Acta Geologica Polonica, Vol. 72 (2022), No. 1, pp. 107–135
DOI: 10.24425/agp.2021.137712

The Jurassic–Cretaceous transition in the High-Tatric succession (Giewont Unit, Western Tatra Mts, Poland): integrated stratigraphy and microfacies

DAMIAN GERARD LODOWSKI[1], ANDRZEJ PSZCZÓŁKOWSKI[2], ANDRZEJ WILAMOWSKI[3] and JACEK GRABOWSKI[3]

[1] *Faculty of Geology, University of Warsaw, ul. Żwirki i Wigury 93, 02-089 Warsaw, Poland.*
E-mail: damian.lodowski@uw.edu.pl
[2] *Institute of Geological Sciences, Polish Academy of Sciences, Warszawa Research Centre, ul. Twarda 51/55, 00-818 Warsaw, Poland.*
E-mail: apszcz@interia.pl
[3] *Polish Geological Institute-National Research Institute, ul. Rakowiecka 4, 00-975 Warsaw, Poland.*
E-mail: andrzej.wilamowski@pgi.gov.pl; jacek.grabowski@pgi.gov.pl

ABSTRACT:

Lodowski, D.G., Pszczółkowski, A., Wilamowski, A. and Grabowski, J. 2022. The Jurassic–Cretaceous transition in the High-Tatric succession (Giewont Unit, Western Tatra Mts, Poland): integrated stratigraphy and microfacies. *Acta Geologica Polonica*, **72** (1), 107–135.

Herein are presented the results of detailed bio- (calcareous dinocysts, calpionellids, foraminifers, saccocomids) and chemostratigraphic ($\delta^{13}C$) studies combined with high-resolution microfacies, rock magnetic and gamma-ray spectrometry (GRS) investigations performed on the upper Kimmeridgian–upper Valanginian carbonates of the Giewont succession (Tatricum, Giewont and Mały Giewont sections, Western Tatra Mountains, Poland). The interval studied covers the contact between the Raptawicka Turnia Limestone (RTL) Fm. and the Wysoka Turnia Limestone (WTL) Fm. Their sedimentary sequence is composed of micrites, pseudonodular limestones, cyanoid packstones, lithoclastic packstone and encrinites. A precise correlation with the previously published Mały Giewont section is ensured by biostratigraphy, rock magnetic and GRS logs. The methodology adopted has enabled the recognition of two stratigraphic discontinuities, approximated here as corresponding to the latest Tithonian–early (late?) Berriasian and the early Valanginian. The hiatuses are evidenced by biostratigraphic data and the microfacies succession as well as by perturbations in isotopic compositions and rock magnetic logs; they are thought to result from a conjunction of tectonic activity and eustatic changes. A modified lithostratigraphic scheme for the Giewont and the Osobita High-Tatric successions is proposed. The top of the RTL Fm. falls in the upper Tithonian, where cyanoid packstones disappear. At the base of the WTL Fm. a new Giewont Member is defined as consisting of a basal lithoclastic packstone and following encrinites.

Key words: Microfossils; Rock magnetism; Carbon isotopes; Western Carpathians; Tatra Mountains.

INTRODUCTION

One of the key problems for consistent regional-scale paleoenvironmental interpretations and models is the sometimes problematic correlation between pelagic-, swell- and platform-type deposits (e.g. Pasquier and Strasser 1997; Morales *et al.* 2013, 2016). A variety of the Late Jurassic–Early Cretaceous depositional environments may be traced within the Central Western Carpathians (CWC) (Vašíček *et al.* 1994).

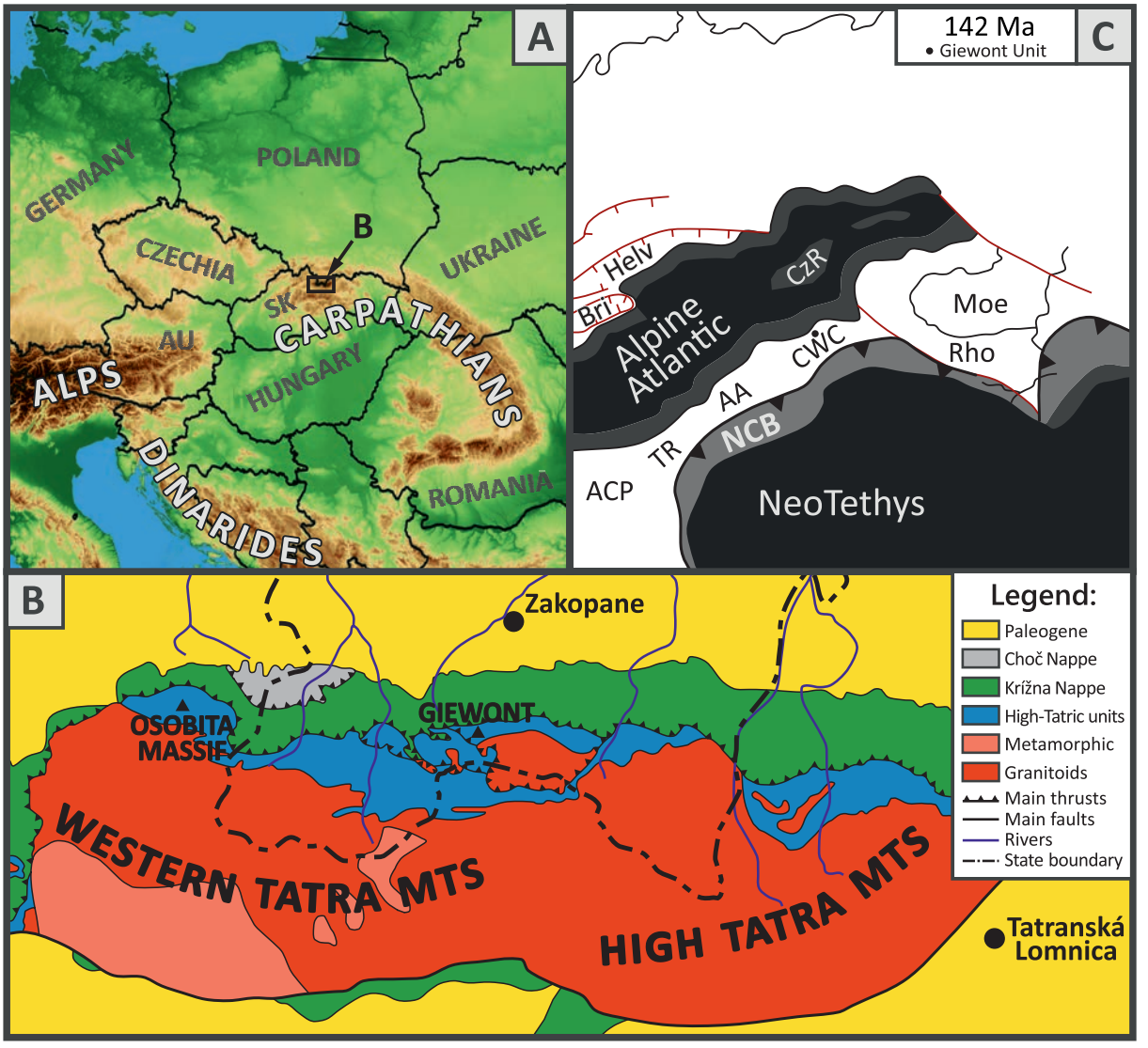

Text-fig. 1. Geological setting of this study area. A – Localization of the Tatra Mountains; Abbreviations: AU – Austria; SK – Slovakia. B – Geological map of the Tatra Mts (modified after Nemčok et al. 1994 and Jurewicz 2005). C – Simplified paleogeographic map of the circum-Carpathian region during the Berriasian; modified after Stampfli and Hochard (2009). Abbreviations: AA – Austro Alpine; ACP – Adriatic Carbonate Platform; CWC – Central Western Carpathians; NCB – Neotethyan Collision Belt; Bri – Brianconnais; CzR – Czorsztyn Ridge; Helv. – Helvetic units; Moe – Moesian Platform; Rho – Rhodopes; TR – Transdanubian Range.

This tectonic mega-unit was located at this time between the Alpine Atlantic (sensu Missoni and Gawlick 2011; equivalent of Alpine Tethys of Schmid *et al.* 2008) to the north and the Tethys ocean to the south (Text-fig. 1), providing an insight into sediments both typically pelagic (deposited in the Zliechov Basin; e.g. Jach *et al.* 2014a) and shallow water (originated on the so-called Tatric Ridge; e.g. Lefeld 1968; Vašíček *et al.* 1994; Pszczółkowski *et al.* 2016). Open-marine, basinal-type deposits are yielded by the Krížna (Lower Sub-Tatric) succession. The Tithonian–Berriasian of this unit possesses a well-established stratigraphic framework (e.g. Pszczółkowski 1996, 2003; Grabowski and Pszczółkowski 2006) which allowed for the recent paleoenvironment-focused studies of Grabowski *et al.* (2013) and Grabowski and Sobień (2015). These resulted in the recognition of a late Berriasian trend of increasing lithogenic supply, suggested to have been related to either climatic and/or eustatic changes. However, correlation of the J/K boundary interval between the Lower Sub-Tatric and the High-Tatric (Tatric Ridge) successions is vague due to the ambiguous stratigraphy of the latter (in particular the Berriasian is poorly or even not documented; compare Lefeld 1968

and Pszczółkowski *et al.* 2016). Consequently, the relations between the different sedimentary zones of the CWC remain unclear also in the context of the latest Jurassic–earliest Cretaceous deposition environments and their controls.

According to literature data (e.g. Kotański 1959; Lefeld 1968) the record of the Jurassic–Cretaceous boundary interval in the High-Tatric succession may be followed on the northern slopes of Mt. Giewont (Western Tatra Mts, Poland). In this study we present data from two sections (Mały Giewont and Giewont), adopting modern research techniques in order to provide a consistent stratigraphic interpretation of the uppermost Jurassic–lowermost Cretaceous beds of the Giewont Unit. Integration of detailed microfacies analysis with high resolution bio- (calcareous dinoflagellates, chitinoidellids, foraminifers), chemo- ($\delta^{13}C$ and $\delta^{18}O$ stratigraphy) and rock magnetic stratigraphy has allowed for precise correlation between the studied sections, interpreted herein as spanning the upper Kimmeridgian–upper Valanginian. A separate paper will be devoted to a detailed paleoenvironmental interpretation of this study area and its relations to adjacent sedimentary zones.

GEOLOGICAL SETTING AND PREVIOUS STUDIES

The Tatra Mountains are located in the northernmost Central Western Carpathians, a part of the vast Alpine-Carpathian-Dinaric orogen (Text-fig. 1). The Tatras are composed of a crystalline core and a latest Paleozoic–Mesozoic sedimentary cover. The crystalline basement consists of granitoids of the High Tatra Mts as well as granitoid and metamorphic rocks of the Western Tatra Mts, whilst the sedimentary cover consists of: 1) High-Tatric autochthonous unit and nappes; and 2) Sub-Tatric (Krížna and Choč) Nappes (for more information see e.g. Jurewicz 2005 and references therein).

The area of this study is located within the Giewont Nappe, one of the High-Tatric allochthonous units, providing the record of its Lower Triassic–Upper Cretaceous evolution (e.g. Kotański 1959; Lefeld 1968; Jurewicz 2005; Bąk and Bąk 2013). According to Lefeld *et al.* (1985) the Jurassic–Cretaceous boundary falls in the Raptawicka Turnia Limestone Formation (RTL Fm). This ca. 100 m thick formation is customarily subdivided into three informal members: 1) the lower member (Callovian–Oxfordian), consisting of pinkish pelitic limestones with ammonites (Kotański 1959; Lefeld *et al.* 1985); 2) the middle member (upper Oxfordian–Berriasian), with light gray Lombardia (= *Saccocoma*)-pseudo-oolitic limestones (Passendorfer 1928; Kotański and Radwański 1959; Lefeld and Radwański 1960; Lefeld 1968; Lefeld *et al.* 1985); and 3) the upper member (Valanginian–Hauterivian), characterized by dark brown (almost black) onco-oolitic limestones (Kotański 1959; Lefeld 1968; Lefeld *et al.* 1985). Lefeld (1968) described also Hauterivian crinoidal limestones (= encrinites), however these were not included in the later lithostratigraphic scheme of Lefeld *et al.* (1985). The RTL Fm. is followed by the Barremian–Aptian Wysoka Turnia Limestone Formation (WTL Fm.), which consists of Urgonian type limestones abundant in reef corals, orbitolinids, brachiopods, bivalves, calcareous algae, bryozoans, hydrozoans and gastropods (Lefeld *et al.* 1985; Masse and Uchman 1997).

Integrated bio- and chemostratigraphy of the Upper Jurassic of the Mały Giewont section was provided by Pszczółkowski *et al.* (2016). There authors proposed also a modification of the RTL Fm. lithostratigraphy, suggesting a late Oxfordian–early Tithonian age for the middle member of the Fm. However, the uppermost Tithonian and the lowermost Cretaceous beds were not documented due to lack of their exposure. An insight into this interval is however provided by the Giewont section (see below).

Description of the sections

This study was conducted based on the material collected from two localities, namely the Mały Giewont and the Giewont sections (Text-figs 1–2). The Mały Giewont section (49°15'09" N; 19°55'30" E) was first described by Lefeld (1968). It provides a record of ca. 80 m thick Kimmeridgian–Lower Cretaceous rocks (Pszczółkowski *et al.* 2016). A substantial part of the section is made of the dark gray to gray oncoid-bearing limestones of the RTL Fm. followed by the light gray bioclastic limestones of the WTL Fm.; nevertheless, the section is characterized by numerous observational gaps, covering also the boundary between the RTL and the WTL Fms.

A continuous, yet stratigraphically more restricted record characterizes the Giewont section (49°15'15" N; 19°55'52" E). This is a new section located on the northern slopes of Mount Giewont, in the foothills of Kirkor's Gully (pol. Żleb Kirkora), giving an insight into the 40 m thick record of the RTL Fm. to the WTL Fm. transition (Text-fig. 3). Massive, thick to medium bedded, gray to dark gray pelitic limestones with rare macrofossils (ammonites, bivalves) characterize the lowermost 12 m of the section (G1–G15

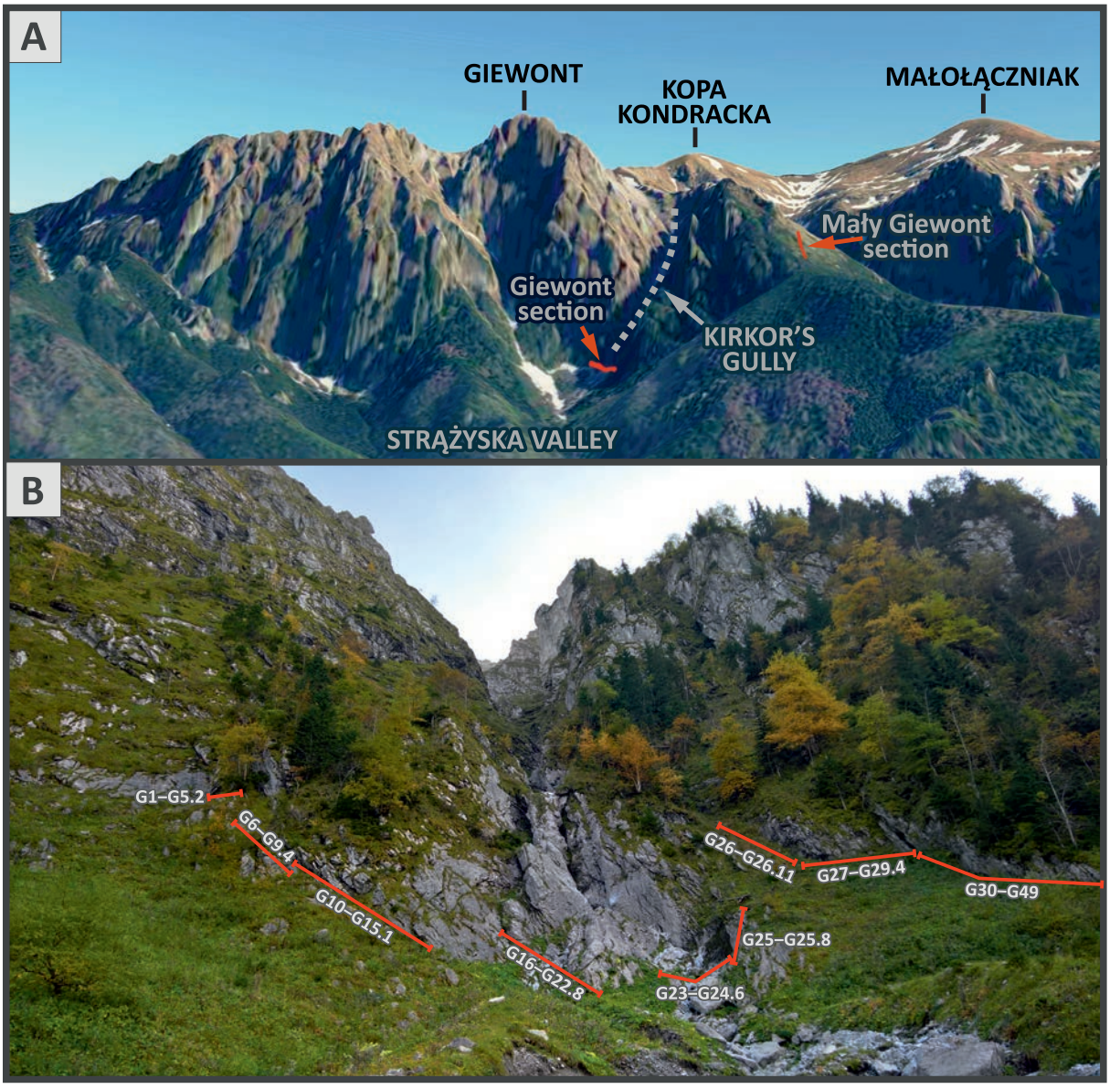

Text-fig. 2. Area of this study. A – Localization of the Giewont and the Mały Giewont sections in the Western Tatra Mountains. B – General outlook of the Giewont section; red lines indicate intervals in which given samples were taken from (for details see Appendix 1 – Supplementary material available only in the online version).

samples). Above (12–32.5 m; samples G15.1–G28.13) the rocks gradually become darker and reflect some signs of cross-stratification. Between samples G27 and G28 (ca. 27 m) a fault zone with tectonic breccia and a slight differentiation of dip are observed. The topmost investigated part of the section (32.5–40 m; G29–G49) consists of light gray, medium to thin bedded crinoidal packstones (encrinites) with cross-beddings. Basic observations were conducted also within the following 10 m interval; these rocks are identical in lithology to those below. Detailed photographic documentation of the Giewont section is presented in Appendix 1 (Supplementary material available only in the online version).

MATERIALS AND METHODS

Field measurements and laboratory analyses of the Mały Giewont section were conducted in years 2013–2014; here we interpret them in the light of recently collected data. The Giewont section was inves-

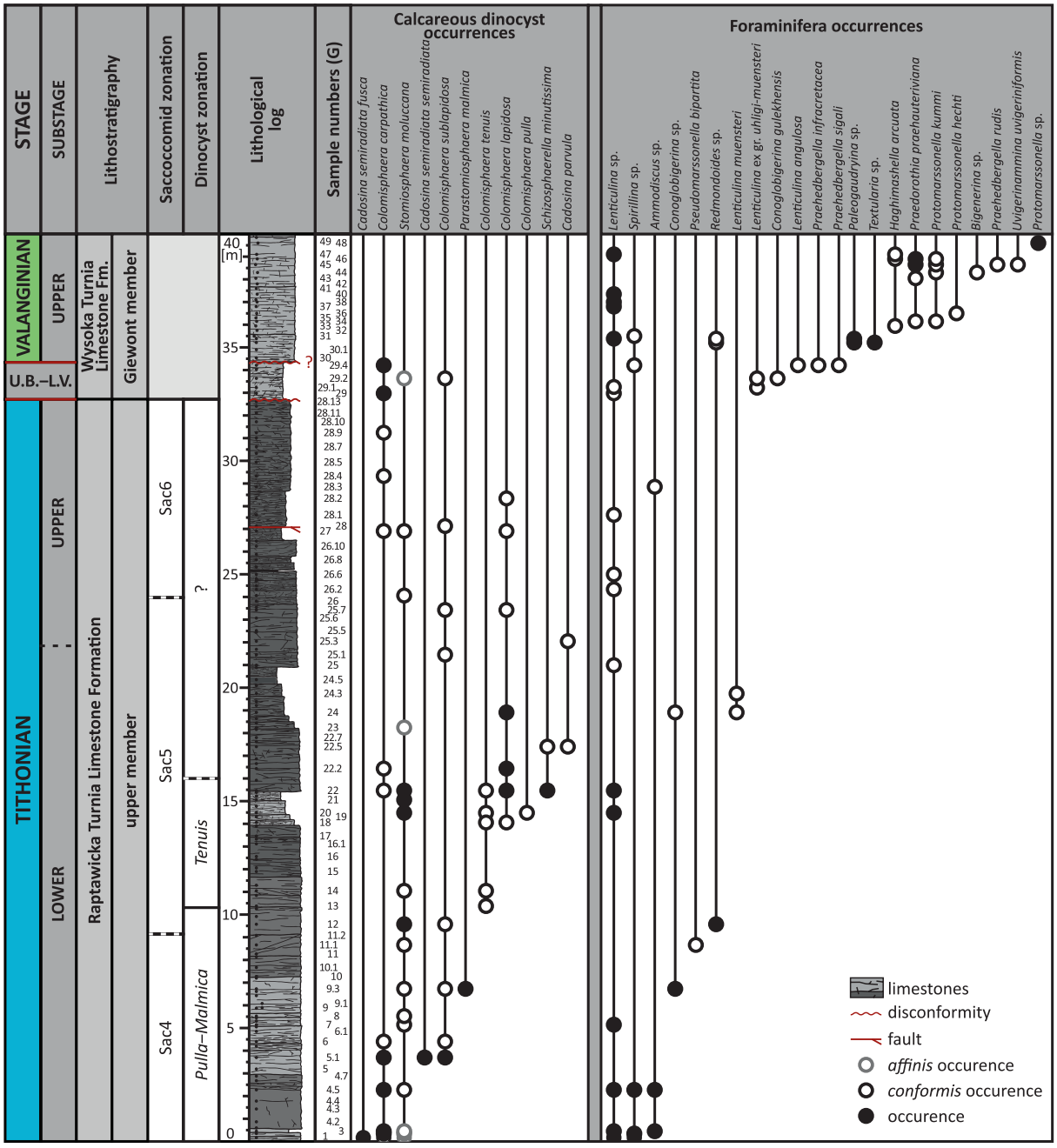

Text-fig. 3. Calcareous dinoflagellates and foraminifers range charts from the Giewont section. Dinocyst zonation after Reháková (2000); Saccocomid zonation after Benzaggagh *et al.* (2015a). Abbreviations: U.B–L.V. – upper Berriasian–lower Valanginian. Colors on lithological log correspond to the colors of the fresh rock surfaces.

tigated in years 2018–2020; also microfacies analysis of the Mały Giewont section was performed in this time, in order to enable direct correlation with observations from the Giewont section. The data used in this study are presented in tabular form (.xlsx file) in Appendix 2 (Supplementary material available only in the online version).

Microfossil biostratigraphy and microfacies analysis

A total number of 79 thin sections from the material collected in the Giewont section was prepared in the Laboratory of Geological Education (ECEG) in Chęciny, Poland (affiliated with the University

of Warsaw) using a Logitech PM5 Lapping and Polishing System. Additional 66 thin sections from the Mały Giewont sections were taken for investigations from the archives of the Polish Geological Institute-National Research Institute. Microfossil biostratigraphy was investigated using Nikon ECLIPSE LV100POL polarizing microscope (Institute of Geological Sciences, Polish Academy of Sciences). In this study we adopted the calcareous dinoflagellate and calpionellid zonation after Reháková (2000) and the *Saccocoma* zonation after Benzaggagh *et al.* (2015a).

Microfacies analyses were performed using Nikon ECLIPSE LV100POL (for 2× and higher magnification) and NIKON SMZ1000 (for 0.8x magnification) microscopes, both in the Optical Microscopy Lab of the Faculty of Geology, University of Warsaw. Images were taken in natural and cross polarized light (XPL) using Nikon NIS software. Microfacies analysis was performed using ImageJ software. On a 0.8× magnification image a 20×30 grid was put in order to determine the general microfacies characteristics of the sample and to estimate the percentage of oncoids, burrows and lithoclasts. Subsequently, a 23×30 grid was put on a 2× magnified representative area of the sample in order to count cyanoids, cortoids, peloids, (other) biogenic detritus and matrix (spar and micrite).

Magnetic susceptibility and rock magnetism

Magnetic susceptibilities (MS) of 209 stratigraphic horizons (138 in the Giewont and 71 in the Mały Giewont section) were measured during the field work using ZH Instruments SM30 Magnetic Susceptibility Meter; MS of each horizon was measured three times in order to calculate its mean value. Among them, 144 horizons (77 from Giewont and 70 from the Mały Giewont section) were intended for sampling and detailed laboratory investigations of rock magnetic properties in the Paleomagnetic Laboratory of the Polish Geological Institute-National Research Institute (PGI-NRI). Rock samples were crushed into a homogenous fine-gravel fraction and packed in 8 cm^3 sample boxes. Rock magnetic investigations comprised mass-normalized measurements of the MS and laboratory induced magnetizations: isothermal remanent magnetization (IRM) and anhysteretic remanent magnetization (ARM). MS measurements were performed using Agico KLY2 kappabridge; susceptibilities of sample boxes were subtracted from the results. IRM was applied along the Z axis in the field of 1 T (IRM_{1T}) and then antiparallel in the field of 100 mT (IRM_{100mT}) using Magnetic Measurements MMPM Pulse Magnetizer; measurements were performed using Agico JR6A spinner magnetometer. ARM was produced in a Molspin pARM device with peak alternating field of 100 mT and a steady field bias of 0.1 mT. All the measurements were processed using Agico Rema6 software. S-ratio ($-IRM_{100mT}/IRM_{1T}$) was calculated in order to indicate proportions between low and high coercivity minerals (e.g. Opdyke and Channell 1996). Domination of low coercivity fraction (e.g. magnetite) is characterized by high S-ratio values (above 0.6), whilst the lower S-ratio the higher is contribution of high coercivity minerals, e.g. hematite. ARM/IRM_{1T} ratio is often used as a proxy for magnetic grains size or magnetite/hematite ratio. (e.g. Opdyke and Channell 1996; Jovane *et al.* 2007; Venuti *et al.* 2007).

Gamma-ray spectrometry (GRS) and elements geochemistry

Field gamma-ray spectrometric measurements were carried out using a Georadis GT-32 portable natural radioisotope assay analyzer with BGO 2×2" detector. Energy windows of potassium, uranium and thorium were analyzed in 300 s time intervals. The results account for the value of the total dose (nGy/h), SGR (standard gamma ray; ppm), counts per minute (cpm) for K, U and Th as well as their converted concentrations (% for K and ppm for U and Th). A total number of 162 measurements was performed (88 in the Giewont and 74 in the Mały Giewont section); those were fully integrated with the horizons of the MS measurements and rock sampling. Due to the fact that K concentrations were usually near or below the cpm to % conversion limit of the handheld device, in this paper we consider CGR (computed gamma ray index), which is calculated using the following formula: CGR [API] = Th [ppm] × 3.93 + K [%] × 16.32 (Rider 1999). CGR is regarded as a good proxy for terrigenous contribution in carbonates (e.g. Kumpan *et al.* 2014; Grabowski *et al.* 2019).

Additional chemical analyzes of 79 whole-rock samples (49 from the Giewont and 30 from the Mały Giewont section) were performed at the Bureau Veritas Mineral Laboratories, Canada (ACME) using multi-acid MA250 method (for details see Bureau Veritas Minerals Schedule of Services and Fees 2020). In this study GRS data and laboratory-measured Th concentrations are used and discussed for correlation purposes only.

Stable carbon and oxygen isotopes

A total number of 128 bulk rock samples (only from the Giewont section) were intended to $\delta^{13}C$ and $\delta^{18}O$ analysis. Homogenous powder was obtained by dry micro-drilling in the same samples as were used for rock magnetic investigations. Analyses were carried out in the Stable Isotope Laboratory of the GeoZentrum Nordbayern, Erlangen, Germany. Carbonate powders were analyzed using a Gasbench II connected to a ThermoFisher Delta V Plus mass spectrometer. All values are reported in per mil relative to V-PDB scale. Reproducibility and accuracy was monitored by replicate analysis of laboratory standards calibrated by assigning $\delta^{13}C$ values of +1.95‰ to NBS19 and -47.3‰ to IAEA-CO9 references and $\delta^{18}O$ values of -2.20‰ to NBS19 and -23.2‰ to NBS18. Reproducibility for both $\delta^{13}C$ and $\delta^{18}O$ was ±0.0 (1 std. dev.). Oxygen isotope values of dolomite, siderite, aragonite etc. were corrected using the phosphoric acid fractionation factors given by Kim *et al.* (2007) and Rosenbaum and Sheppard (1986). Data for the Mały Giewont section comes from the Pszczółkowski *et al.* (2016) dataset.

RESULTS

Microfossil biostratigraphy

The calcareous dinoflagellate and calpionellid stratigraphies of the Mały Giewont section have been already published by Pszczółkowski *et al.* (2016). Their study provided also a documentation of relatively rich, however of limited stratigraphic value, assemblage of planktonic and benthic foraminifers, as well as a detailed commentary on the Late Jurassic ammonites reported over the years from the area of this study. Although we adopt the stratigraphic framework of Pszczółkowski *et al.* (op. cit.), based on correlation with the Giewont section we revise the stratigraphic position of the basal and the topmost intervals of their section (see Interpretation chapter).

Only calcareous dinoflagellates, foraminifers and saccocomids were found to provide significant stratigraphic information in the Giewont section. Nevertheless, both dinocysts and foraminifers are rare and poorly preserved, which usually prevented their exact taxonomic designation; in turn the *Saccocoma* stratigraphy (Benzaggagh *et al.* 2015a, b) has limited stratigraphic resolution. Worth noting also is the almost complete absence of calpionellids; only a single specimen of indeterminable ?*Calpionellidae* sp. was observed in sample G29.1. Consequently, only two calcareous dinoflagellate biozones and three *Saccocoma* zones were recognized. Occurrences of recorded taxa are depicted on Text-fig. 3. For details on the stratigraphic interpretation of the studied sections see Interpretation chapter.

Calcareous dinoflagellates of the Giewont section

The basal part of the Giewont section (G1–G12 samples) accounts for the association of *Cadosina semiradiata fusca*, *Cadosina semiradiata semiradiata*, *Colomisphaera carpathica*, *Colomisphaera sublapidosa*, *Stomiosphaera moluccana* and *Parastomiosphaera malmica* dinoflagellates (Text-fig. 3). This assemblage – in particular *P. malmica* – is characteristic of the early Tithonian (compare e.g. with Benzaggagh *et al.* 2015b; Grabowski *et al.* 2019; Lodowski *et al.* 2021; Michalík *et al.* 2021), thus is assigned here to the *Pulla–Malmica* Zone. The first occurrence (FO) of *Colomisphaera tenuis* in sample G13 evidences the mid-Tithonian *Tenuis* calcareous dinoflagellate Zone (Reháková 2000). The *Tenuis* Zone is correlated with the upper part of the *Chitinoidella* calpionellid Zone (= *Chitinoidellidae* Zone after Benzaggagh 2021). Above, the only observed FO's are those of *Colomisphaera lapidosa*, *Colomisphaera pulla*, *Schizosphaerella minutissima* and *Cadosina parvula* (Text-fig. 3), therefore an assemblage that does not yield any significant information in the context of upper Tithonian stratigraphy. Selected specimens of calcareous dinoflagellates of the Giewont section are presented on Pl. 1.

Foraminifers of the Giewont section

Foraminifers of the Giewont section are rare and in most cases did not allow an exact taxonomical determination. Among planktonic foraminifers a few specimens of genera *Conoglobigerina* and *Praehedbergella* were documented; benthic forams are represented by genera *Ammodiscus*, *Bigenerina*, *Haghimashella*, *Lenticulina*, *Paleogaudryina*, *Praedorothia*, *Protomarssonella*, *Pseudomarssonella*, *Redmondoides*, *Spirillina*, *Textularia* and *Uvigerinammina* (Text-fig. 3). Within the lower and the middle part of the section (samples G1–G28.13) only three specimens were identified to species level; these are *Pseudomarssonella bipartita* documented in sample G11.1 and *Lenticulina* cf. *muensteri* recognized in samples G24 and G24.3 (Text-fig. 3). More diverse associations are observed from sample G29 upwards. There, benthic foraminifers are

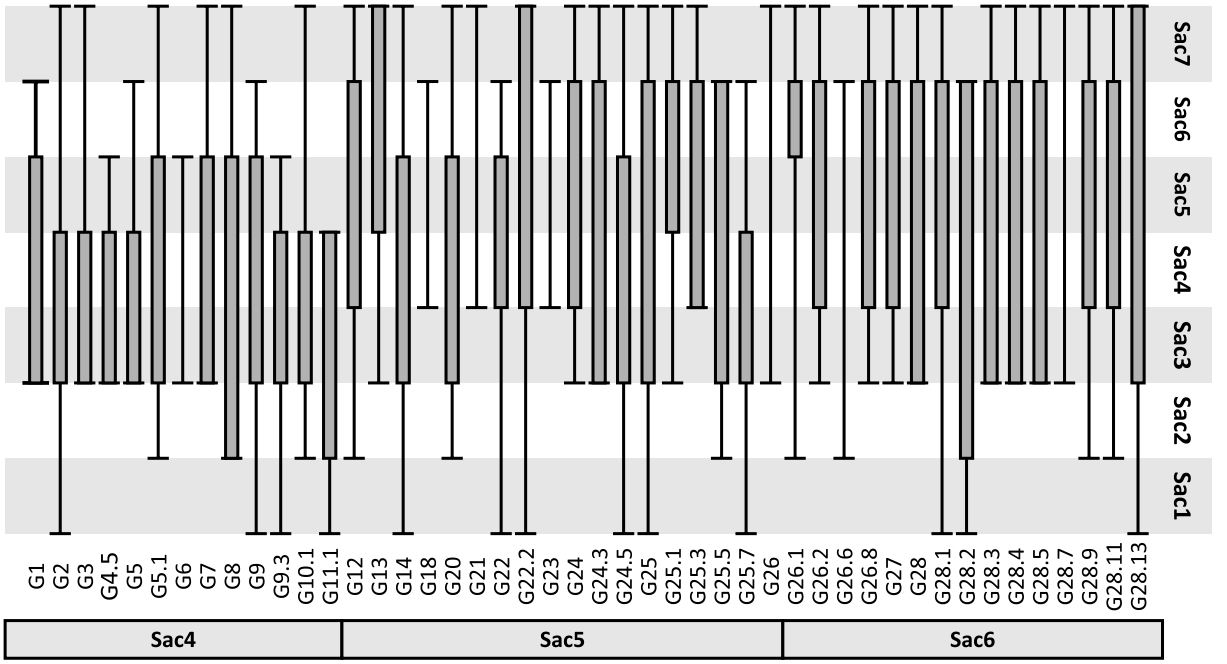

Text-fig. 4. Ranges of *Saccocoma* skeletal elements occurring in the studied samples of the RTL Fm. in the Kirkor's Gully (Western Tatra Mts.). Saccocomid zones (Sac1 to Sac7) after Benzaggagh *et al.* (2015a).

represented by *Lenticulina* ex gr. *uhligi–muensteri* (G29.1 and G29.2 samples), *Lenticulina angulosa* (G29.4), *Haghimashella* cf. *arcuata* (FO in G33 sample), *Praedorothia praehauteriviana* (FO in sample G34), *Protomarssonella kummi* (FO in sample G34), *Protomarssonella hechti* (G36) and *Uvigerinammina uvigeriniformis* (G45). In turn the assemblage of planktonic forams consists of *Conoglobigerina gulekhensis* (G29.2), *Praehedbergella infracretacea* (G29.4), *Praehedbergella sigali* (G29.4) and *Praehedbergella rudis* (G45) (Text-fig. 3). These taxa account for the predominantly Valanginian age of the interval (for detailed discussion see Interpretation chapter). Selected specimens of foraminifers (and a single specimen of gastropod) are shown on Pl. 2.

Saccocomids of the Giewont section

In principle, Saccocomidae zonation is based on the variable geometry and relative abundance of their skeletal elements (Benzaggagh *et al.* 2015a). During this study elements of relatively wide stratigraphic range (even Sac1–Sac7) were observed in most of samples. However, the most frequent are those characteristic of zones Sac4–Sac6, which belong to the lower–lower upper Tithonian interval (Text-fig. 4). The boundary between Sac4 and Sac5 zones was put between samples G11.1 and G12, where Sac3 Zone and older elements become less common. In turn, the boundary between the Sac5 and Sac6 zones was established between samples G26 and G26.1, where *Saccocoma* skeletal elements are the most characteristic of Sac6 Zone (Text-fig. 4). Nevertheless, due to stratigraphic inaccuracy this interpretation has to be regarded as an approximation. Examples of characteristic *Saccocoma* skeletal elements are shown on Pls 3–5.

Microfacies

According to Pszczółkowski *et al.* (2016), the microfacies succession of the Mały Giewont section may be simplified to: 1) upper Kimmeridgian oncolitic limestones and following biomicrites, both with *Globochaete* algae, thin-shelled bivalves and

Text-fig. 5. Microfacies of the upper Kimmeridgian–upper Valanginian limestones of the Giewont Unit. A – MF IA, sample MG64; B – MF IB, sample MG75A; C – MF II, sample MG84; D – MF III, sample MG95; E – MF III, sample G17; F – MF IV, sample G28.4; G – MF V, sample G29.1; H – MF VI, sample G36. Abbreviations: bf – benthic foraminifera; c – cyanoid; co – cortoid; cr – crinoid; d – dissolution features; *G.a.* – *Globochaete alpina*; l – lithoclast; p – peloid; r – radiolarians; *S* – *Saccocoma* skeletal element; G – Giewont section; MG – Mały Giewont section. →

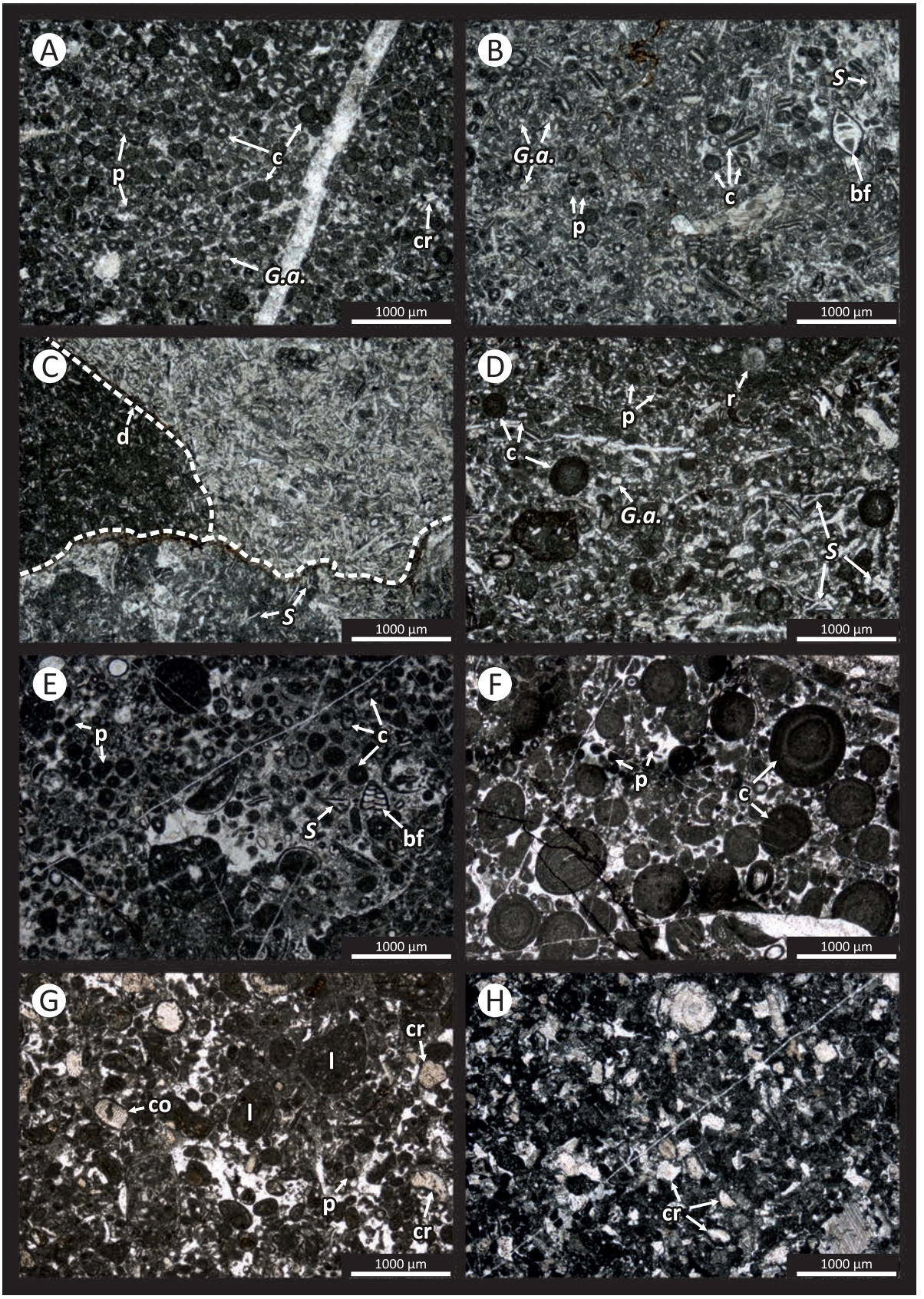
A
p
c
cr
G.a.
1000 µm
B
S
G.a.
c
bf
p
1000 µm
C
d
S
1000 µm
D
p
r
c
G.a.
S
1000 µm
E
p
c
S
bf
1000 µm
F
p
c
1000 µm
G
cr
l
co
l
p
cr
1000 µm
H
cr
1000 µm

Saccocomidae elements; 2) lower Tithonian biomicrites with *Saccocoma* and *Globochaete*, gradually passing into the upper Tithonian oncosparites; and 3) echinoderm-dominated Lower Cretaceous (?Barremian–Aptian) limestones. In this study we provide more detailed insight into the microfacies succession of both the Giewont and Mały Giewont sections (see below).

Pszczółkowski (2018) confirmed the assumption of Lefeld and Radwański (1960) that the Upper Jurassic coated grains of the Giewont Unit (previously regarded also as "oolites") are predominantly of bacterial (cyanobacteria) origins, and thus should be regarded rather as porostromate (micro)oncoids or cyanoids. During this study two kinds of oncoidal structures were observed. Those of the first group are usually larger than 2 mm in diameter, have ovoidal, elongate or lobate shape, often manifesting aggregation of smaller bodies while the nucleus may be either simple (e.g. bioclast) or compound. The second group accounts for smaller coated grains (usually below 1 mm in diameter), more regular in shape (usually cylindrical or ovoidal), with tangential or no inner structure and a single bioclast or peloid as a nucleus. Based on it, for the purpose of microfacies analysis two separate classes for 1) oncoids and 2) microoncoids (here referred simply as "cyanoids" *sensu* Pszczółkowski 2018; compare with cyanoids *sensu* Riding 1983) were set aside. The other class of coated grains are cortoids, here defined as bioclasts with a thin bacterial coating, in the order of 0.02 mm. Besides, dark-gray rounded grains with blurred edges and no internal structure, usually smaller than 0.2 mm in diameter, are interpreted here as peloids. The microfacies of the Giewont and Mały Giewont sections are presented in Text-fig. 5, whilst the relative shares of selected rock constituents and structures (matrix, biodetritus, oncoids, microoncoids, cortoids, peloids, burrows) are visualized in Text-fig. 6. Photographs of polished rock surfaces of samples G28.13 and G29 are shown in Text-fig. 7.

Mały Giewont

The basal part of the section (MF IA; 0–11 m, samples MG56–MG69; lower part of the upper Kimmeridgian) consists of wackestones-packstones abundant in cyanoids and peloids. Stylolites and dissolution seams are observed; *Globochaete* algae dominate among bioclasts, however ammonites, benthic foraminifers, as well as crinoidal and shelly detritus also occur. Microoncoids are small and relatively spherical; micrite dominates the matrix, however spar sectors are also observed.

Above, (MF IB; 11–22 m, samples MG70–MG80; upper part of the upper Kimmeridgian) the succession becomes more densely packed in bioclasts and rich in burrowing structures. Pressure dissolution features are observed; the matrix is dominated by micrite, however spar sectors also occur. Cyanoids and peloids gradually disappear, whilst *Saccocoma* skeletal elements and *Globochaete* algae are still common.

The following beds (MF II; 22–33 m, samples MG81–MG91; Kimmeridgian/Tithonian transition) are barren in coated grains. A patchwork of *Saccocoma–Globochaete* packstone and wackestone sectors combined with common pressure dissolution features (both dissolution seams and stylolites) and micrite matrix account for the pseudonodular texture of the interval.

Cyanoids reappear gradually from sample MG92. The entire interval of samples MG92–MG104C (33–53 m; lower Tithonian) is characterized by heterogenous wackestones and packstones (MF III). Oncoids are common at the basal part of the interval; upwards they are replaced by cyanoids. Stylolites and dissolution seams occur, yet the pseudonodular texture is observed no longer. Bioclasts are dominated by *Saccocoma* and *Globochaete* elements; matrix is dominated by micrite, spar is rare.

Samples MG105–MG116 (56–65 m; uppermost lower–upper Tithonian) were taken from cyanoid packstone with peloids (MF IV). Uncoated bioclasts almost do not occur; *Saccocoma* elements and shelly material are the most common nuclei of coated grains, however they are less frequent than in underlying beds. Pressure dissolution features are uncommon; both micrite and spar matrix sectors occur.

Crinoidal packstones (encrinites) with peloids constitute the topmost part of the section (MF VI; MG117–MG120; 77–80 m; lower Cretaceous); these calcarenites are poor in other microfossils, amongst which benthic foraminifers are the most common.

Text-fig. 6. Correlation between the Giewont and Mały Giewont section in the light of relative share of microscopically observed rock constituents. GRS total dose logs are shown for comparison. Stratigraphy of the Mały Giewont section after Pszczółkowski *et al.* (2016; modified, see text for discussion). Thick dashed lines indicate correlation horizons. Explanations: MF IA – cyanoid-peloid wackestones and packstones; MF IB – cyanoid-peloid wackestones and packstones with other bioclasts; MF II – *Saccocoma–Globochaete* pseudonodular limestones; MF III – heterogenous wackestones and packstones with cyanoids; MF IV – cyanoid packstones with peloids; MF V – lithoclastic packstone with crinoids; MF VI – crinoidal packstones (encrinites). Abbreviations: U.B–L.V. – upper Berriasian–lower Valanginian; VAL. – Valanginian; U. – Upper; WTL Fm. – Wysoka Turnia Limestone Formation; Bor – Borzai. →

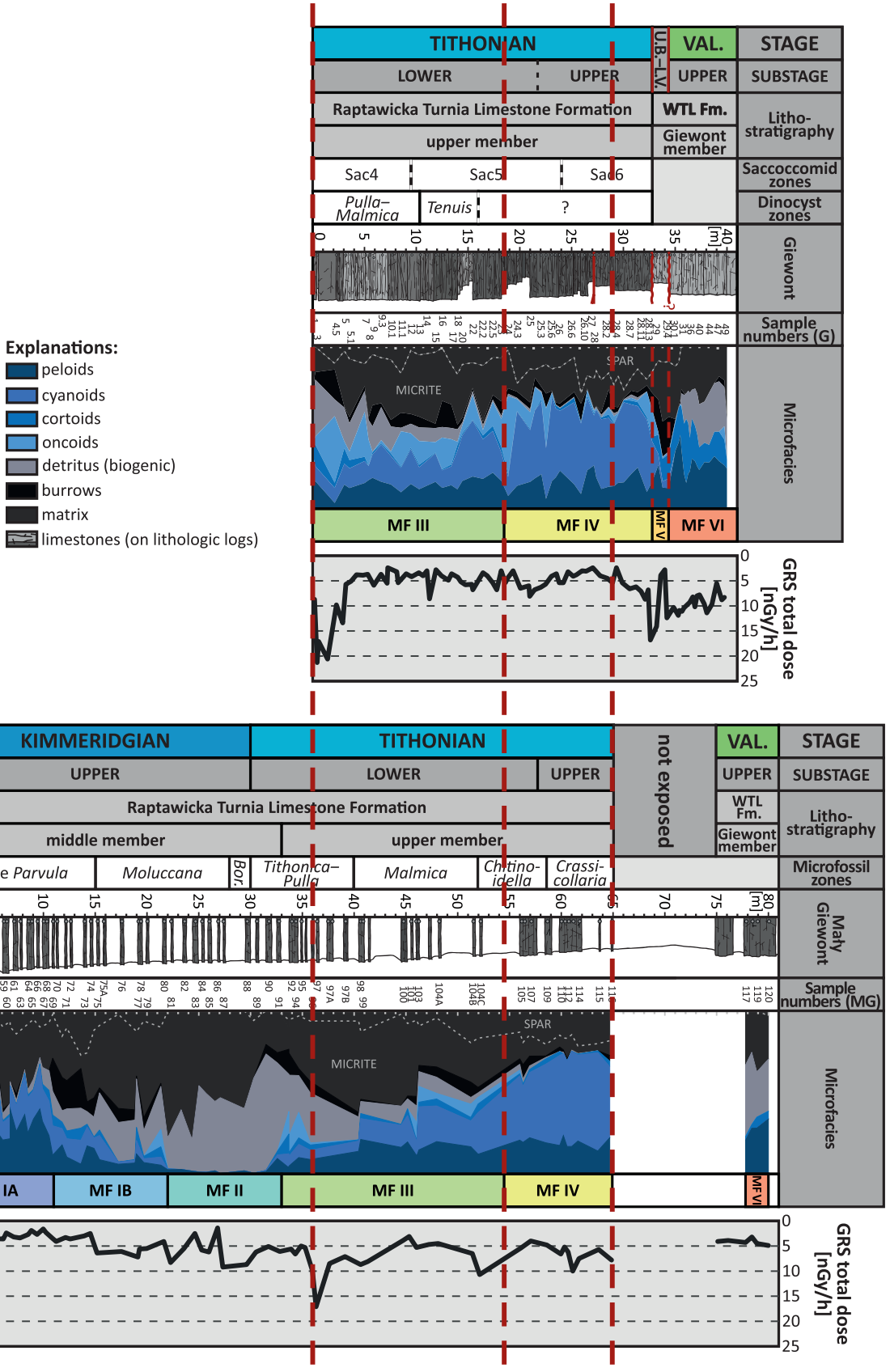
Explanations:
peloids
cyanoids
cortoids
oncoids
detritus (biogenic)
burrows
matrix
limestones (on lithologic logs)
TITHONIAN
U.B.–LV.
VAL.
STAGE
LOWER
UPPER
UPPER
SUBSTAGE
Raptawicka Turnia Limestone Formation
WTL Fm.
Litho-stratigraphy
upper member
Giewont member
Sac4
Sac5
Sac6
Saccoccomid zones
Pulla–Malmica
Tenuis
?
Dinocyst zones
Giewont
Sample numbers (G)
SPAR
MICRITE
Microfacies
MF III
MF IV
MF V
MF VI
GRS total dose [nGy/h]
KIMMERIDGIAN
TITHONIAN
not exposed
?
UPPER
LOWER
UPPER
middle member
upper member
Acme Parvula
Moluccana
Bor.
Tithonica–Pulla
Malmica
Chitino-idella
Crassi-collaria
Microfossil zones
Mały Giewont
Sample numbers (MG)
MF IA
MF IB
MF II
MF III
MF IV
MF VI

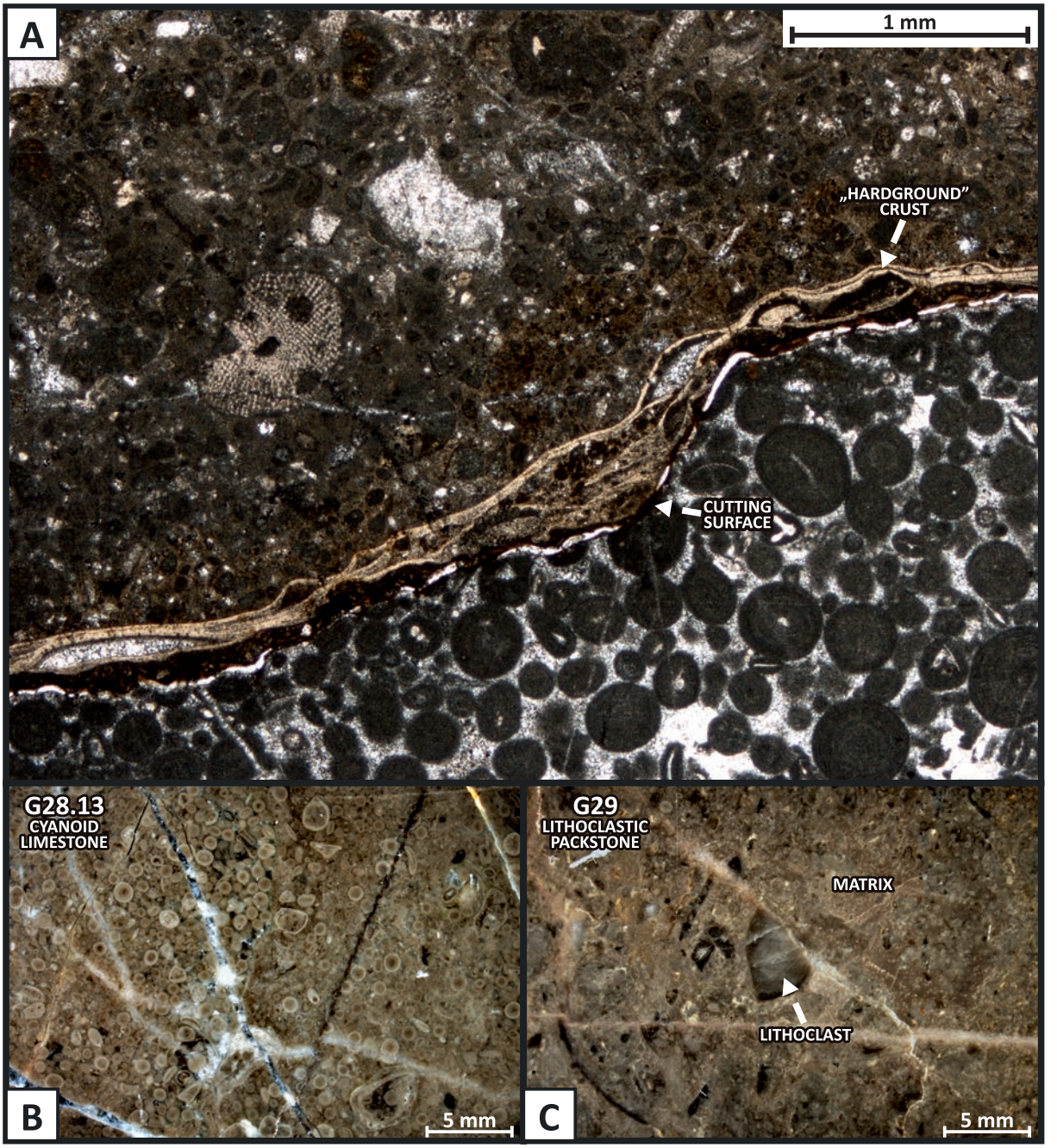

Text-fig. 7. Microphotographs of cyanoid packstone (MF IV) and lithoclastic packstone (MF V). A – Contact between the cyanoid packstone (below) and lithoclastic packstone (above) in sample G29 (thin section). Cutting surface and a hardground crust are indicated by arrows. B – Cyanoid packstone in sample G28.13 (polished rock surface). C – Lithoclastic packstone in sample G29 (polished rock surface).

Giewont

The microfacies succession in the Giewont section corresponds well to that of the Mały Giewont (Text-fig. 6), starting with heterogenous wackestones and packstones (MF III; G1–G23 samples, 0–18.2 m), subsequent cyanoid packstones (MF IV; G24–G28.13, 18.85–32.95 m) and lithoclastic packstone and encrinites on top (MF V and MF VI; G29–G49, 32.95–40 m). This allowed an initial (however precise; see Interpretation chapter) correlation between the studied sections, putting the base of the

Giewont section at or near the 36 m level of the Mały Giewont section (Text-fig. 6).

A new feature in the Giewont section, not observed in the Mały Giewont, is a thin interval of lithoclastic packstone (MF V; samples G29–G29.4, 32.95–34.20 m; Text-figs 5–7). It is characterized by abundant peloids, cortoids (with crinoidal elements as nuclei as usual) and burrows. Noteworthy, the contact between MF IV and MF V is marked by an erosion surface, covered by a thin (?)hardground crust (Text-fig. 7). Lithoclasts of MF V are variable in size, sub-rounded to rounded-edged and falling in the sand fraction (0.125–2 mm in diameter; Text-fig. 5G), however larger clasts also occur (see Text-fig. 7C). They have wackestone characteristics, with a dark-gray to dark-brown matrix (Text-fig. 5G and 7C) and indeterminable bioclasts (Text-fig. 5G). Above, lithoclastic packstone encrinites of MF VI occur (samples G30–G49; 34.8–40 m); they are rich in peloids, cortoids and bioclasts, and are characterized by predominantly homogenous texture (see Text-figs 5–6). Although contact between MF V and MF VI is not observed in thin sections, field observations suggests the discordant character of this boundary. Occurrence of a fault is rather excluded as no near-fault structures – such as tectonic breccia, mineralization or slickensides – were observed, whilst slight differentiation in dip may be noticed (see Appendix 1, photograph 43). Finally, four samples were collected from the following 10 m thick interval (40–50 m; not shown on text-figures); these also represent microfacies MF VI.

Rock magnetism

Mały Giewont

The magnetic susceptibility log obtained from the Mały Giewont section (Text-figs 8–9) may be divided in three intervals with clearly different trends: 1) the upper Kimmeridgian, characterized by slightly increasing MS (5–20 × 10^{-9} m^3/kg); 2) the lower Tithonian, elevated MS values (15–60 × 10^{-9} m^3/kg); and 3) the uppermost lower Tithonian–lower Cretaceous, which manifests decreasing MS (-5–10 × 10^{-9} m^3/kg).

Both IRM_{1T}, IRM_{100mT} and ARM (Text-fig. 8)

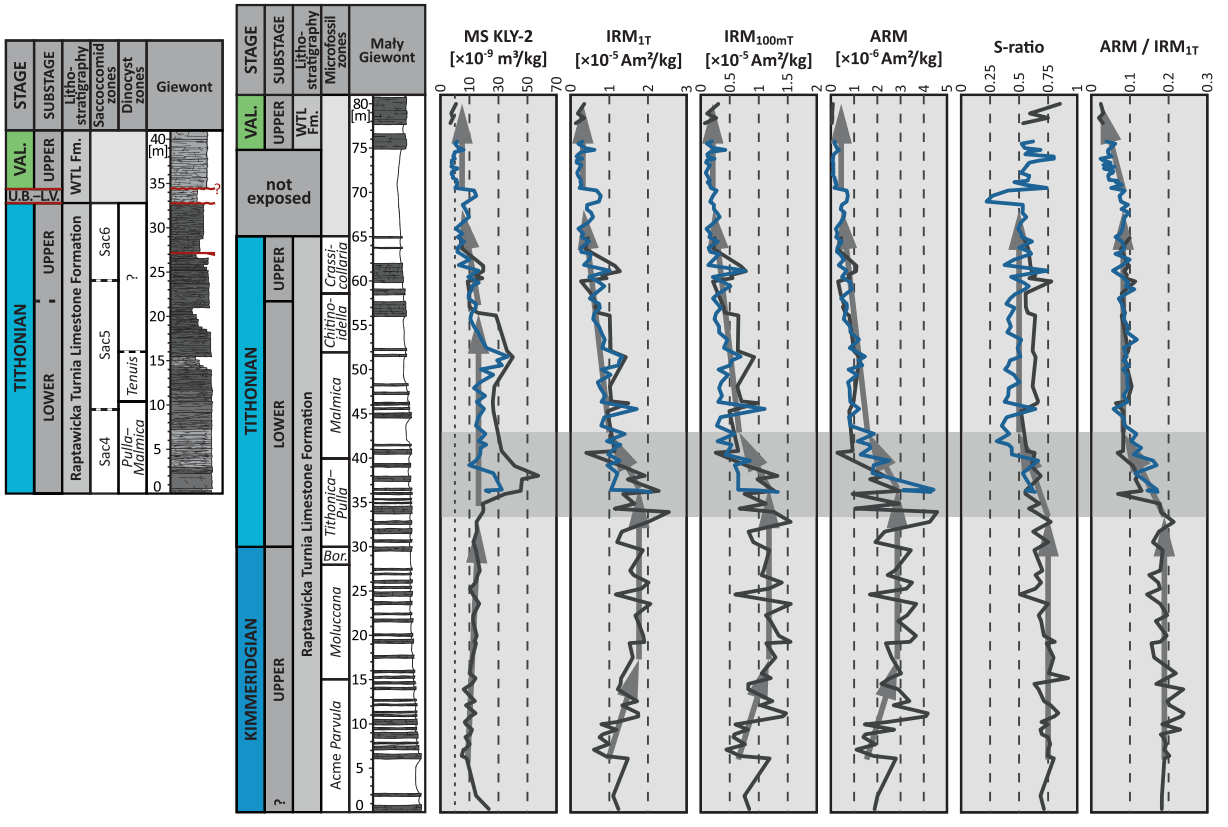

Text-fig. 8. Magnetic susceptibility, IRM_{1T} and IRM_{100mT}, ARM, S-ratio and ARM / IRM_{1T} logs from the Giewont Unit of the High-Tatric succession. IRM100mT is presented in absolute values. Gray arrows indicate trends; gray belt indicates an interval of rock magnetic perturbations. Gray lines – Mały Giewont section logs; blue lines – Giewont section logs. Dashed red lines indicate levels of possible discontinuities. Abbreviations: U.B.–L.V. – upper Berriasian–lower Valanginian; Val. – Valanginian; WTL Fm. – Wysoka Turnia Limestone Formation; Bor. – Borzai.

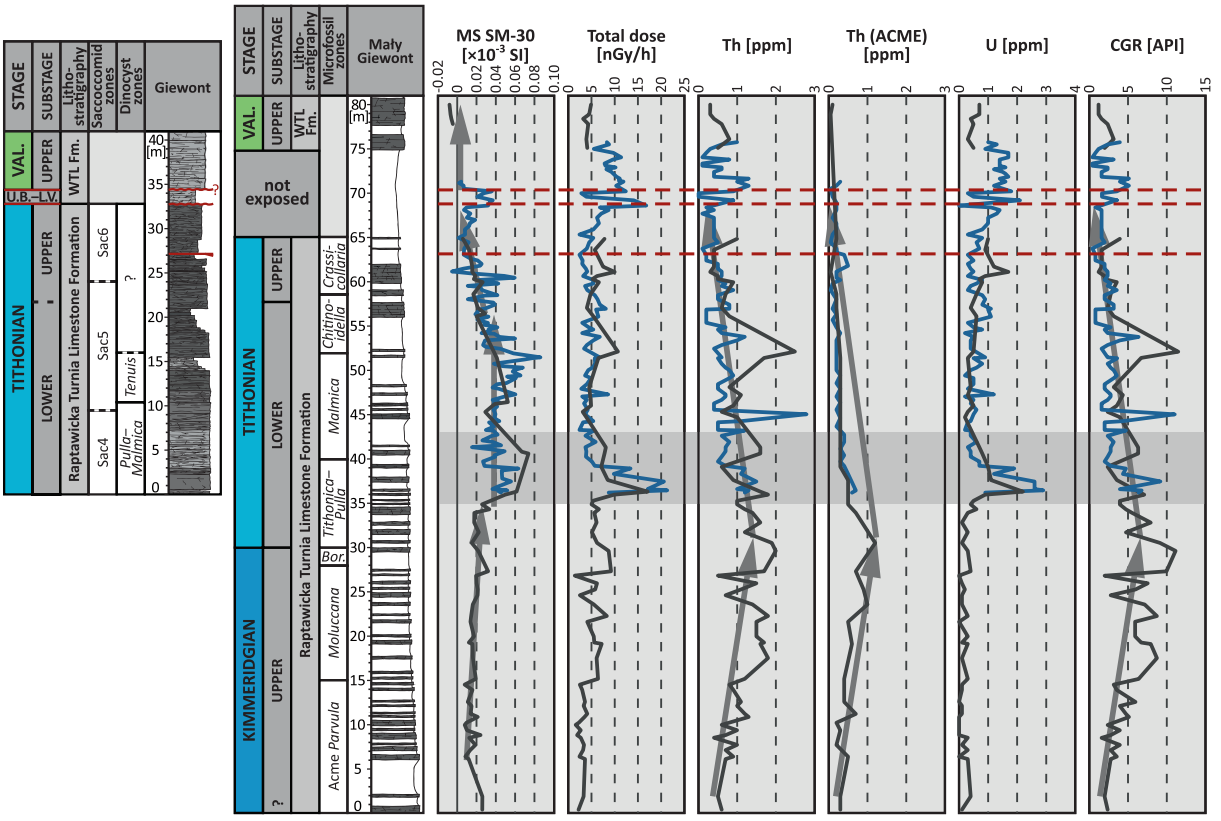

Text-fig. 9. The results of portable MS and gamma-ray spectrometry measurements performed in the upper Kimmeridgian–Valanginian of the Giewont Unit. For comparison laboratory Th concentrations (ACME) are shown. MS, Th and Al trends are indicated by arrows. Explanations and abbreviations as on Text-fig. 8. Note that interval of rock magnetic perturbations (gray belt) correlates with maximum content of U and GRS total dose.

manifest coherent trends through the entire upper Kimmeridgian–Lower Cretaceous. They are characterized by initially slightly increasing and subsequently relatively stable values, with maximum in the *Tithonica–Pulla* Zone of the lower Tithonian. They decrease sharply above, towards the *Malmica* calcareous dinocyst Zone; decreasing, however more gentle trends continue upwards, up to the top of the succession studied.

S-ratio and ARM/IRM$_{1T}$ logs depict relatively high and stable values through the upper Kimmeridgian–lowermost Tithonian (ca. 0.75 and 0.2 respectively; Text-fig. 8). Both ratios depict decreasing trends starting in the *Tithonica–Pulla* calcareous dinocyst Zone, however in case of the S-ratio the drop is only slightly pronounced. Following beds, up to the top of the Tithonian, manifest stable S-ratio (ca. 0.65) and ARM/IRM$_{1T}$ values (ca. 0.1). The topmost beds of the Mały Giewont section show variable and relatively high S-ratio (0.5–0.8) and lowered ARM/IRM$_{1T}$ (ca. 0.025).

Giewont

Rock magnetic logs obtained during investigations of the Giewont sections agree well along with those of the Mały Giewont (Text-fig. 8). The most important differences are that: 1) the lower Tithonian interval of elevated MS is characterized by lower laboratory-measured values than in the Mały Giewont section (compare MS on Text-figs 8 and 9); and 2) the *Tithonica–Pulla* drop in the S-ratio is more distinct in the Giewont section; similarly, the following beds manifest lower values of the ratio (ca. 0.5). Noteworthy, the collected rock magnetic data fully support the microfacies-based correlation of the studied sections (compare Text-fig. 6 and Text-figs 8–9).

In addition, the Giewont section provides a rock magnetic record of the Jurassic/Cretaceous boundary interval, which is not exposed on the slopes of the Mały Giewont. The topmost Tithonian beds manifest continuation of the previous trends, both in the MS, IRM, ARM, S-ratio and ARM/IRM$_{1T}$ logs

(Text-fig. 8). The basal Cretaceous of the Giewont section (G29–G29.4 samples; 32.95–34.20 m) is characterized by slightly elevated MS (Text-figs 8–9) and IRM_{1T}, as well as a significant drop in the S-ratio (Text-fig. 8), which might support the occurrence of the hiatus between samples G28.13 and G29 (as induced from microfacies analysis; MF IV/MF V boundary). Above (samples G30-upwards) a noticeable drop is observed in both MS (Text-figs 8–9) and IRM_{1T}, ARM reaches its lowest values, whilst IRM_{100mT} becomes highly variable (Text-fig. 8). This results in a relatively high but variable S-ratio, as well as decreasing ARM/IRM_{1T}; besides, these perturbations may serve as a support for another hiatus between samples G29.4 and G30 (MF V/MF VI boundary; see the Microfacies chapter above).

Gamma-ray spectrometry and geochemistry of elements

The total dose of the gamma-ray radiation in the Mały Giewont section increases through the upper Kimmeridgian, depicting a significant peak already within the lowermost Tithonian beds (*Tithonica–Pulla* calcareous dinocyst Zone; Text-fig. 9). Above it decreases and remains relatively stable from the *Malmica* calcareous dinocyst Zone up to the top of the studied section. One may notice that in the upper Kimmeridgian–lowermost Tithonian (up to 35 m) the total dose apparently correlates with the CGR ($r_{CGR} = 0.90$), which might indicate that in this interval GRS predominantly reflects the contribution of the detrital fraction. In turn above (35–80 m) the total dose is much more prone to the U content ($r_U = 0.87$ vs. $r_{CGR} = 0.47$), which suggests decreasing lithogenic influx and relative increase of U content.

The GRS measured Th content (Text-fig. 9) increases through the upper Kimmeridgian reaching a broad maximum within the Kimmeridgian/Tithonian boundary interval. Besides one second-order peak, the Tithonian is characterized by the consecutively decreasing contribution of Th. Noteworthy, these observations are coherent with laboratory ICP-MS Th concentrations (Text-fig. 9). The same trend is observed in the CGR curve, which approximates terrigenous input utilizing both Th and K data.

The upper Kimmeridgian is characterized by very low U concentrations (Text-fig. 9). A major peak is observed within the lowermost Tithonian beds; above it decreases, however remaining higher than in the Kimmeridgian. The uranium content increases again within the upper Tithonian and decreases only in the topmost part of the succession studied.

Similarly as in the case of rock magnetic data, GRS logs from the Giewont section correspond well to those of the Mały Giewont (Text-fig. 9); the most prominent is flawless correlation between the lowermost Tithonian total dose and U peaks. This additionally supports the adopted correlation of the studied sections. Furthermore, within the uppermost Tithonian–lowermost Cretaceous beds (G28.3–G47 samples), the total dose of radiation, U and CGR manifest elevated values.

Stable carbon and oxygen isotopes

Stable carbon and oxygen isotope curves from the Mały Giewont section have been already published by Pszczółkowski *et al.* (2016). They correlate well with the more detailed logs from the Giewont section (this study) (Text-fig. 10); single outstanding negative peaks are thought to result from diagenetic overprint.

The upper Kimmeridgian is characterized by relatively high (ca. 2.5‰ VPDB) and stable $\delta^{13}C$ values (Text-fig. 10). Near the Kimmerdigian/Tithonian boundary $\delta^{13}C$ decreases by approximately 0.5–0.6‰ and remains at ca. 1.8–1.9‰ VPDB through the entire lower–upper Tithonian. No clear trend is observed within the MF V lithoclastic packstone interval (samples G29–G29.4). Although four samples depict values similar to those of the upper Tithonian beds, sample G29.4 manifests a significantly lighter carbon isotope signature (0.99‰ VPDB). From above the sample G30, $\delta^{13}C$ manifests an increasing trend, reaching values as high as 2.45‰ in sample G48; similarly, the topmost part of the Mały Giewont section is also characterized by elevated $\delta^{13}C$ (2.35‰ in sample MG120).

The stable oxygen isotopes curve (Text-fig. 10) increases from ca. -4‰ VPDB at the base of the Mały Giewont section to ca. -2.5‰ VPDB within the upper Kimmeridgian *Moluccana* calcareous dinocyst Zone. From below the Kimmeridgian/Tithonian boundary upwards a generally decreasing $\delta^{18}O$ trend is observed, reaching ca. -4‰ VPDB in the topmost Tithonian beds. Nevertheless, local fluctuations and minima are observed within the *Tithonica–Pulla*, *Malmica* and *Crassicollaria* zones, reaching as low as -5‰ VPDB. Values near -4‰ VPDB characterize also the basal Cretaceous beds, however a significant drop (to ca. -6‰ VPDB) is observed above, between samples G29.4 and G30. This phenomenon is thought to evidence the discordant character of the boundary between the MF V (lithoclastic packstone) and MF VI (encrinites). The following beds (MF VI) account for an increasing trend, up to ca. -5‰ VPDB.

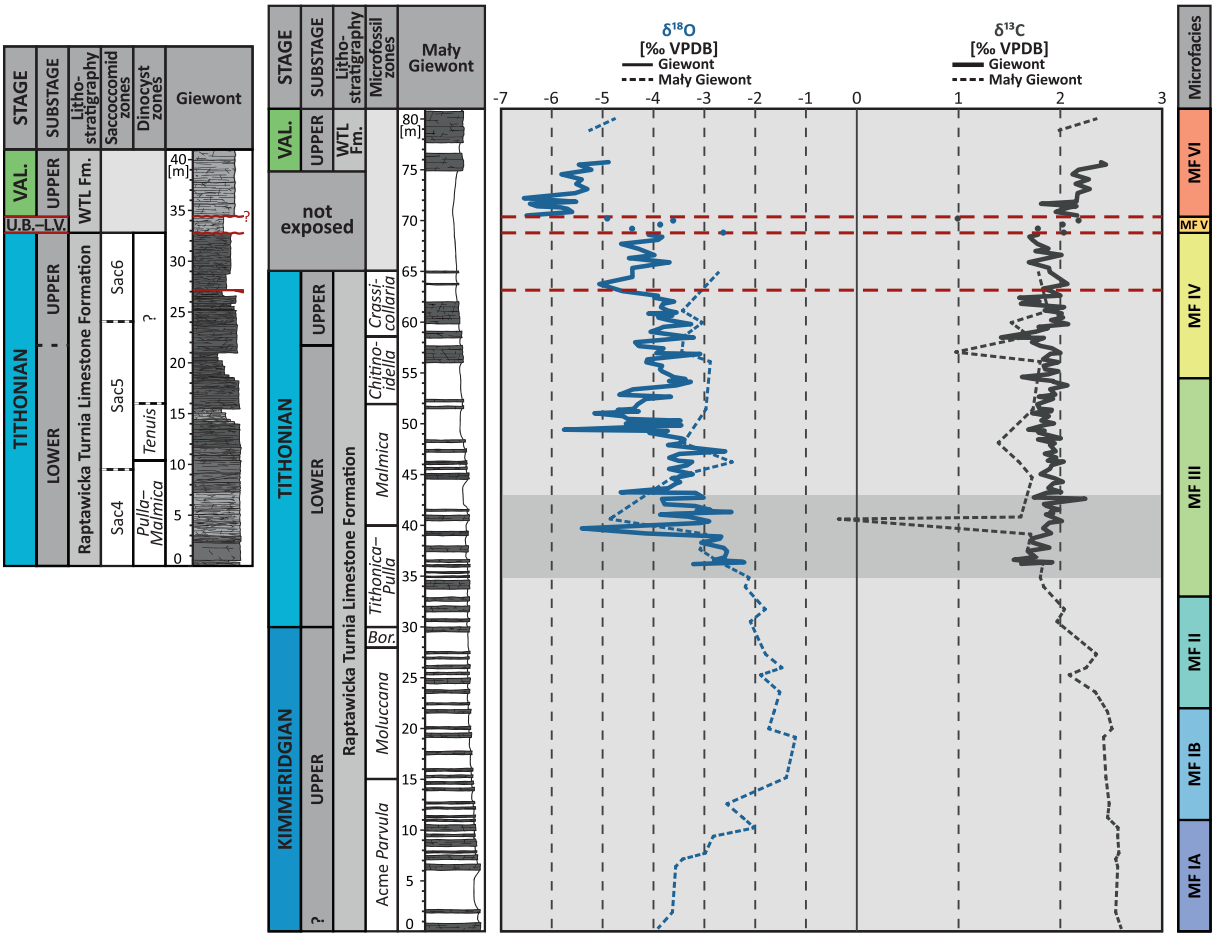

Text-fig. 10. Stable oxygen and carbon isotopes in the Upper Jurassic–lowermost Cretaceous of the Giewont Unit. Note different scales for $\delta^{18}O$ and $\delta^{13}C$ curves. Microfacies types log (composite) is put for context. Abbreviations as on Text-fig. 8. Note that interval of rock magnetic perturbations (gray belt) correlates with change in trends of both isotopic curves.

Pszczółkowski *et al.* (2016) considered the possibility of a diagenetic alteration of the isotope record (e.g. Colombie *et al.* 2011), relying on an apparently positive correlation between carbon and oxygen isotopes within the upper Kimmeridgian–Tithonian of the Mały Giewont section. However, when both the Mały Giewont and Giewont section isotope data are plotted, it appears that the $\delta^{13}C$ and $\delta^{18}O$ signatures do not correlate (Text-fig. 11), which is confirmed by the Pearson correlation coefficient (r = 0.17; for Giewont section alone r = -0.1). Therefore, we can safely assume that at least primary $\delta^{13}C$ trends are preserved. The burial diagenesis (e.g. Moore 2001) most likely affected oxygen isotopic ratios, as they manifest significantly lower values than other Western Tethyan successions (either bulk or belemnite; e.g. compare Text-fig. 10 with fig. 26.1 in Hesselbo *et al.* 2020). Although the paleoenvironmental significance of stable carbon and oxygen isotopes is not yet clear and is not discussed in this paper, it is worth noting an apparent correlation between the uppermost Kimmeridgian–lowermost Tithonian change in their trends and an interval of rock magnetic perturbations, elevated GRS parameters and U peak (compare Text-figs 8–10).

INTERPRETATION

Correlation between the Giewont and Mały Giewont sections

Based on microfacies observations, the base of the Giewont section was initially correlated with meter 36 of the Mały Giewont section (Text-fig. 6). Here we summarize rock magnetic and GRS observations

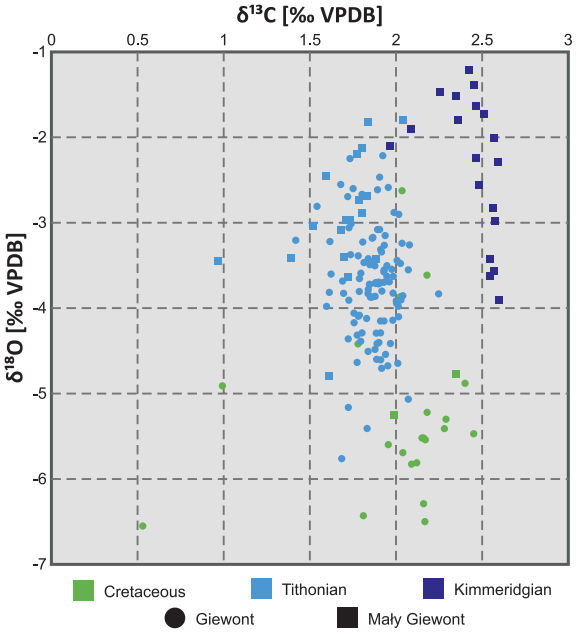

Text-fig. 11. Cross-plot of stable carbon and oxygen isotopes values in the Giewont (this study) and Mały Giewont (Pszczółkowski *et al.* 2016) sections.

(Text-figs 8–9), which provide evidence for the correctness of this interpretation.

The basal part of the Giewont section is characterized by elevated MS (Text-figs 8–9) as well as decreasing trends in IRM (both 1 T and 100 mT), ARM, S-ratio and ARM/IRM_{1T} logs (Text-fig. 8). Corresponding characteristics of these rock magnetic proxies are found near meter 36 of the Mały Giewont section. Similarly, near-zero MS and very low IRM and ARM values are observed in the topmost intervals of both sections.

Besides rock magnetic perturbations, the basal part of the Giewont section depicts significant peaks in GRS total dose and U concentration; a similar phenomenon is observed at 36–37 m (*Tithonica–Pulla* calcareous dinocyst Zone) of the Mały Giewont section (Text-fig. 9). Noteworthy, also Th (both GRS and ICP-MS) and CGR reach their highest values within the *Tithonica–Pulla* Zone, which is coherent with observations from the Giewont section (Text-fig. 9).

Biostratigraphy of the Giewont section

The biostratigraphic data collected during this study allows for only a rough dating of the Giewont section. Therefore, the stratigraphic scheme of the Giewont succession presented in this paper was developed based on an integrated stratigraphy approach, including biostratigraphy, chemostratigraphy and MS stratigraphy, as well as detailed correlation with the Mały Giewont section (Pszczółkowski *et al.* 2016).

The calcareous dinoflagellates assemblage of the Giewont section allowed for determination of only two biozones, namely the lower Tithonian *Pulla–Malmica* Zone and the lower–lower upper Tithonian *Tenuis* Zone. These ages are supported by the correlation with the Sac4–Sac6 Saccocomidae zones of Benzaggagh *et al.* (2015a, b) (Text-fig. 3).

Stratigraphically significant data for the upper part of the Giewont section (G29–G49 samples interval) is provided by foraminiferal assemblages (Text-fig. 3). *Conoglobigerina* cf. *gulekhensis* from sample G29.2 indicates its late Berriasian–early Valanginian age (cf. Omaña *et al.* 2017; Gradstein *et al.* 2020). In turn, a specimen of the early Valanginian–Aptian (Coccioni *et al.* 2007; Barchetta 2015) *Praehedbergella* cf. *sigali* was observed in sample G29.4. Noteworthy, both taxa come from the matrix of lithoclastic packstone (MF V; Pl. 2), hence were most probably not redeposited.

The most common species within G30–G49 samples are *Praedorothia praehauteriviana* and *Protomarssonella kummi*, indicating the Valanginian–early Hauterivian (Desai and Banner 1987; Kaminski *et al.* 1992; Olszewska *et al.* 2012) and the Berriasian–Hauterivian (?Barremian) (Gradstein *et al.* 1999; Olszewska *et al.* 2008; Borowska 2015) age of the interval, respectively. Finally, *Uvigerinammina* cf. *uvigeriniformis* recognized in sample G45 was reported to have become extinct during the Valanginian (Krajewski and Olszewska 2007; Olszewska *et al.* 2008; Borowska 2015). Also, the occurrence of the small gastropod *Pseudonerinea* cf. *vaceki* (sample G48), according to Kollmann (2002), suggests the late Valanginian–early Hauterivian age of the sample. The approximated stratigraphic position of selected (= biostratigraphically significant) samples are visualized in Text-fig. 12.

$\delta^{13}C$ stratigraphy

A decreasing upper Kimmeridgian–Tithonian carbonate carbon isotopes trend has been already correlated with Hlboča (Malé Karpaty; Grabowski *et al.* 2010), Brodno (Pieniny Klippen Belt; Michalík *et al.* 2009) and Długa Valley (Fatric succession of the Western Tatra Mts, Jach *et al.* 2014a) sections by Pszczółkowski *et al.* (2016). Here we provide additional correlations with the Hárskút (Transdanubian Range; Főzy *et al.* 2010; Lodowski *et al.* 2021) and Velykyi Kamianets (Pieniny Klippen Belt; Gra-

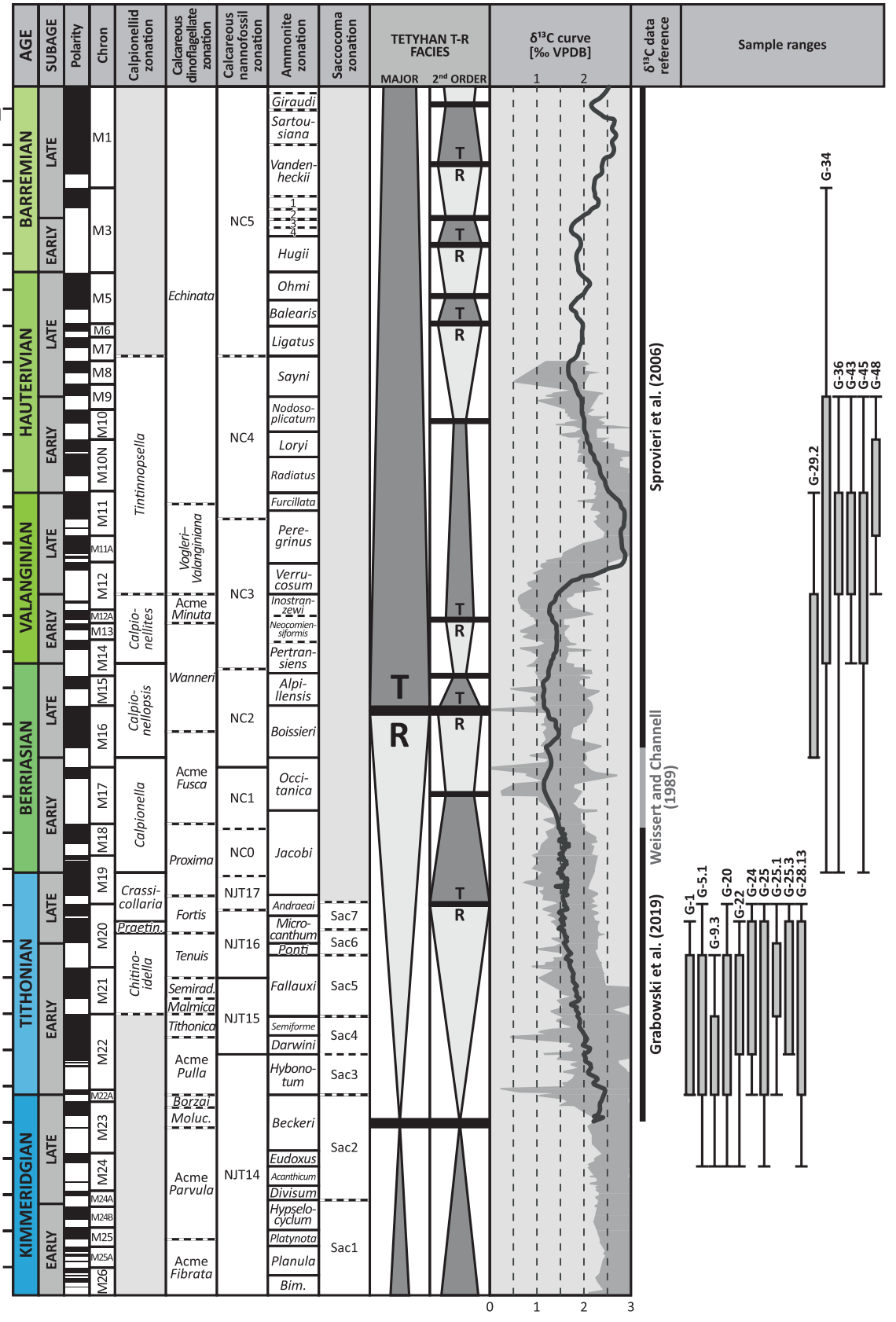
AGE
SUBAGE
Polarity
Chron
Calpionellid zonation
Calcareous dinoflagellate zonation
Calcareous nannofossil zonation
Ammonite zonation
Saccocoma zonation
TETYHAN T-R FACIES
MAJOR
2nd ORDER
δ13C curve [‰ VPDB]
δ13C data reference
Sample ranges
122 [Ma]
KIMMERIDGIAN
TITHONIAN
BERRIASIAN
VALANGINIAN
HAUTERIVIAN
BARREMIAN
EARLY
LATE
M1
M3
M5
M6
M7
M8
M9
M10
M10N
M11
M11A
M12
M12A
M13
M14
M15
M16
M17
M18
M19
M20
M21
M22
M22A
M23
M24
M24A
M24B
M25
M25A
M26
Tintinnopsella
Calpio-nellites
Calpio-nellopsis
Calpionella
Crassi-collaria
Praetin.
Chitino-idella
Echinata
Vogleri–Valanginiana
Acme Minuta
Wanneri
Acme Fusca
Proxima
Fortis
Tenuis
Semirad.
Malmica
Tithonica
Acme Pulla
Borzai
Moluc.
Acme Parvula
Acme Fibrata
NC5
NC4
NC3
NC2
NC1
NC0
NJT17
NJT16
NJT15
NJT14
Giraudi
Sartou-siana
Vanden-heckii
Pseudo-thurmannia
Hugii
Ohmi
Balearis
Ligatus
Sayni
Nodoso-plicatum
Loryi
Radiatus
Furcillata
Pere-grinus
Verru-cosum
Inostran-zewi
Neocomien-siformis
Pertran-siens
Alpi-llensis
Boissieri
Occi-tanica
Jacobi
Andraeai
Micro-canthum
Ponti
Fallauxi
Semiforme
Darwini
Hybono-tum
Beckeri
Eudoxus
Acanthicum
Divisum
Hypselo-cyclum
Platynota
Planula
Bim.
Sac7
Sac6
Sac5
Sac4
Sac3
Sac2
Sac1
T
R
0
1
2
3
Sprovieri et al. (2006)
Weissert and Channell (1989)
Grabowski et al. (2019)
G-1
G-5.1
G-9.3
G-20
G-22
G-24
G-25
G-25.1
G-25.3
G-28.13
G-29.2
G-34
G-36
G-43
G-45
G-48

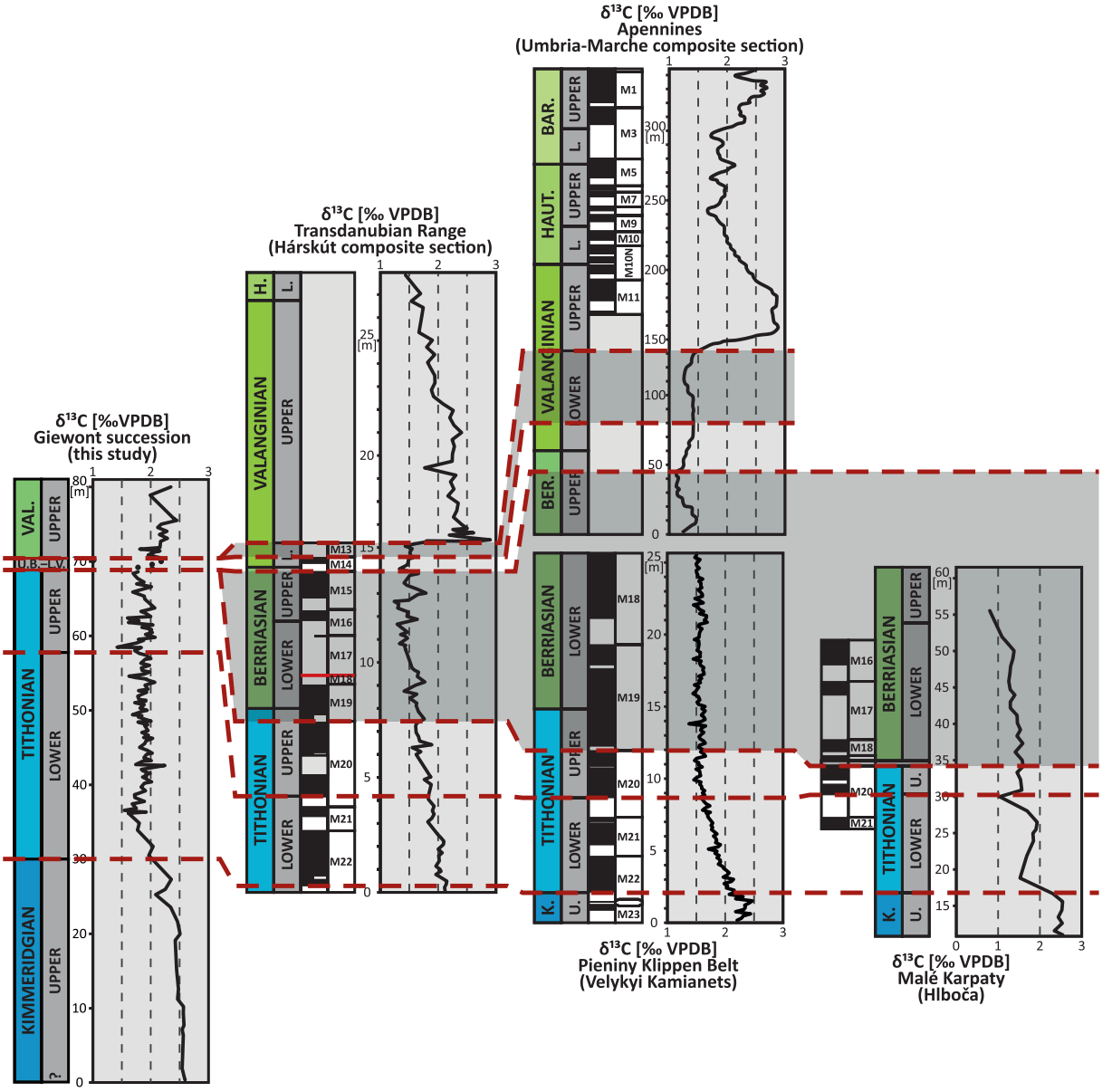

Text-fig. 13. Correlation of the stable carbon isotope curves between the Giewont Unit and selected western Tethyan successions: Transdanubian Range (Főzy *et al.* 2010 and Lodowski et al. 2021), Pieniny Klippen Belt (Grabowski *et al.* 2019), Apennines (Sprovieri *et al.* 2006) and Malé Karpaty (Grabowski *et al.* 2010). Gray areas represent stratigraphic ranges of hiatuses within the Giewont succession, as interpreted in this study. Abbreviations: BAR. – Barremian; BER. – Berriasian; H., HAUT. – Hauterivian; K. – Kimmeridgian; Val. – Valanginian; U.B–L.V. – upper Berriasian–lower Valanginian; L. – Lower; U. – Upper.

← Text-fig. 12. Stratigraphic framework of selected stratigraphically important Giewont section samples. Magnetostratigraphy and timescale after Ogg (2020). Calpionellid zonation as presented in Lodowski *et al.* (2021), supplemented by the data from Reháková and Michalík (1997) for the upper Valanginian–Barremian. Calcareous dinoflagellate zonation after Reháková (2000) supplemented by Jach *et al.* (2014a) and Grabowski et al. (2019). Tethyan calcareous nannofossil zonation combined after Erba and Tremolada (2004); Channell *et al.* (2010); Casellato and Erba (2021). Tethyan ammonite zones combined after Zeiss (2003), Reboulet *et al.* (2018) and Hesselbo *et al.* (2020). Saccocomid zonation after Benzaggagh *et al.* (2015a). Major and 2nd order eustatic cycles with respect to Hardenbol *et al.* (1998) and Haq (2014, 2018). Stable carbon isotopes (bulk) combined of Weissert and Channell (1989), Sprovieri *et al.* (2006) and Grabowski *et al.* (2019); gray field represents global $\delta 1^3C$ stack as presented in Price *et al.* (2016). An offset of -0.5‰ has been applied to the oxygen curve of Grabowski *et al.* (2019). Abbreviations: Praetin. – Praetintinnopsella; Bim. – Bimammatum; Moluc. – Moluccana. Explanations: 1 – Moutonianum; 2 – Compressissima; 3 – Pulchella, 4 – Nicklesi.

bowski *et al.* 2019) sections, which agree well with the Pszczółkowski *et al.* (op cit.) interpretation (Text-fig. 13).

Characteristic for the $\delta^{13}C$ curve of the Giewont succession is an increasing trend observed in its uppermost part (for ca. 0.7‰ magnitude, from 1.78‰ VPDB in the uppermost Tithonian sample G28.13 to 2.45‰ VPDB in sample G48; Text-fig. 10). Such heavy carbon isotope signatures are not observed in the Berriasian–lower Valanginian of the Western Tethys (Text-fig. 12). When compared either to the reference Tithonian–Barremian log of Föllmi (2012; combined from Weissert and Channell 1989 and Sprovieri *et al.* 2006), or the stack curve of Price *et al.* (2016), such an increase can be related only to: 1) the upper Valanginian Weissert event; or 2) the Barremian increasing $\delta^{13}C$ signature (see Text-fig. 12). Discovery of hiatuses in sample G29 and between samples G29.4 and G30 (Text-fig. 7) could support either interpretation; nonetheless, due to the fact that: 1) the approximated stratigraphic position of samples G29–G49 cluster within Valanginian–early Hauterivian ages (see Text-fig. 12); and 2) the rocks overlying the hardground do not meet the characteristics of the High-Tatric Urgonian (Barremian–Aptian; see the Discussion chapter), herein the former solution is adopted.

In principle, the Weissert event is characterized by a ca. 1.5‰ increase of $\delta^{13}C$, to values close to 3‰ VPDB (Text-figs 12–13). Consequently, the topmost interval of the Giewont succession (encrinites of MF VI; samples G30-upwards) might be correlated with an onset of the positive carbon isotope excursion, that is the beginning of significantly increasing $\delta^{13}C$ trend near the lower/upper Valanginian boundary, as observed in the Transdanubian Range (Főzy *et al.* 2010; Lodowski *et al.* 2021) and Apennines (Sprovieri *et al.* 2006) (Text-fig. 13). To state unequivocally whether the Giewont section records the Weissert carbon isotope event a high-resolution sampling of the interval following the top of the section studied is required.

A separate issue is the unclear age of the MF V lithoclastic packstone (G29–G29.4 samples). As evidenced by the microfacies succession (MF IV/MF V and MF V/MF VI boundaries; Text-figs 5–7), rock magnetic (Text-fig. 8), GRS (Text-fig. 9) and $\delta^{18}O$ logs (Text-fig. 10) from the top and the bottom it is bounded by disconformities. In addition, the foraminiferal assemblage of the interval suggests its late Berriasian–early Valanginian age or not much later (see chapter above and Text-figs 3 and 12). However, most of datapoints manifest $\delta^{13}C$ values of ca. 2‰ VPDB, hence much heavier than the signatures expected for the upper Berriasian–lower Valanginian (ca. 1‰ VPDB; compare Text-fig. 10 with Text-figs 12–13); only in sample G29.4 $\delta^{13}C$ falls to 0.99‰ VPDB. Nonetheless, taking into account the lithologic appearance of the interval (lithoclastic packstone) we can't exclude that the isotopic composition of the sampled material is (at least partly) affected by older lithoclasts (upper Tithonian–?lower Berriasian); as may be seen on Text-fig. 5 their size and distribution likely prevented successful sampling of matrix material alone. In conclusion, an exact age of the G29–G30 interval must be regarded as an approximation.

DISCUSSION

Remarks on the stratigraphy of the Mały Giewont section

Although a detailed biostratigraphic study of the Mały Giewont section was presented by Pszczółkowski *et al.* (2016) some corrections to their interpretation have to be applied. In their paper they assumed that the Acme *Parvula* dinoflagellate Zone was early Kimmeridgian in age. Nonetheless, more up-to-date research from Velykyi Kamianets (Grabowski *et al.* 2019) has proved the upper Kimmeridgian occurrence of this biozone (?its upper part), as high as within the M23r magnetozone. However, the top of the Acme *Parvula* Zone was earlier correlated with the upper boundary of the early Kimmeridgian *Divisum* ammonite Zone (Fig. 5 in Reháková *et al.* 2011; compare with Hesselbo *et al.* 2020). These (somewhat ambiguous) data from the Velykyi Kamianets section may indicate that in the Mały Giewont section (Pszczółkowski *et al.* 2016) the ammonites studied by Passendorfer (1928; cf. *Divisum* and/or *Acanthicum* ammonite zones, see Pszczółkowski *et al.* 2016) represent the lower/upper Kimmeridgian boundary interval, or even are of the earliest late Kimmeridgian age (M24A–M24 according Hesselbo *et al.* 2020), as adopted in this study.

Also the age of the topmost part of the Mały Giewont section (encrinites of MG117–MG120 samples) has to be revised. Based on its stratigraphic position and the lithostratigraphic scheme of Lefeld *et al.* (1985) Pszczółkowski *et al.* (2016) considered it to be Urgonian (Barremian–Aptian). However, according Lefeld *et al.* (op cit.) and Masse and Uchman (1997) the High-Tatric Urgonian is characterized by an abundance of fossils, including reef corals, orbitolinids, brachiopods and bivalves, which essentially occur neither within the lowermost Cretaceous beds of the Mały Giewont nor the Giewont section. Consequently, as the topmost interval of the Giewont

section is interpreted here as the upper Valanginian, this age is also assigned to the top of the Mały Giewont section (e.g. Text-fig. 6).

Stratigraphy of the Giewont Unit

Lefeld *et al.* (1985) included the Berriasian and Valanginian into the Raptawicka Turnia Limestone Fm. The presence of the Berriasian was established based on the occurrence of *Crassicollaria intermedia*, *Calpionellites darderi* and *Calpionella* sp., whilst the Valanginian was documented by *Tintinnopsella* (*Remaniella*) cf. *cadischiana* and *T. carpathica* (Lefeld 1968). Noteworthy, these forms were reported from within the pseudo-oolite limestones of the Mały Giewont, which is contrary to the results of this and Pszczółkowski *et al.* (2016) studies. Moreover, *Cr. intermedia* and *C. darderi* are not known to co-occur (compare e.g. Grabowski *et al.* 2016 with Grabowski *et al.* 2019 and Lodowski *et al.* 2021), what implies either the wrong taxonomic designation of either of the species or redeposition.

Besides, within the Giewont succession *Saccocoma* skeletal elements are observed through the entire upper Kimmeridgian–upper Tithonian, yet become less frequent already in the upper Tithonian microfacies MF IV and do not occur within the upper Berriasian–lower Valanginian lithoclastic packstone (MF V). This is against the statement of Lefeld and Radwański (1960) who reported *Saccocoma* skeletal elements from as high as the Berriasian–Valanginian (?Hauterivian) limestones. This discrepancy is thought to result from the erroneous stratigraphic calibration adopted by the authors (following Lefeld 1959), namely assigning the gray pseudo-oolitic limestones to the Berriasian (here the upper Tithonian). Moreover, Lefeld and Radwański (op. cit) reported saccocomids from within biodetrital limestones (= encrinites) of the Hauterivian (upper Valanginian herein), what is not confirmed by our observations.

In view of the above considerations we have to assume that some of the taxonomic designations adopted by Lefeld (1968) and Lefeld *et al.* (1985; see also Kotański 1959 and Kotański and Radwański 1960) require revision. In the light of the data presented herein there is no evidence for stratigraphic continuity at the contact of the upper Jurassic and the lower Cretaceous deposits of the Giewont Unit.

Lithostratigraphy of the High-Tatric succession

Based on the data collected during this study the top of the middle member of the RTL Fm. (= gray micrites and the following interval of pseudonodular limestone; MF I and MF II) falls in the lowermost Tithonian *Tithonica–Pulla* dinoflagellate Zone, whilst the upper member (near black cyanoid limestones) is cut by the upper Tithonian–Berriasian disconformity (MF IV/MF V boundary). Interestingly, the basal Cretaceous beds of the Giewont section (upper Berriasian–upper Valanginian) do not resemble either the middle or the upper members of the RTL Fm. nor the Urgonian-type WTL Fm. *sensu* Lefeld *et al.* (1985), yet they meet the definition of the Hauterivian *sensu* Lefeld (1968). This also applies to the topmost interval of the Mały Giewont section.

Consequently, we propose following modifications to the lithostratigraphic scheme of Lefeld *et al.* (1985; Text-fig. 14), to be applied at least to the Giewont Unit and Osobita Massif areas: 1) the top of the middle member of the RTL Fm. falls in the lowermost Tithonian and may be defined as the boundary between the pseudonodular limestone (MF II) and heterogenous limestones with cyanoids and peloids (MF III); 2) the upper boundary of the RTL Fm. (thus the top of the upper member) falls in the upper Tithonian and is cut by the disconformity; 3) in the Osobita massif the RTL Fm. continues as the upper Tithonian–lower Berriasian Sobótka Member (Madzin *et al.* 2014); 4) a new Giewont Member shall be defined and included into the WTL Fm., in concordance with the following definition:

Giewont Member (new member)

Name: After the type section, located in the northern wall of the Mt. Giewont (Western Tatra Mts).

History: The rocks distinguished here as the Giewont Member were assigned by Kotański (1959) to the Urgonian (Barremian–Aptian) and so they were mapped in subsequent cartographic studies. Lefeld (1968) established their age as the Hauterivian, however they were not discussed in the lithostratigraphic scheme of Lefeld (1985); more recently they were assigned to the Barremian–Aptian of the Wysoka Turnia Limestone Fm. (e.g. Pszczółkowski *et al.* 2016).

Type section: Lowermost part of the Kirkor's Gully.

Thickness: At least 17 m at the type locality.

Dominant lithology: Light gray encrinites with peloids. Basal beds comprise a lithoclastic packstone (ca. 1.5 m in thickness).

Boundaries: Lower – sharp, at the hardground on top of the Raptawicka Turnia Limestone Fm; a stratigraphically continuous passage from the Sobótka Member encrinites to the lower beds of the Giewont Member may occur in the Osobita Massif, yet this

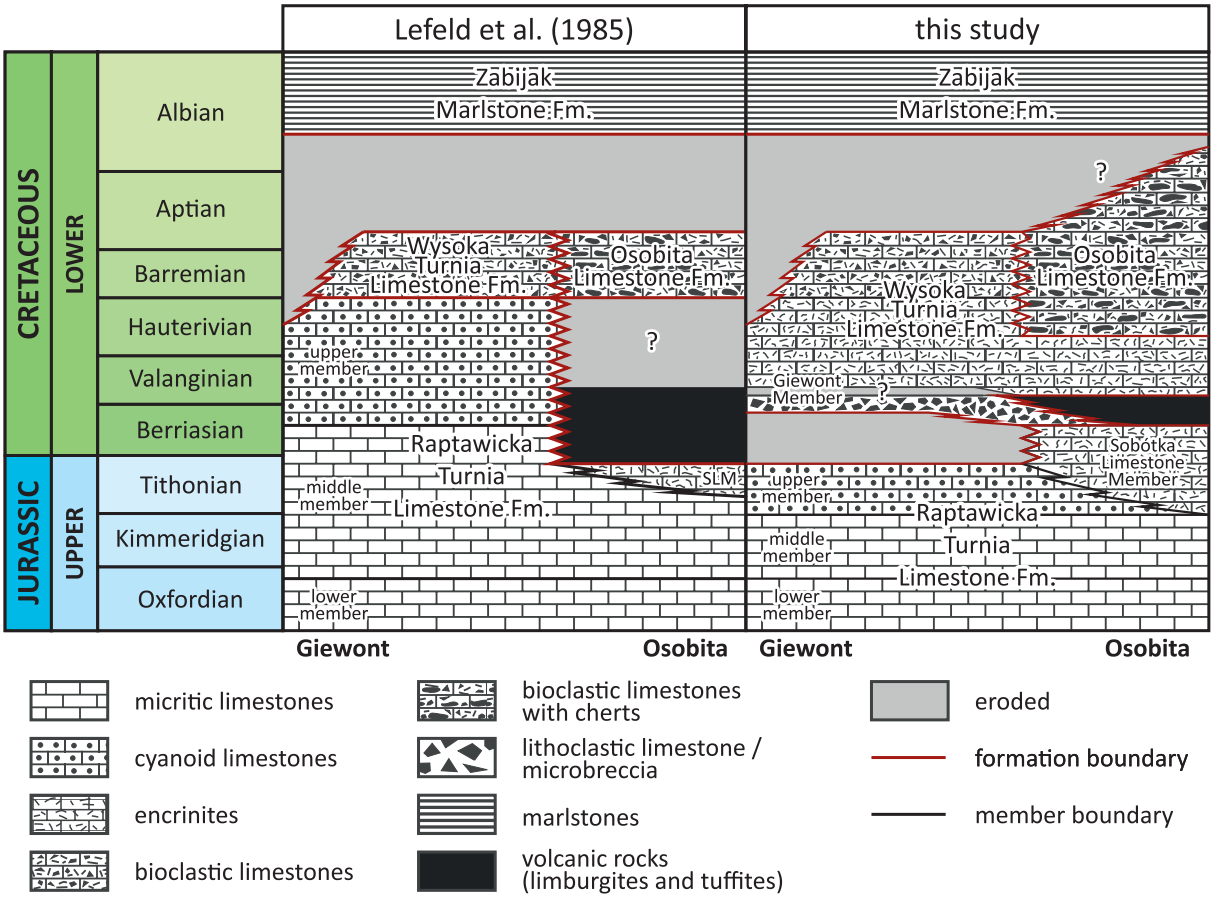

Text-fig. 14. Generalized Upper Jurassic–Lower Cretaceous lithostratigraphic scheme of the High-Tatric series in the para-autochthonous Giewont Unit and the Osobita Massif. Revised scheme (right) is composed of this study and Madzin *et al.* (2014) data. Abbreviations: SLM – Sobótka Limestone Member. Uncertain stratigraphic range of the hiatus between the lower and upper beds of the Giewont Member is marked by a question mark.

is not entirely clear here (see Fig. 3 in Madzin *et al.* 2014). Upper – not defined; according Lefeld (1968) (?)Hauterivian encrinites gradually pass into the Urgonian facies.

Geological age: Late Berriasian–Hauterivian.

Distribution: Lower parts of the Kirkor's Gully, northern slopes of the Mały Giewont Mt., Osobita Massif area; also Kościeliska and Spis-Michałowa valleys according to Lefeld (1968).

Subdivision: Basal beds (upper Berriasian–lower Valanginian) – gray to light gray lithoclastic packstone with cortoids, peloids and burrows. Upper beds (upper Valanginian–Hauterivian) – light gray encrinites with peloids. In the Giewont section a disconformity was documented between the basal and the upper beds (Text-fig. 7).

Equivalents: Basal beds: upper Berriasian microbreccia of the Osobita Massif (Madzin *et al.* 2014; assigned there to the RTL Fm.); ?Berriasian–lower Valanginian of the Niedźwiedź crag (Borowska 2015). The stratigraphic position of the basal beds roughly corresponds to the volcanic rocks (limburgites) of the Osobita Massif.

Upper beds: light gray Urgonian limestones of the Kirkor's Gully section of Kotański (1959), probably their lower part; Hauterivian of the Raptawicka Turnia Limestone Fm. of Lefeld (1985); encrinites of the lowermost part of the Osobita Limestone Fm. (Staniszewska and Ciborowski 2000; Madzin *et al.* 2014); ?Valanginian of the Niedźwiedź crag (Borowska 2015).

Although Madzin *et al.* (2014) included the upper Berriasian microbreccia of the Osobita Massif (see also Staniszewska and Ciborowski 2000) into the RTL Fm., here we suggest its assignation to the basal beds of the Giewont Member (WTL Fm.; Text-

fig. 14). This is because cyanoid limestones of the upper member of the RTL Fm. are not known from the Osobita Massif, where encrinites of the Sobótka Limestone Member (RTL Fm.) overlie directly the Kimmeridgian micrites (Kotański and Radwański 1959; Lefeld *et al.* 1985). Besides, based on lithologic resemblance (compare Text-fig. 5H with fig. 9 in Madzin *et al.* 2014) we suggest the inclusion of the upper Valanginian–lower Hauterivian encrinites of the Osobita Massif into the upper beds of the Giewont Member. These proposed modifications (Text-fig. 14) provide a more consistent definition of the boundary between the RTL Fm. and the WTL Fm., utilizing the discovery of an important hiatus within the Giewont Unit as well as adopting microbreccia and lithoclastic packstone as local stratigraphic markers. Noteworthy, the Upper Jurassic–Lower Cretaceous lithostratigraphic scheme of Lefeld *et al.* (1985) has been adopted by numerous authors (e.g. Pszczółkowski 2003; Jach *et al.* 2014b; Madzin *et al.* 2014; Borowska 2015; Pszczółkowski *et al.* 2016; Łuczyński 2021), therefore the proposed modification is of big importance for local geology. Nevertheless, further studies performed in other High-Tatric autochthonous and para-autochthonous units are required in order to propose a major revision of the Lefeld *et al.* (op. cit.) scheme.

Sedimentary trends and events

Disappearance of Saccocoma skeletal elements

According to Grabowski *et al.* (2019) and Lodowski *et al.* (2021), in the Western Tethyan successions *Saccocoma* MF disappear near the M20n/M19r magnetozones boundary (mid upper Tithonian; see also Benzaggagh et al. 2015b). In the Lower Sub-Tatric succession this phenomenon is observed within the *Praetintinnopsella* Zone and the lower part of the *Crassicollaria* calpionellid Zone, where transitional MF (= decreasing contribution of *Saccocoma* skel-

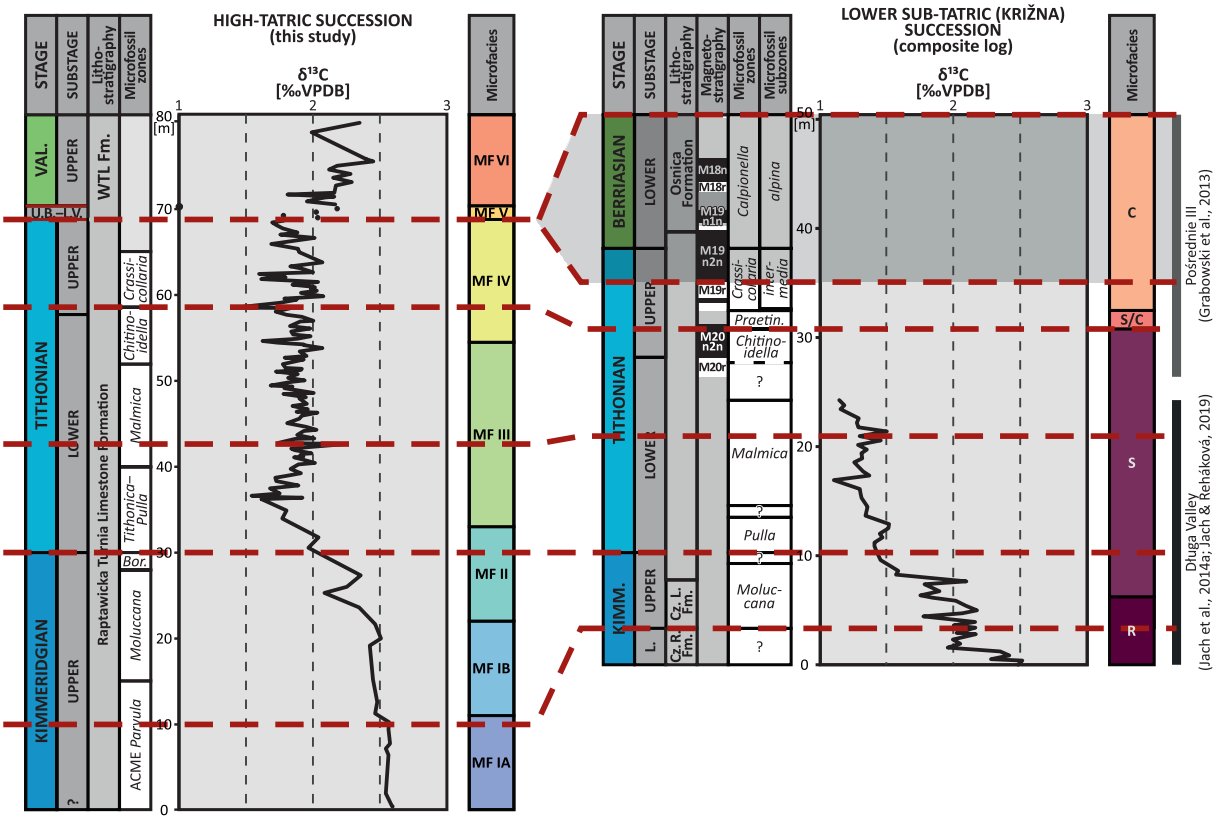

Text-fig. 15. Correlation between the $\delta^{13}C$ and microfacies of the High-Tatric (this study) and Lower Sub-Tatric (Križna) successions (synthetic log composed of the data from Grabowski *et al.* 2013, Jach *et al.* 2014a and Jach and Reháková 2019). Approximated range of the uppermost Tithonian–lower Berriasian erosional gap in the High-Tatric succession (grayed out on the Lower Sub-Tatric logs) is indicated. Microfacies of the lower Sub-Tatric indicate the most common component: R – radiolarian; S – *Saccocoma*; S/C – transition interval between the *Saccocoma*- and calpionellid-dominated microfacies; C – calpionellid. Abbreviations: KIMM. – Kimmeridgian; VAL. – Valanginian; U.B–L.V. – upper Berriasian–lower Valanginian; L. – lower; Cz. L. Fm. – Czorsztyn Limestone Formation; Cz. R. Fm. – Czajakowa Radiolarite Formation; WTL Fm. – Wysoka Turnia Limestone Fm.; Bor. – Borzai; Praetin. – Praetintinnopsella.

etal elements) was documented (Grabowski and Pszczółkowski 2006 and unpublished data; Text-fig. 15). This most likely corresponds to the cyanoid packstones of the Giewont succession (MF IV), characterized by less common saccocomids (in relation to underlying beds, especially the MF III interval). Consequently, the topmost Tithonian beds of the Giewont section are thought to record an interval of *Saccocoma* vanishing or slightly below, and thus they might be roughly correlated with magnetozones M20n and/or M19r. This assumption is in concordance with biostratigraphic data, namely the topmost Tithonian beds of the Mały Giewont section falling in the *Crassicollaria* calpionellid Zone (Text-fig. 6).

Origins of the upper Tithonian–(?)upper Berriasian disconformity

Stratigraphic gaps discovered within the upper part of the Giewont section are thought to result from the combination of eustasy and tectonic uplift. These eventually led to erosion, caused by long-term wave processes in a shallow paleobathymetric setting, however also (?periodic) emersion during the Berriasian cannot be excluded. The trend of decreasing depths of deposition is supported by the microfacies succession, as well as via correlation with neighboring successions.

Cyanobacteria are known to obtain energy from photosynthesis, thus also the most of cyanoids should be restricted to the photic zone, whose base is customarily approximated to ca. 200 m below the sea surface (e.g. Sutton 2013; see also Jenkyns 1972). Noteworthy, allochthonous origins of the High-Tatric cyanoids was already rejected by Pszczółkowski *et al.* (2016) and Pszczółkowski (2018; compare with Lefeld and Radwański 1960), therefore they can be reliably used for paleobathymetric considerations. Consequently, the vanishing of cyanoids during the late Kimmeridgian (MF IA–IB on Text-fig. 6) and the gradual passage from the latest Kimmeridgian–earliest(?) Tithonian pseudonodular limestone (MF II) towards the late Tithonian cyanoid limestones (MF III–IV) is thought to document the latest Kimmeridgian paleoenvironmental perturbations and the Tithonian trend of decreasing depths of deposition, respectively.

Although intensified lithogenic influx (= less clear water column) during the latest Kimmeridgian–earliest Tithonian (increasing Th content on Text-fig. 9) might have efficiently reduced the depth of the photic zone (hence the paleobathymetric range of cyanoids), relative deepening is also thought to be important for vanishing of cyanoids within the MF II. Accordingly, it is suggested that during the late Kimmeridgian the High-Tatric area was subjected to vertical tectonic movements, likely connected with the pull-apart tectonics within the Zliechov Basin (see Jach and Reháková 2019), however the impact of rising sea-level during the transgressive cycle (Text-fig. 12) also cannot be excluded. These are in turn thought to result in the late Kimmeridgian trend of increasing depths of deposition, temporal disappearance of cyanoids (MF IA–IB on Text-fig. 6) and the formation of the pseudonodular limestone (MF II).

Irrespective of the processes controlling the presence of cyanoids, the key to understanding the mechanisms responsible for the late Tithonian–Berriasian discordance is to estimate the paleobathymetry during the formation of the pseudonodular limestone. Since MF II lacks cyanoids and is rich in dissolution seams and stylolites (Text-fig. 5), the nodular structure is interpreted here as resulting from early-diagenetic (partial) dissolution (see Jenkyns 1974), possibly in depths of ?several hundred meters, fairly below the base of the photic zone (Text-fig. 6). Besides, sedimentation of the Kimmeridgian–Tithonian nodular limestones of the Manín Unit (transitional zone between the South Tatric Ridge and the Zliechov Basin, e.g. Plašienka 2019) was interpreted to taken place at depths of ca. 750–1000 m (Michalík and Vašiček 1987; see also Michalík *et al.* 2012). This may be indirect evidence, that – although inevitably shallower – the paleobathymetric setting of the Giewont Unit during this time was also relatively deep. Consequently, even though the late Berriasian was characterized by the maximum of a major regressive cycle (Text-fig. 12; Hardenbol *et al.* 1998; Haq 2014), we assume that such a dramatic paleobathymetric change (from more than 200 m during the Kimmeridgian/Tithonian transition to depths enabling wave erosion during the Berriasian) cannot be related to sea-level fall alone. Accordingly, latest Jurassic–earliest Cretaceous tectonic activity is evidenced in the High-Tatric area by the microbreccia and volcanic rocks of the Osobita Massif (Kotański 1961; Staniszewska and Ciborowski 2000; Madzin *et al.* 2014; see Text-fig. 14). The Tithonian–Berriasian tectonic uplift of the Pieniny Klippen Belt has been discussed by Krobicki (1994); also the increasing energy of the environment documented by Grabowski *et al.* (2019) in the Velykyi Kamianets section is most likely related to this phenomenon. In addition, in the Manín Unit the Lower Cretaceous sequence starts with a hiatus – the stratigraphic range of which perfectly corresponds to that observed in the Giewont succession – and a basal breccia comprising Tithonian and Berriasian clasts

(Michalík and Vašíček 1987; Michalík *et al.* 2005). Michalík *et al.* (2012) interpreted this phenomenon as resulting from "an extensive bottom denivelation due to tectonic stress and by submarine erosion of older strata"; a similar solution is proposed to explain the gap in the Giewont succession. Furthermore, a discontinuity within the J/K boundary interval is observed also in the Vysoká Unit of the Malé Karpaty, which provides an insight into the slope facies of the Zliechov Basin (Grabowski *et al.* 2010). In the view of the above, paleobathymetric perturbations during the latest Jurassic–earliest Cretaceous were of big importance for sedimentation in the Central Western Carpathians, in particular its shallower (= ridge) zones (see also Michalík *et al.* 1995; Rehákova 2000; Michalík *et al.* 2012). Ultimately, erosional gap and Berriasian bauxites document episodes of aerial exposure in the Villány Hills (southern Hungary; e.g. Szederkényi *et al.* 2013). There, bauxites overlie the upper Jurassic microoncoid facies (e.g. Török 1999) resembling much the cyanoid limestones documented in this study (MF IV), which suggests that (?temporal) emersion could have been possible also in the case of the Giewont Unit. The latest Jurassic–earliest Cretaceous evolution of the High-Tatric succession will be considered in detail in a separate paper.

CONCLUSIONS

- The J/K boundary interval of the Giewont succession has been investigated in terms of bio- and chemostratigraphy, microfacies, rock magnetism and GRS. Biostratigraphic investigations performed in the Giewont section (Text-fig. 3) resulted in the recognition of two calcareous dinocyst zones (*Pulla–Malmica* and *Tenuis*) as well as three saccocomid zones (Sac4–Sac6). The stratigraphic framework of Pszczółkowski *et al.* (2016) was adopted for the Mały Giewont section, albeit reinterpreted in terms of its lowermost and topmost intervals. High resolution rock magnetic and GRS data allowed precise correlation between the studied sections (Text-figs 6, 8–10).
- Two hiatuses have been recognized within the lowermost Cretaceous of the Giewont Unit. The lower one, documented by the disconformity and the hardground crust (Text-fig. 7) is estimated to span the latest Tithonian–early (?and partly late) Berriasian. The upper one is approximately dated to the early Valanginian and is evidenced by a contrasting microfacies (MF V/MF VI boundary; Text-figs 5–6) as well as perturbations in rock magnetic (Text-fig. 8) and oxygen isotopes record (Text-fig. 10). Both disconformities are thought to result from an interplay of tectonics and eustasy. A restricted interval of late Berriasian–early Valanginian age (MF V) is evidenced by the occurrence of *Conoglobigerina* cf. *gulekhensis* and *Praehedbergella* cf. *sigali* (Text-fig. 3 and Pl. 2).
- The onset of an increasing $\delta^{13}C$ trend above the upper hiatus (Text-fig. 10) is compared to trends and events documented in other Western Tethyan successions (Text-fig. 13). This allowed for a rough dating of the uppermost part of the studied interval as upper Valanginian, however most likely below the maximum of the Weissert event.
- A modification of the High-Tatric lithostratigraphic scheme (Lefeld *et al.* 1985) is proposed (Text-fig. 14) based on this study and Madzin *et al.* (2014; Osobita Massif) data. This accounts for the new stratigraphic ranges of the middle and upper members of the RTL Fm., as well as the description of the Giewont Member of the WTL Fm. The upper Berriasian–lower Valanginian lithoclastic packstone (MF V) of the Giewont succession is correlated here with the upper Berriasian microbreccia of the Osobita Massif; these are included into the basal beds of the Giewont Member. Subsequently, the upper Valanginian encrinites of the Giewont Unit are correlated with the upper Valanginian–lower Hauterivian crinoidal limestones of the Osobita Massif; these are defined as the upper beds of the Member. Nevertheless, a systematic revision of the Lefeld *et al.* (op. cit.) scheme requires further studies focused on other High-Tatric successions.

Acknowledgements

These investigations were financially supported by the National Science Center, Poland (projects no.: 2016/21/B/ST/10/02941 and 2011/03B/ST10/05256; leader: J. Grabowski; PGI-NRI, Warsaw). We would like to thank the management of the Tatra National Park (Tatrzański Park Narodowy) for allowing us to conduct the research, including rock-sampling and entering restricted areas. D.G. Lodowski thanks also to Prof. Bruno Granier (Department of Earth Sciences and Universe, Université de Bretagne Occidentale) for discussions on microfacies of the Giewont succession. Last, but not least, we would like to warmly thank reviewers of this manuscript: PhD Renata Jach (Institute of Geological Sciences, Jagiellonian University, Poland) and PhD Jozef Michalík (Earth Science Institute, Slovak Academy of Sciences, Slovakia) for an inspiring discussion on presented data and their interpretation.

REFERENCES

Barchetta, A. 2015. The Tethys (Cismon core) and Pacific (DSDP Site 463) Ocean record of OAE1a: a taxonomic and quantitative analyses of planktonic foraminifera and their biological response across the Selli Level equivalent. Ph.D. Thesis, Università Degli Studi di Milano, DOI: http://dx.doi.org/10.13130/barchetta-alessia_phd2015-02-11

Bąk, K. and Bąk, M. 2013. Foraminiferal and radiolarian biostratigraphy of the youngest (Late Albian through Late Cenomanian) sediments of the Tatra massif, Central Western Carpathians. *Acta Geologica Polonica*, **63** (2), 223–237.

Benzaggagh, M. 2021. Systematic revision and evolution of the Tithonian family Chitinoidellidae Trejo, 1975. *Carnets de Geologie*, **21** (2), 27–53.

Benzaggagh, M., Homberg, C., Schnyder, J. and Abdesselam-Mahdaoui, S.B. 2015a. Description et biozonation des sections de crinoïdes saccocomidés du Jurassique supérieur (Oxfordien–Tithonien) du domaine téthysien occidental. *Annales de Paléontologie*, **101** (2), 95–117. [In French with English abstract]

Benzaggagh, M., Homberg, C., Schnyder, J., Razgallah, S. and Hssaida, T. 2015b. Intérêt des kystes de dinoflagellés calcaires et du biomicrofaciès pélagique dans la datation des terrains du sommet du Jurassique et de la base du Berriasien dans le domaine téthysien occidental. *Annales de Paléontologie*, **101** (4), 251–263. [In French with English abstract]

Borowska, U. 2015. Stratigraphy of the Lower Tithonian–Lower Aptian limestones of the Niedźwiedź crag from the High-Tatric allochthon, Polish Western Tatra Mountains (in Polish with English summary). *Przegląd Geologiczny*, **63**, 164–171.

Bureau Veritas Minerals Schedule of Service & Fees 2020. http://acmelab.com/wp-content/uploads/2020/01/BV_Fees-Schedule-2020_CAD_v2_08Jan2020.pdf

Casellato, C.E. and Erba, E. 2021. Reliability of calcareous nannofossil events in the Tithonian–early Berriasian time interval: Implications for a revised high resolution zonation. *Cretaceous Research*, **117**, 104611.

Channell, J.E.T., Casellato, C.E., Muttoni, G. and Erba, E. 2010. Magnetostratigraphy, nannofossil stratigraphy and apparent polar wander for Adria-Africa in the Jurassic–Cretaceous boundary interval. *Palaeogeography, Palaeoclimatology, Palaeoecology*, **293**, 51–75.

Coccioni, R., Silva, I.P., Marsili, A. and Verga, D. 2007. First radiation of Cretaceous planktonic foraminifera with radially elongate chambers at Angles (Southeastern France) and biostratigraphic implications. *Revue de Micropaléontologie*, **50** (3), 215–224.

Colombie, C., Lécuyer, C. and Strasser, A. 2011. Carbon- and oxygen-isotope records of palaeoenvironmental and carbonate production changes in shallow-marine carbonates (Kimmeridgian, Swiss Jura). *Geological Magazine*, **148** (1), 133–153.

Desai, D. and Banner, F.T. 1987. The evolution of Early Cretaceous Dorothiinae (Foraminiferida). *Journal of Micropaleontology*, **6** (2), 13–27.

Erba, E. and Tremolada, F. 2004. Nannofossil carbonate fluxes during the Early Cretaceous: Phytoplankton response to nutrification episodes, armospheric CO_2, and anoxia. *Paleoceanography*, **19**, PA1008, DOI: 10.1029/2003PA000884.

Föllmi, K.B. 2012. Early Cretaceous life, climate and anoxia. *Cretaceous Research*, **35**, 230–257.

Főzy, I., Janssen, N.M.M., Price, G.D., Knauer, J. and Pálfy, J. 2010. Integrated isotope and biostratigraphy of a Lower Cretaceous section from the Bakony Mountains (Transdanubian Range, Hungary): A new Tethyan record of the Weissert event. *Cretaceous Research*, **31**, 525–545.

Grabowski, J., Bakhmutov, V., Kdýr, Š., Krobicki, M., Pruner, P., Reháková, D., Schnabl, P., Stoykova, K. and Wierzbowski, H. 2019. Integrated stratigraphy and palaeoenvironmental interpretation of the Upper Kimmeridgian to Lower Berriasian pelagic sequences of the Velykyi Kamianets section (Pieniny Klippen Belt, Ukraine). *Palaeogeography, Palaeoclimatology, Palaeoecology*, **532**, 109216. DOI: 10.1016/j.palaeo.2019.05.038.

Grabowski, J., Lakova, I., Petrova, S., Stoykova, K., Ivanova, D. Wójcik-Tabol, P., Sobień, K. and Schnabl, P. 2016. Paleomagnetism and integrated stratigraphy of the Upper Berriasian hemipelagic succession in the Barlya section Western Balkan, Bulgaria: Implications for lithogenic input and paleoredox variations. *Palaeogeography, Palaeoclimatology, Palaeoecology*, **461**, 156–177.

Grabowski, J., Michalík, J., Pszczółkowski, A. and Lintnerová, O. 2010. Magneto-, and isotope stratigraphy around the Jurassic/Cretaceous boundary in the Vysoká Unit (Malé Karpaty Mountains, Slovakia): correlations and tectonic implications. *Geologica Carpathica*, **61** (4), 309–326.

Grabowski, J. and Pszczółkowski, A. 2006. Magneto- and biostratigraphy of the Tithonian–Berriasian pelagic sediments in the Tatra Mountains (Central Western Carpathians, Poland): sedimentary and rock magnetic changes at the Jurassic/Cretaceous boundary. *Cretaceous Research*, **27**, 398–417.

Grabowski, J., Schnyder, J., Sobień, K., Koptíková, L., Krzemiński, L., Pszczółkowski, A., Hejnar, J. and Schnabl, P. 2013. Magnetic susceptibility and spectral gamma logs in the Tithonian–Berriasian pelagic carbonates in the Tatra Mts (Western Carpathians, Poland): Palaeoenvironmental changes at the Jurassic/Cretaceous boundary. *Cretaceous Research*, **43**, 1–17.

Grabowski, J. and Sobień, K. 2015. Variation in clastic input in the Berriasian of the Lower Sub-Tatric (Krížna) succession in the Tatra Mountains (Central Western Carpathians, Poland): data from magnetic susceptibility and inorganic

geochemistry). *Annales Societatis Geologorum Poloniae*, **85**, 139–150.

Gradstein, F.M., Kaminski, M.A. and Agterberg, F.P. 1999. Biostratigraphy and paleoceanography of the Cretaceous seaway between Norway and Greenland. *Earth-Science Reviews*, **46**, 27–98.

Gradstein, F.M., Waskowska, A. and Glinskikh, L. 2020. The first 40 milion years of planktonic foraminifera. *Preprints*, **2020**, DOI:10.20944/202012.0319.v1.

Haq, B.U. 2014. Cretaceous eustasy revisited. *Global and Planetary Change*, **113**, 44–58.

Haq, B.U. 2018. Jurassic sea-level variations: A reappraisal. *GSA Today*, **28** (1). DOI: 10.1130/GSATG359A.1.

Hardenbol, J., Thierry, J., Harley, M.B., Jacquin, Th., de Graciansky, P.-C. and Vail, P.R. 1998. Mesozoic and Cenozoic sequence chronostratigraphic framework of European basins. Appendix. *SEPM Special Publication*, **160**, 763–786.

Hesselbo, S.P., Ogg, J.G. and Ruhl, M. 2020. The Jurassic Period. In: Gradstein, F.M., Ogg, J.G., Schmitz, M.D. and Ogg, G.M. (Eds), The Geologic Time Scale 2020, 955–1022. Elsevier; Amsterdam, London, Cambridge.

Jach, R., Djerić, N., Goričan, Š. and Rehákova, D. 2014a. Integrated stratigraphy of the Middle–Upper Jurassic of the Krížna Nappe, Tatra Mountains. *Annales Societatis Geologorum Poloniae*, **84**, 1–33.

Jach, R. and Rehákova, D. 2019. Middle to Late Jurassic carbonate-biosiliceous sedimentation and palaeoenvironment in the Tethyan Fatricum domain, Krížna Nappe, Tatra Mts, Western Carpathians. *Annales Societatis Geologorum Poloniae*, **89**, 1–46.

Jach, R., Rychliński, T. and Uchman, A. (eds.). 2014b. Sedimentary Rocks of the Tatra Mountains, 278 pp. Wydawnictwa Tatrzańskiego Parku Narodowego; Zakopane.

Jenkyns, H.C. 1972. Pelagic "oolites" from the Tethyan Jurassic. *The Journal of Geology*, **80**, 21–33.

Jenkyns, H.C. 1974. Origin of red nodular limestones (Ammonitico Rosso, Knollenkalke) in the Mediterranean Jurassic: a diagenetic model. *Special Publications of the International Association of Sedimentologists*, **1**, 249–271.

Jovane, L., Sprovieri, M., Florindo, F., Acton, G., Coccioni, R., Dall'Antonia, B. and Dinarès-Turell, J. 2007. Eocene-Oligocene paleoceanographic changes in the stratotype section, Massignano, Italy: Clues from rock magnetism and stable isotopes. *Journal of Geophysical Research*, **112**, B11101, DOI: 10.1029/2007JB004963.

Jurewicz, E. 2005. Geodynamic evolution of the Tatra Mts. And the Pieniny Klippen Belt (Western Carpathians): problems and comments. *Acta Geologica Polonica*, **55** (3), 295–338.

Kaminski, M.A., Gradstein, F.M. and Geroch, S. 1992. Uppermost Jurassic to Lower Cretaceous deep-water benthic foraminiferal assemblages from site 765 on the Argo Abyssal Plain. *Proceedings of the Ocean Drilling Program, Scientific Results*, **123**, 239–269.

Kim, S.T., Mucci, A. and Taylor, B.E. 2007. Phosphoric acid fractionation factors for calcite and aragonite between 25 and 75°C: Revisited. *Chemical Geology*, **246**, 135–146.

Kollmann, H.A. 2002. Gastropods from the Lower Cretaceous of Vorarlberg, Austria. A systematic review. *Annales des Naturhistorischen Museums in Wien. Serie A für Mineralogie und Petrographie, Geologie und Paläontologie, Anthropologie und Prähistorie*, **103**, 23–73.

Kotański, Z. 1959. Z badań geologicznych wykonanych w Tatrach. Tom IV. Profile stratygraficzne serii wierchowej Tatr Polskich. *Biuletyn Instytutu Geologicznego*, **139**, 1–160.

Kotański, Z. 1961. Tectogenese et reconstitution de la paleogeographie de la zone Haut-Tatrique dans les Tatras. *Acta Geologica Polonica*, **11**, 187–475. [In Polish with French summary]

Kotański, Z. and Radwański, A. 1959. High-Tatric Tithonian in the Osobita Region, its fauna with Pygope diphya and products of volcanoes. *Acta Geologica Polonica*, **9**, 519–538. [In Polish with English summary]

Kotański, Z. and Radwański, A. 1960. Les crinoides planctoniques Saccocoma Agassiz dans le Malm et le Néocomien Haut-Tatrique des Tatras polonaises. *Przegląd Geologiczny*, **8**, 477–479. [In Polish with French summary]

Krajewski, M. and Olszewska, B. 2007. Foraminifera from the Late Jurassic and Early Cretaceous carbonate platform facies of the southern part of the Crimea Moutnains, Southern Ukraine. *Annales Societatis Geologorum Poloniae*, **77**, 291–311.

Krobicki, M. 1994. Stratigraphic significance and palaeoecology of the Tithonian–Berriasian brachiopods in the Pieniny Klippen Belt, Carpathians, Poland. *Studia Geologica Polonica*, **106**, 89–156.

Kumpan, T., Bábek, O., Kalvoda, J., Grygar, T.M. and Frýda, J. 2014. Sea-level and environmental changes around the Devonian–Carboniferous boudnary in the Namur–Dinant Basin (S Belgium, NE France): A multi-proxy stratigraphic analysis of carbonate ramp archives and its use in regional and interregional correlations. *Sedimentary Geology*, **311**, 43–59.

Lefeld, J. 1959. Tintinnidae z serii Kominów Tylkowych. *Przegląd Geologiczny*, **8**, 358.

Lefeld, J. 1968. Stratigraphy and palaeogeography of the High-Tatric Lower Cretaceous in the Tatra Mountains. *Studia Geologica Polonica*, **24**, 1–115. [In Polish with English summary]

Lefeld, J., Gaździcki, A., Iwanow, A., Krajewski, K. and Wójcik, K. 1985. Jurassic and Cretaceous lithostratigraphic units of the Tatra Mountains. *Studia Geologica Polonica*, **84**, 7–93.

Lefeld, J. and Radwański, A. 1960. Les Crinoides planctoniques Saccocoma Agassiz dans le Malm et le Néocomien haut-tatrique des Tatras Polonaises. *Acta Geologica Polonica*, **10**, 593–618. [In Polish with French summary]

Lodowski, D.G., Pszczółkowski, A., Szives, O., Főzy, I. and

Grabowski, J. 2021. Jurassic–Cretaceous transition in the Transdanubian Range (Hungary): integrated stratigraphy and paleomagnetic study of the Hárskút and Lókút sections. *Newsletters on Stratigraphy*, DOI: 10.1127/nos/2021/0656.

Łuczyński, P. 2021. Early and Middle Jurassic tectonically controlled deposition in the High-Tatric succession (Tatricum), Tatra Mountains, southern Poland: a review. *Geological Quarterly*, **65**, DOI: 10.7306/gq.1583

Madzin, J., Sýkora, M. and Soták, J. 2014. Stratigraphic position of alkaline volcanic rocks in the autochtonous cover of the High-Tatric Unit (Western Tatra Mts., Central Western Carpathians, Slovakia). *Geological Quarterly*, **58**, 163–180.

Masse, J.-P. and Uchman, A. 1997. New biostratigraphic data on the Early Cretaceous platform carbonates of the Tatra Mountains, Western Carpathians, Poland. *Cretaceous Research*, **18** (5), 713–729.

Michalík, J., Grabowski, J., Lintnerová, O., Reháková, D., Kdýr, S. and Schnabl, P. 2021. Jurassic–Cretaceous boundary record in Carpathian sedimentary sequences. *Cretaceous Research*, **118**, 104659, DOI: 10.1016/j.cretres.2020.104659.

Michalík, J., Lintnerová, O., Reháková, D., Boorová, D. and Šimo, V. 2009. Early Cretaceous sedimentary evolution of a pelagic basin margin (the Manín Unit, central Western Carpathians, Slovakia). *Cretaceous Research*, **38**, 68–79.

Michalík, J., Reháková, D., Halásová, E. and Lintnerová, O. 2009. The Brodno section – a potential regional stratotype of the Jurassic/Cretaceous boundary (Western Carpathians). *Geologica Carpathica*, **60** (3), 213–232.

Michalík, J., Rehákova, D. and Vašíček, Z. 1995. Early Cretaceous sedimentary changes in West-Carpathian area. *Geologica Carpathica*, **46** (5), 285–296.

Michalík, J. and Vašíček, Z. 1987. Geology and stratigraphy of the Butkov Lower Cretaceous limestone deposits, Manín Unit, Middle Váh Valley (Western Slovakia). *Mineralia slovaca*, **19** (2), 115–134. [In Slovak with English summary]

Michalík, J., Vašíček, Z., Skupien, P., Kratochvílova, L., Rehákova, D. and Halásová, E. 2005. Lower Cretaceous sequences of the Manín Unit (Butkov Quarry, Strážovské vrchy Mts, Western Carpathians) – integrated biostratigraphy and sequence stratigraphy. *Slovak Geological Magazine*, **11** (1), 29–35.

Missoni, S. and Gawlick, H.-J. 2011. Evidence for Jurassic subduction from the Northern Calcareous Alps (Berchtesgaden; Austroalpine, Germany). *International Journal of Earth Sciences*, **100**, 1605–1631.

Moore, C.H. 2001. Carbonate Reservoirs: Porosity evolution and diagenesis in a sequence stratigraphic framework, 460 pp. Elsevier; Amsterdam.

Morales, C., Gardin, S., Schnyder, J., Spangenberg, J., Arnaud-Vanneau, A., Arnaud, H., Adatte, T. and Föllmi, K.B. 2013. Berriasian and early Valanginian environmental change along a transect from the Jura Platform to the Vocontian Basin. *Sedimentology*, **60**, 36–63.

Morales, C., Spangenberg, J.E., Arnaud-Vanneau, A., Adatte, T. and Föllmi, K.B. 2016. Evolution of the northern Tethyan Helvetic Platform during the late Berriasian and early Valanginian. *The Depositional Record*, **2** (1), 47–73.

Nemčok, J., Bezák, V., Biely, A., Gorek, A., Gross, P., Halouzka, R., Janák, M., Kahan, Š., Kotański, Z., Lefeld, J., Mello, J., Reichwalder, P., Raczkowski, W., Roniewicz, P., Ryka, W., Wieczorek, J. and Zelman, J. 1994. Geological map of the Tatra Mountains. MŽP SR, GÚDŠ; Bratislava.

Ogg, J.G. 2020. Geomagnetic polarity time scale. In: Gradstein, F.M., Ogg, J.G., Schmitz, M.D. and Ogg, G.M. (Eds), The Geologic Time Scale 2020, 159–192. Elsevier; Amsterdam, London, Cambridge.

Olszewska, B., Matyszkiewicz, J., Król, K. and Krajewski, M. 2012. Correlation of the Upper Jurassic–Cretaceous epicontinental sediments in southern Poland and southwestern Ukraine based on thin sections. *Biuletyn Państwowego Instytutu Geologicznego*, **453**, 29–79.

Olszewska, B., Szydło, A., Jugowiec-Nazarkiewicz, M. and Nescieruk, P. 2008. Integrated biostratigraphy of carbonate deposits of the Cieszyn Beds in the Polish Western Carpathians. *Geologia*, **34** (3), 33–59.

Omaña, L., Gonzáles-Arreola, C. and Núñez-Useche, F. 2017. The Berriasian–Valanginian boundary interval based on calpionellids from the Taraises Formation, Cuencamé de Ceniceros, Durango, NW Mexico: Bisotratigraphic, paleoecologic and paleobiogeographic significance. *Journal of South American Earth Sciences*, **80**, 589–600.

Opdyke, N.D. and Channell, J.E.T. 1996. Magnetic Stratigraphy, 346 pp. Academic Press; San Diego.

Pasquier, J.-B. and Strasser, A. 1997. Platform-to-basin correlation by high-resolution sequence stratigraphy and cyclostratigraphy (Berriasian, Switzerland and France). *Sedimentology*, **44**, 1071–1092.

Passendorfer, E. 1928. Kimeryd w Tatrach (Le Kimeridgien dans la Tatra). *Sprawozdania PIG*, **4**, 491–499. [In Polish with French summary]

Plašienka, D. 2019. Linkage of the Manín and Klape units with the Pieniny Klippen Belt and Central Western Carpathians: balancing the ambiguity. *Geologica Carpathica*, **70** (1), 35–61.

Price, G.D., Főzy, I. and Pálfy, J. 2016. Carbon cycle history through the Jurassic–Cretaceous boundary: a new global $\delta^{13}C$ stack. *Palaeogeography, Palaeoclimatology, Palaeoecology*, **451**, 46–61.

Pszczółkowski, A. 1996. Calpionellid stratigraphy of the Tithonian–Berriasian pelagic limestones in the Tatra Mts. (Western Carpathians). *Studia Geologica Polonica*, **109**, 103–130.

Pszczółkowski, A. 2003. Tithonian–Hauterivian events from the Lower Subtatric succession of the Tatra Mountains (Western Carpathians) in the framework of calpionellid stratigraphy (southern Poland). *Przegląd Geologiczny*, **51** (11), 987–994. [In Polish with English summary]

Pszczółkowski, A. 2018. Upper Jurassic bacteria from the Raptawicka Turnia Limestone Formation in the Mały Giewont area (Western Tatra Mountains, Poland), *Geological Quarterly*, **62** (4), 840–857.

Pszczółkowski, A., Grabowski, J. and Wilamowski, A. 2016. Integrated biostratigraphy and carbon isotope stratigraphy of the Upper Jurassic shallow water carbonates of the High-Tatric Unit (Mały Giewont area, Western Tatra Mountains, Poland). *Geological Quarterly*, **60** (4), 893–918.

Reboulet, S., Szives, O., Aguirre-Urreta, B., Barragán, R., Company, M., Frau, C., Kakabadze, M.V., Klein. J., Moreno-Bedmar, J.A., Lukeneder, A., Pictet, A., Ploch, I., Raisossadat, S.N., Vašíček, Z., Baraboshkin, J. and Mitta, V.V. 2018. Report on the 6th International Meeting of the IUGS Lower Cretaceous Ammonite Working Group, the Kilian Group (Vienna, Austria, 20th August 2017). *Cretaceous Research*, **91**, 100–110.

Reháková, D. 2000. Calcareous dinoflagellate and calpionellid bioevents versus sea-level fluctuations recorded in the West-Carpathian (Late Jurassic/Early Cretaceous) pelagic environments. *Geologica Carpathica*, **51** (4), 229–243.

Reháková, D., Matyja, B., Wierzbowski, A., Schlögl, J., Krobicki, M. and Barski, M. 2011. Stratigraphy and microfacies of the Jurassic and lowermost Cretaceous of the Veliky Kamenets section (Pieniny Klippen Belt, Carpathians, Western Ukraine). *Volumina Jurassica*, **IX**, 61–104.

Reháková, D. and Michalík, J. 1997. Evolution and distribution of calpionellids – the most characteristic constituents of Lower Cretaceous Tethyan microplankton. *Cretaceous Research*, **18**, 493–504.

Rider, M.H. 1999. The Geological Interpretation of Well Logs, 288 pp. Whittles Publishing Services; Southerland, Scotland.

Rosenbaum, J. and Sheppard, S.M. 1986. An isotopic study of siderites, dolomites and ankerites at high temperatures. *Geochimica et Cosmochimica Acta*, **50**, 1147–1150.

Schmid, S.M., Bernoulli, D., Fügenschuh, B., Matenco, L., Schefer, S., Schuster, R., Tischler, M. and Ustaszewski, K. 2008. The Alpine-Carpathian-Dinaridic orogenic system: correlation and evolution of tectonic units. *Swiss Journal of Geosciences*, **101**, 139–183.

Sprovieri, M., Coccioni, R., Lirer, F., Pelosi, N. and Lozar, F. 2006. Orbital tuning of a lower Cretaceous composite record (Maiolica Formation, central Italy). *Paleoceanography*, **21**, PA421. DOI: 10.1029/2005PA001224.

Stampfli, G.M. and Hochard, C. 2009. Plate tectonics of the Alpine realm. In: Murphy, J.B., Keppie, J.D. and Hynes, A.J. (Eds), Ancient Orogens and Modern Analogues. *Geological Society, London, Special Publications*, **327**, 89–111.

Staniszewska, A. and Ciborowski, T. 2000. Lower Cretaceous breccia from autochthonous High-Tatric succession in Western Tatra Mts. *Przegląd Geologiczny*, **48** (3), 246–250. [In Polish with English summary]

Sutton, T.T. 2013. Vertical ecology of the pelagic ocean: classical patterns and new perspectives. *Journal of Fish Biology*, **83** (6), 1508–1527.

Szederkényi, T., Haas, J., Nagymarosy, A. and Hámor, G. 2013. Geology and History of Evolution of the Tisza Mega-Unit. In: Haas, J. (Ed.), Geology of Hungary, 103–148. Regional Geology Reviews, Springer; Heidelberg, New York, Dordrecht, London.

Török, Á. 1999. Petrophysical and sedimentological analyses of Siklós ornamental limestones, S-Hungary. *Periodica Polytechnica Civil Engineering*, **43** (2), 187–205.

Vašíček, Z., Michalík, J. and Reháková, D. 1994. Early Cretaceous stratigraphy, paleogeography and life in Western Carpathians. *Beringeria*, **10**, 5–168.

Venuti, A., Florindo, F., Michel, E. and Hall, I.R. 2007. Magnetic proxy for deep (Pacific) western boundary current variability across the mid-Pleistocene climate transition. *Earth and Planetary Science Letters*, **259**, 107–118.

Weissert, H. and Channell, J.E.T. 1989. Tethyan carbonate carbon isotope stratigraphy across the Jurassic–Cretaceous boundary: an indicator of decelerated global carbon cycling? *Paleoceanography*, **4**, 483–494.

Zeiss, A. 2003. The Upper Jurassic of Europe: its subdivision and correlation. *Geological Survey of Denmark and Greenland*, **1**, 75–114.

Manuscript submitted: 17th May 2021
Revised version accepted: 2nd September 2021

PLATE 1

Calcareous dinoflagellates of the Giewont section.

A – *Cadosina* cf. *semiradiata fusca* Wanner (sample G1); B – *Colomisphaera carpathica* Borza (sample G1); C – *Colomisphaera* cf. *carpathica* Borza (sample G4.5); D – *Stomioshpaera* aff. *mollucana* Wanner (sample G1); E, F – *Stomioshpaera mollucana* Wanner (E: sample G12; F: sample G21); G – *Cadosina semiradiata semiradiata* Wanner (sample G5.1); H, I – *Colomisphaera* cf. *sublapidosa* Vogler (H: sample G12; I: sample G28); J – *Colomisphaera* cf. tenuis Nagy (sample G22); K, L – *Colomisphaera lapidosa* Vogler (K: sample G22.2; L: sample G27); M – *Schizosphaerella minutissima* (Colom) (sample G22); N – *Schizosphaerella* cf. *minutissima* (Colom) (sample G22.5); O – *Cadosina* cf. *parvula* Nagy (sample G22.5).

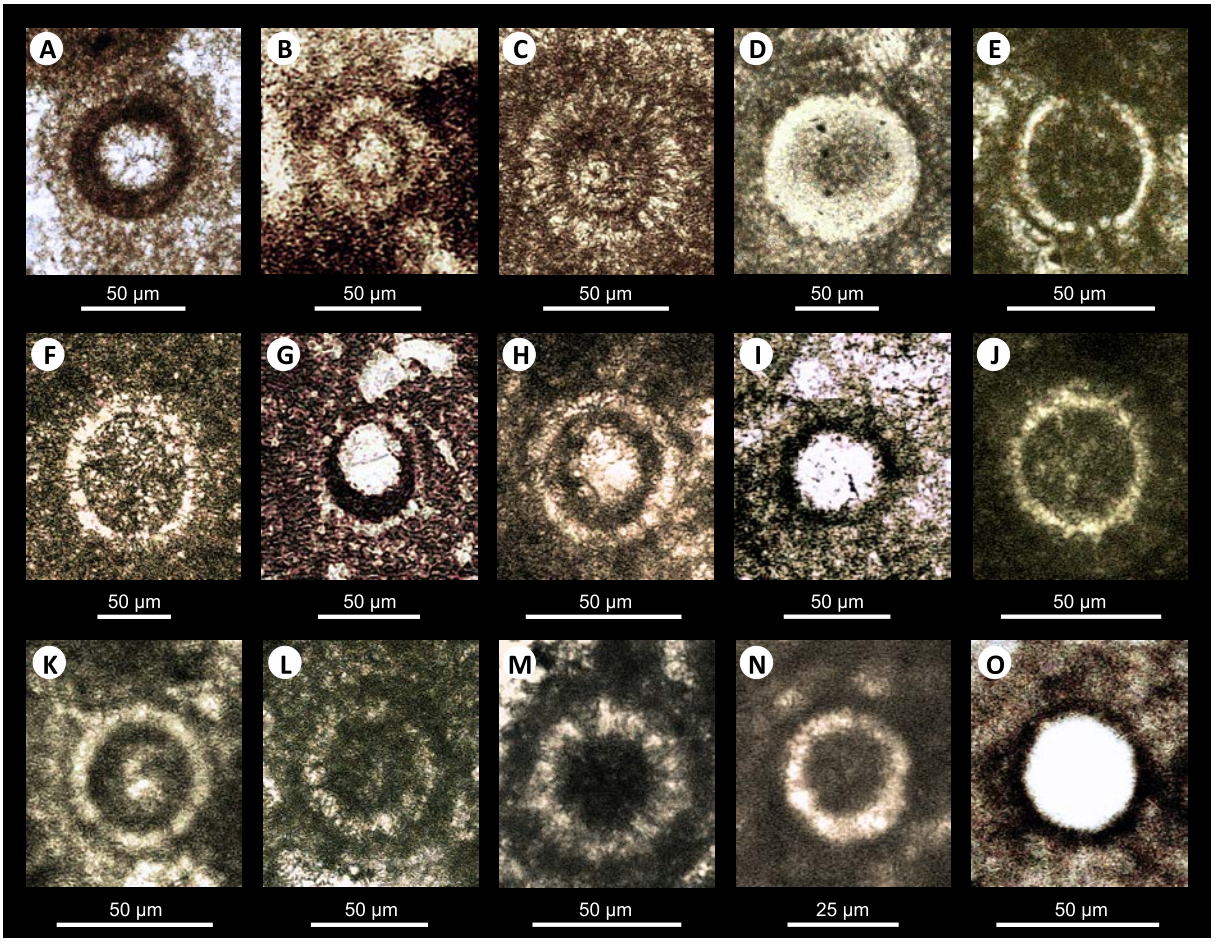
A
50 µm
B
50 µm
C
50 µm
D
50 µm
E
50 µm
F
50 µm
G
50 µm
H
50 µm
I
50 µm
J
50 µm
K
50 µm
L
50 µm
M
50 µm
N
25 µm
O
50 µm

PLATE 2

Foraminifers (1–12; 14–15) and a gastropod (13) of the Giewont section.

1) Lenticulina cf. *muensteri* (Roemer) (sample G24); 2) *Lenticulina* ex gr. *uhligi–muensteri* (G29.2); 3) Conoglobigerina cf. *gulekhensis* (Gorbachik and Poroshina) (G29.2); 4) *Lenticulina* cf. *angulosa* (Chapman) (G29.4); 5) *Praehedbergella* cf. *infracretacea* (Glaessner) (G29.4); 6) *Praehedbergella* cf. SIGALI (Moullade) (G29.4); 7) *Praedorothia* cf. *praehauteriviana* (Dieni and Massari) (G34); 8) *Praedorothia praehauteriviana* (Dieni and Massari) (8: G43) 9) *Haghimashella* cf. *arcuata* (Haeusler) (G47); 10–11) *Protomarsonella* cf. *kummi* (Zedler) (10: G34; 11: G44); 12) *Protomarsonella* cf. *hechti* (Dieni and Massari) (12: G53); 13) *Pseudonerinea* cf. *vaceki* Kollmann (G48); 14) *Uvigerinammina uvigeriniformis* (Seibold and Seibold) (G45); 15) *Praehedbergella* cf. *rudis* (Banner, Copestake and White) (G45).

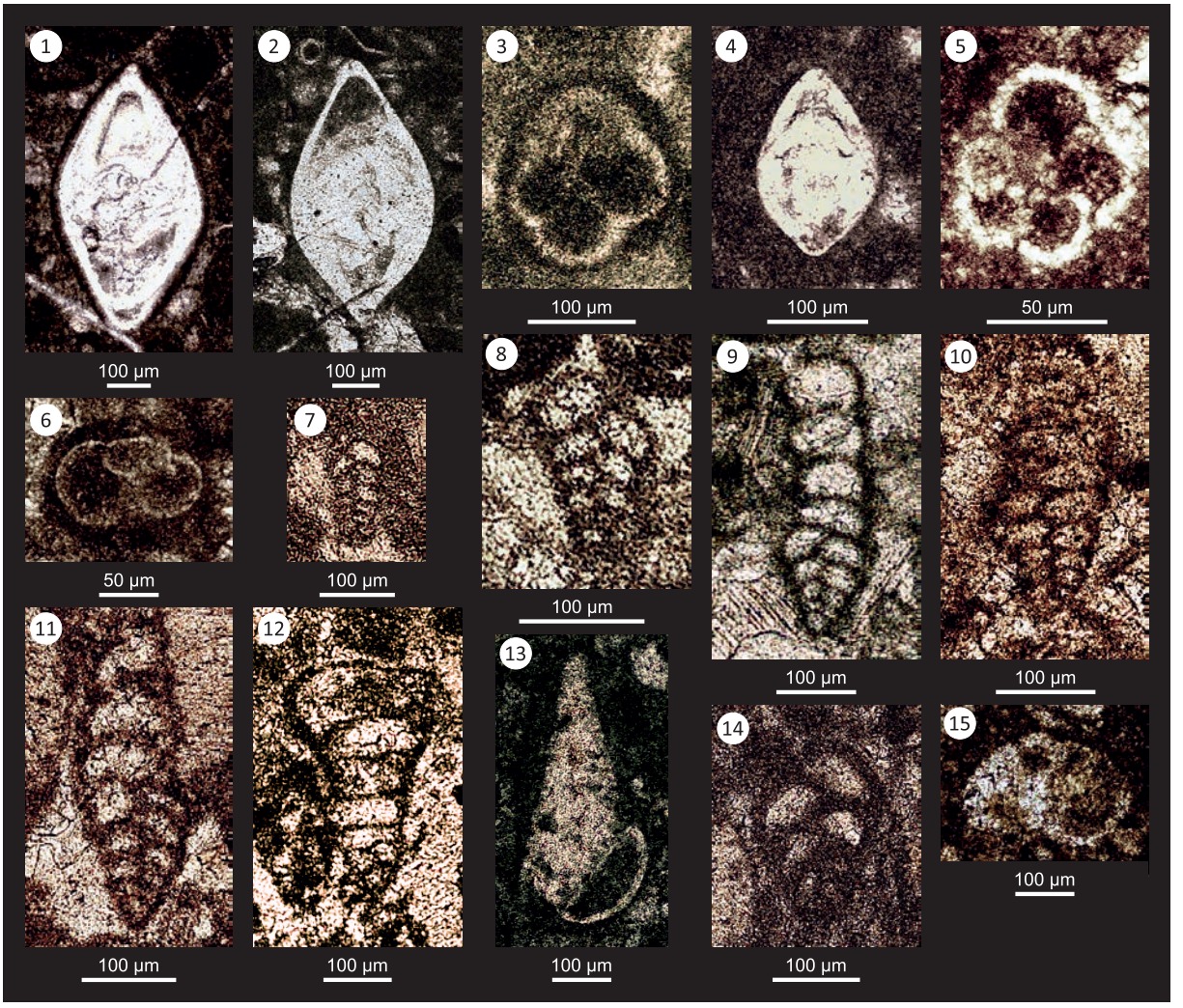
1
100 µm
2
100 µm
3
100 µm
4
100 µm
5
50 µm
6
50 µm
7
100 µm
8
100 µm
9
100 µm
10
100 µm
11
100 µm
12
100 µm
13
100 µm
14
100 µm
15
100 µm

PLATE 3

Sections of saccocomid skeletal elements Sac4 Zone, compared with those shown in the reference paper (Benzaggagh *et al.* 2015a).

A – skeletal element not found in the scheme of Benzaggagh *et al.* (2015a), sample G1; B – skeletal element similar to: P in Fig. 3, AI in Fig. 9, G in Fig. 17 (op. cit.), sample G3; C – section similar to elements: K in Fig. 4 and AN–AO in Fig. 17 (op. cit.), sample G4.5; D – section similar to elements: CV in Fig. 3 and J in Fig. 17 (op. cit.), sample G5.1; E – section similar to elements: G, J–K in Fig. 3, AJ in Fig. 6, AG in Fig. 9 and C in Fig. 17 (op. cit.), sample G5.1; F – section similar to skeletal elements: AC in Fig. 3 and in Fig. 17 (op. cit.), sample G6; G – section similar to skeletal elements: CX?, DG? in Fig. 3, U? in Fig. 9, D? in Fig. 13, J? in Fig. 15 (op. cit.), sample G7; H – section similar to elements: AI?–AJ in Fig. 4 and BJ?–BK in Fig. 17 (op. cit.), sample G11.1; I – section from sample G11.1, exactly similar skeletal element not found in the scheme of Benzaggagh *et al.* (2015a).

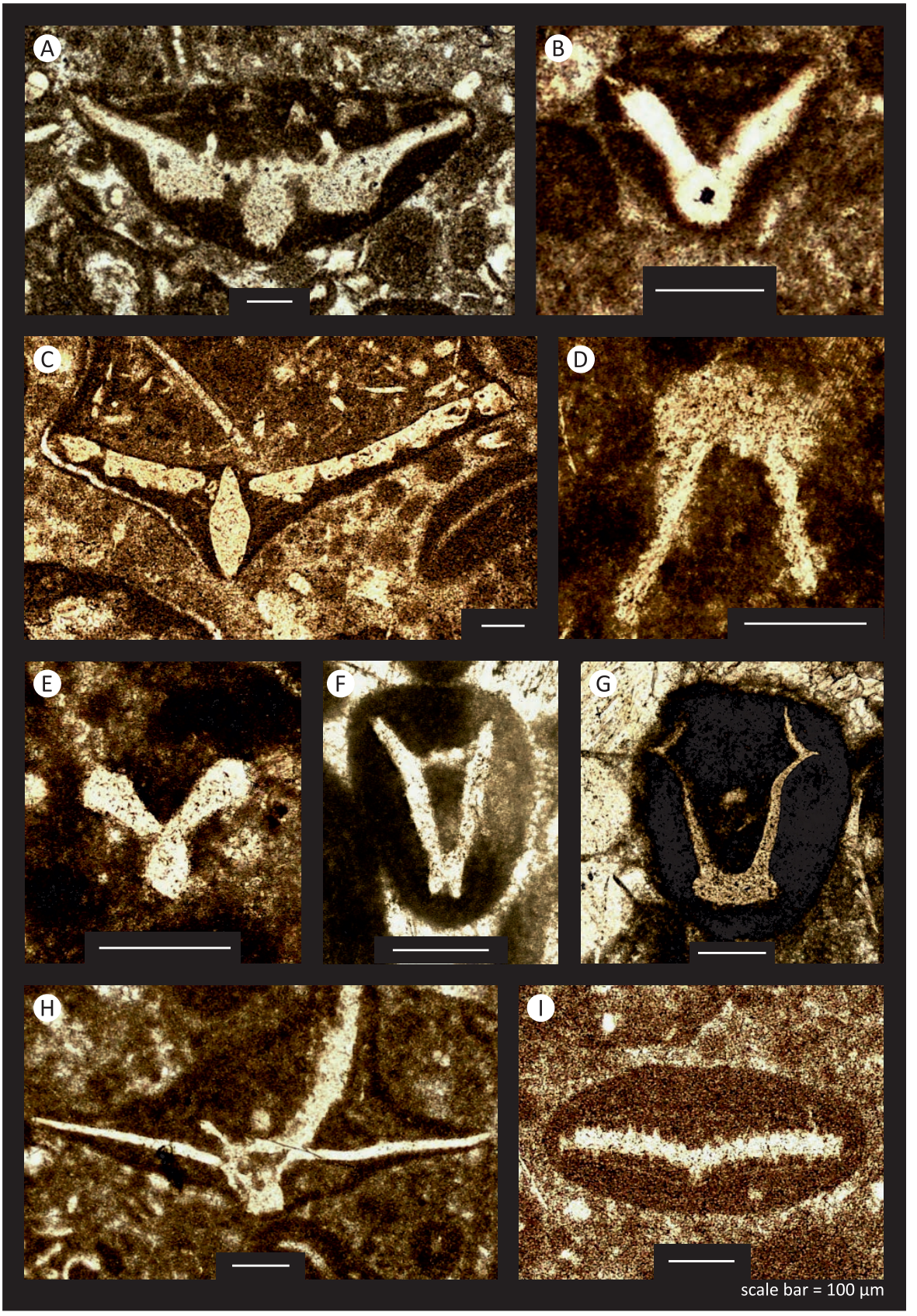
A
B
C
D
E
F
G
H
I
scale bar = 100 µm

PLATE 4

Sections of saccocomid skeletal elements of Sac5 Zone.

A – section similar to skeletal elements: J–K in Fig. 3, AO? in Fig. 10 and D in Fig. 17 (*et al.* 2015a), sample G14; B – skeletal element not found in the reference paper (Benzaggagh *et al.* 2015a), sample G18; C – section similar to skeletal elements: M in Fig. 4, C? in Fig. 12 and AN in Fig. 17 (op. cit.), sample G18; D – section partly similar to AD? in Fig. 8 (op. cit.), however it seems that there is no exact counterpart of it among the skeletal elements included in the scheme of Benzaggagh *et al.* (2015a), sample G20; E – section partly similar to skeletal elements: BQ? in Fig. 5, AJ? In Fig. 6, U? in Fig. 10 and BN? in Fig. 13 (op. cit.), sample G24; F – section similar to skeletal elements: AE?, AG? in Fig. 3, AY? in Fig. 8, W? in Fig. 12, and AD in Fig. 17 (op. cit.), sample G24.3; G – section similar to skeletal elements: C in Fig. 4, N? in Fig. 9, AC, AE in Fig. 10 and AP in Fig. 17 (op. cit.), sample G25.3; H – section similar to skeletal elements: E in Fig. 4, X in Fig. 10 and AL in Fig. 17 (op. cit.), sample G25.5; I – section similar to skeletal elements: N? in Fig. 3, AK? in Fig. 6, AI in Fig. 9, BI? in Fig. 13, K–L? in Fig. 16 and E–G in Fig. 17 (op. cit.), sample G25.7.

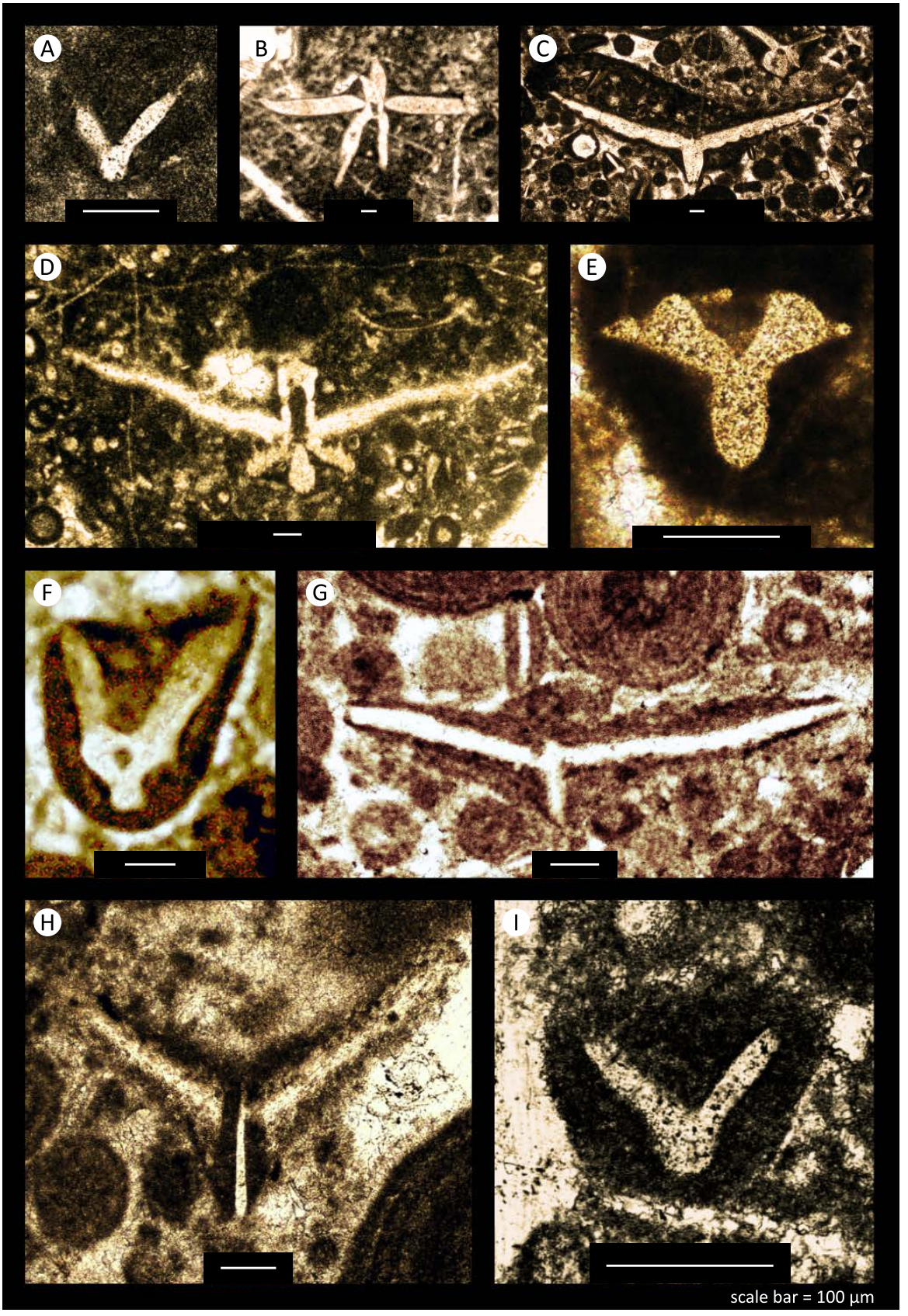
A
B
C
D
E
F
G
H
I
scale bar = 100 µm

PLATE 5

Sections of saccocomid skeletal elements of Sac6 Zone.

A – section similar to skeletal elements: AN? in Fig. 4 and BY–BS in Fig. 17 (Benzaggagh *et al.* 2015a), sample G26.6; B – section similar to skeletal elements: J in Fig. 3, AO? in Fig. 10, BO? in Fig. 13, N in Fig. 14, A–B? in Fig. 16 and D in Fig. 17 (op. cit.), sample G26.8; C – section similar to skeletal elements: W-X in Fig. 4, AY? in Fig. 6, AM? in Fig. 8, AV? in Fig. 9, AL? in Fig. 15 and BY in Fig. 17 (op. cit.), sample G27; D – section similar to skeletal elements: F–G in Fig. 4, V, Z in Fig. 12 and AM, AP in Fig. 17 (op. cit.), sample G27; E – section similar to skeletal elements: AX, AZ in Fig. 4, D? in Fig. 8, C, G in Fig. 11 and BD in Fig. 17 (op. cit.), sample G28.1; F – section similar to skeletal elements: L in Fig. 3, AG? in Fig. 9, BO in Fig. 13, N in Fig. 14, AK? in Fig. 16 and F? in Fig. 17 (op. cit.), sample G28.1; G – section similar to skeletal elements: K–L in Fig. 3, AW? in Fig. 6, BZ in Fig. 13 and F? in Fig. 17 (op. cit.), sample G28.2; H – section similar to skeletal elements: AV in Fig.3, AL? in Fig. 15 and BX in Fig. 17 (op. cit.), sample G28.2; I – section from sample G28.13; similar skeletal element was not found in Benzaggagh *et al.* (2015).

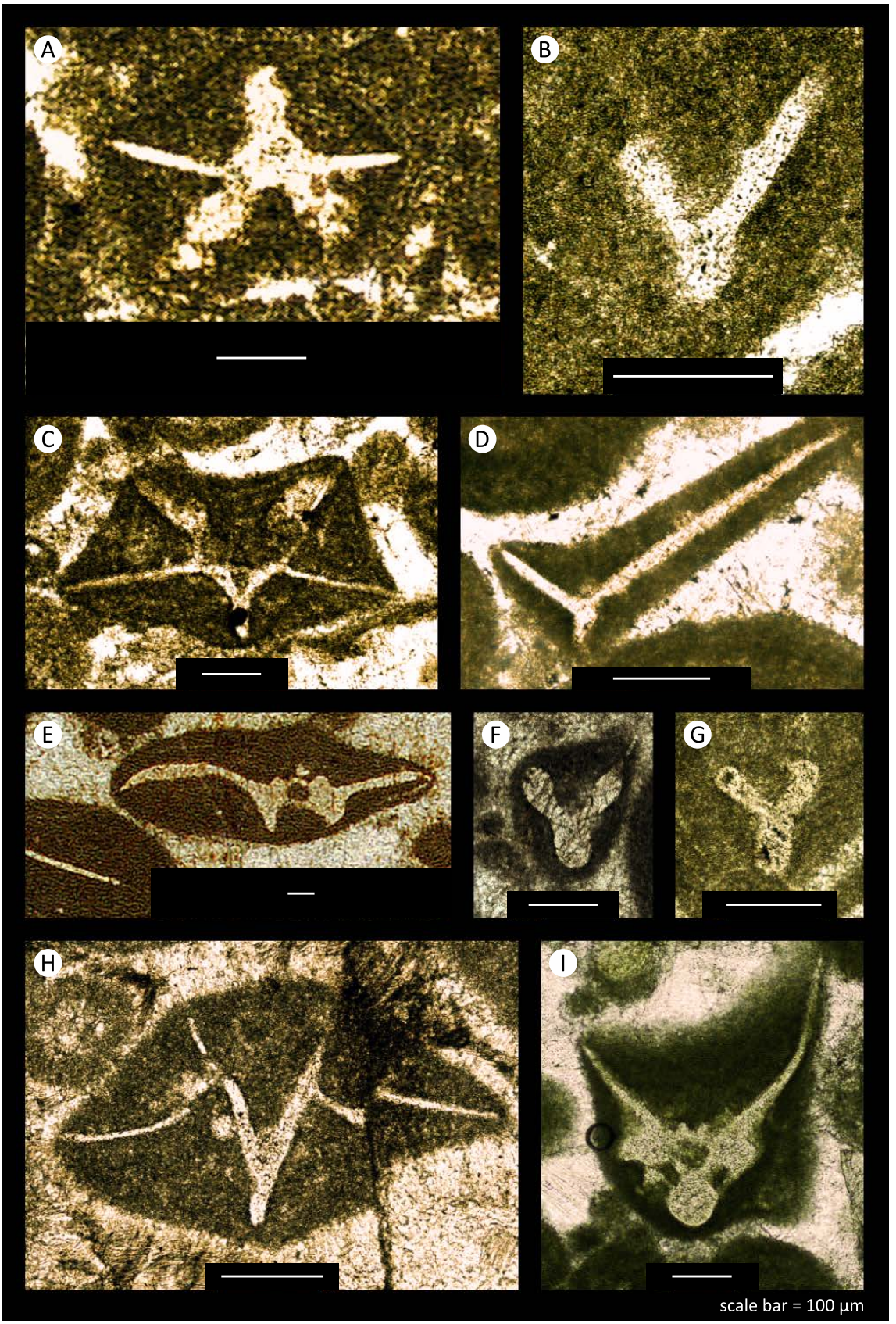
A
B
C
D
E
F
G
H
I
scale bar = 100 µm

APPENDIX 1

Photographic documentation of the Giewont section.

APPENDIX 2

Rock magnetic, geochemical (GRS + ICP-MS measured Th content) and stable isotopes ($\delta^{13}C$ and $\delta^{18}O$) data (Giewont and Mały Giewont sections) as well as occurrences of recorded microfossils (Giewont section).

Sample	[m]	[m] succession	MS KLY-2 [m^3/kg]	MS SM-30 [$\times10^{-3}$ SI]	NRM [A/m]	IRM [A/m/10cm^3]		IRM [Am^2/kg]		ARM [A/m/10cm^3]	ARM [Am^2/kg]	S-ratio	ARM / IRM_{1T}
						IRM_{1T}	IRM_{100mT}	IRM_{1T}	IRM_{100mT}				
G 49	39.75	75.75	1.46E-06		8.34E-05	7.79E-03	-4.86E-03	3.12E-06	-1.94E-06	4.15E-04	1.66E-07	0.62	0.05
G 48	39.50	75.50	-4.44E-08		2.75E-05	4.89E-03	-2.56E-03	1.96E-06	-1.02E-06	4.06E-04	1.62E-07	0.52	0.08
G 47	39.00	75.00	2.53E-06		2.37E-05	9.59E-03	-5.28E-03	3.84E-06	-2.11E-06	6.36E-04	2.54E-07	0.55	0.07
G 46	38.80	74.80	6.02E-06		3.69E-04	1.54E-02	-1.06E-02	6.17E-06	-4.25E-06	8.75E-04	3.50E-07	0.69	0.06
G 45	38.55	74.55	-1.28E-07		6.86E-05	7.00E-03	-4.05E-03	2.80E-06	-1.62E-06	5.77E-04	2.31E-07	0.58	0.08
G 44	38.30	74.30	-5.86E-07		4.51E-05	5.08E-03	-2.82E-03	2.03E-06	-1.13E-06	3.11E-04	1.24E-07	0.56	0.06
G 43	38.05	74.05	-1.18E-06		2.03E-05	3.79E-03	-3.04E-03	1.52E-06	-1.22E-06	2.53E-04	1.01E-07	0.80	0.07
G 42	37.80	73.80	-4.44E-08		2.28E-04	7.46E-03	-5.99E-03	2.98E-06	-2.40E-06	2.38E-04	9.53E-08	0.80	0.03
G 41	37.60	73.60	-2.15E-06		4.43E-05	3.96E-03	-2.69E-03	1.58E-06	-1.08E-06	1.66E-04	6.62E-08	0.68	0.04
G 40	37.35	73.35	-2.29E-06		1.54E-04	3.86E-03	-2.27E-03	1.54E-06	-9.08E-07	2.43E-04	9.72E-08	0.59	0.06
G 39	37.10	73.10	-1.94E-06		1.83E-05	6.93E-03	-3.98E-03	2.77E-06	-1.59E-06	2.75E-04	1.10E-07	0.57	0.04
G 38	36.90	72.90	-2.56E-06		1.52E-04	2.33E-03	-1.35E-03	9.32E-07	-5.40E-07	2.40E-04	9.62E-08	0.58	0.10
G 37	36.70	72.70	1.86E-06		2.01E-05	2.42E-03	-1.39E-03	9.68E-07	-5.56E-07	2.70E-04	1.08E-07	0.57	0.11
G 36	36.40	72.40	-1.58E-06		4.43E-05	2.88E-03	-1.52E-03	1.15E-06	-6.08E-07	2.67E-04	1.07E-07	0.53	0.09
G 35	36.20	72.20	-2.29E-06		4.90E-05	4.20E-03	-2.18E-03	1.68E-06	-8.72E-07	2.91E-04	1.16E-07	0.52	0.07
G 34	36.05	72.05	-2.31E-06		3.11E-05	2.90E-03	-1.73E-03	1.16E-06	-6.92E-07	1.71E-04	6.86E-08	0.60	0.06
G 33	35.85	71.85	-1.28E-06		3.70E-05	4.94E-03	-2.91E-03	1.98E-06	-1.16E-06	2.76E-04	1.10E-07	0.59	0.06
G 32	35.65	71.65	-1.52E-06		4.23E-05	4.16E-03	-9.20E-04	1.66E-06	-3.68E-07	4.08E-04	1.63E-07	0.22	0.10
G 31	35.40	71.40	1.08E-06		3.82E-05	6.72E-03	-3.89E-03	2.69E-06	-1.56E-06	4.19E-04	1.68E-07	0.58	0.06
G 30.3	35.30	71.30	1.14E-06	0.0041	3.16E-05	6.99E-03	-4.02E-03	2.80E-06	-1.61E-06	5.44E-04	2.18E-07	0.57	0.08
G 30.2	35.15	71.15	1.49E-06	0.0018	3.04E-05	6.30E-03	-2.90E-03	2.52E-06	-1.16E-06	4.71E-04	1.88E-07	0.46	0.07
G 30.1	34.85	70.85	1.59E-06	0.0066	5.21E-05	7.11E-03	-3.92E-03	2.84E-06	-1.57E-06	6.43E-04	2.57E-07	0.55	0.09
G 30	34.50	70.50	1.22E-07	0.0068	3.51E-05	5.82E-03	-4.32E-03	2.33E-06	-1.73E-06	3.65E-04	1.46E-07	0.74	0.06
G 29.4	34.20	70.20	1.32E-05	0.0358	2.74E-04	1.69E-02	-6.86E-03	6.74E-06	-2.74E-06	1.71E-03	6.83E-07	0.41	0.10
G 29.3	34.00	70.00		0.0278									
G 29.2	33.60	69.60	1.47E-05	0.0207	8.53E-05	1.96E-02	-5.27E-03	7.82E-06	-2.11E-06	1.83E-03	7.32E-07	0.27	0.09
G 29.1	33.20	69.20		0.0368									
G 29	32.95	68.95	8.59E-06	0.0334	5.37E-05	1.83E-02	-4.03E-03	7.32E-06	-1.61E-06	1.70E-03	6.78E-07	0.22	0.09
G 28.13	32.60	68.60	5.27E-06	0.0319	3.56E-05	1.07E-02	-5.71E-03	4.27E-06	-2.28E-06	1.18E-03	4.73E-07	0.53	0.11
G 28.12	32.40	68.40		0.0098									
G 28.11	32.10	68.10	7.18E-06	0.0069	2.44E-05	1.05E-02	-5.60E-03	4.19E-06	-2.24E-06	1.05E-03	4.19E-07	0.53	0.10
G 28.10	31.70	67.70	8.45E-06	0.0136	8.55E-05	1.32E-02	-7.00E-03	5.29E-06	-2.80E-06	1.47E-03	5.89E-07	0.53	0.11
G 28.9	31.22	67.22	9.78E-06	0.0099	4.31E-05	1.45E-02	-8.21E-03	5.81E-06	-3.28E-06	1.40E-03	5.58E-07	0.57	0.10
G 28.8	30.98	66.98		0.0186									
G 28.7	30.60	66.60	5.41E-06	0.0129	7.07E-05	1.13E-02	-5.87E-03	4.53E-06	-2.35E-06	1.05E-03	4.20E-07	0.52	0.09
G 28.6	30.30	66.30		0.0124									
G 28.5	29.89	65.89	4.76E-07	0.0079	1.81E-05	5.03E-03	-2.48E-03	2.01E-06	-9.91E-07	5.28E-04	2.11E-07	0.49	0.11
G 28.4	29.33	65.33	5.20E-06	0.0081	4.35E-05	8.20E-03	-4.28E-03	3.28E-06	-1.71E-06	7.35E-04	2.94E-07	0.52	0.09
G 28.3	28.95	64.95	1.90E-06	0.0013	3.33E-05	7.07E-03	-3.71E-03	2.83E-06	-1.48E-06	5.61E-04	2.24E-07	0.52	0.08
G 28.2	28.45	64.45	6.26E-06	0.0118	6.86E-05	1.20E-02	-7.39E-03	4.81E-06	-2.96E-06	1.18E-03	4.71E-07	0.61	0.10
G 28.1	27.75	63.75	1.85E-06	0.0072	4.73E-05	6.77E-03	-3.39E-03	2.71E-06	-1.36E-06	7.02E-04	2.81E-07	0.50	0.10
G 28	27.28	63.28	1.67E-06	0.531	2.28E-05	6.87E-03	-4.08E-03	2.75E-06	-1.63E-06	6.30E-04	2.52E-07	0.59	0.09
G 27	27.05	63.05	4.08E-06	0.0066		1.32E-02	-7.97E-03	5.26E-06	-3.19E-06	9.65E-04	3.86E-07	0.61	0.07
G 26.11	26.60	62.60		0.0138									
G 26.10	26.40	62.40	1.02E-05	0.0211	5.98E-05	1.22E-02	-5.58E-03	4.86E-06	-2.23E-06	1.40E-03	5.62E-07	0.46	0.12
G 26.9	26.02	62.02		0.0253									
G 26.8	25.80	61.80	2.65E-06	0.0237	2.87E-05	8.62E-03	-3.24E-03	3.45E-06	-1.30E-06	8.37E-04	3.35E-07	0.38	0.10
G 26.7	25.47	61.47		0.0063									
G 26.6	25.15	61.15	1.62E-05	-0.0055	1.10E-03	2.54E-02	-1.90E-02	1.02E-05	-7.60E-06	1.69E-03	6.78E-07	0.75	0.07
G 26.5	24.95	60.95		0.0137									
G 26.4	24.85	60.85		0.534									
G 26.3	24.65	60.65		0.0487									
G 26.2	24.45	60.45	9.15E-06	0.0595	5.67E-05	1.20E-02	-5.16E-03	4.78E-06	-2.06E-06	1.18E-03	4.72E-07	0.43	0.10
G 26.1	24.20	60.20		0.0222									
G 26	23.80	59.80	1.65E-05	0.0425	1.33E-04	1.87E-02	-1.01E-02	7.50E-06	-4.05E-06	2.12E-03	8.48E-07	0.54	0.11
G 25.8	23.53	59.53		0.0108									
G 25.7	23.40	59.40	1.15E-05	0.0238	1.98E-04	2.19E-02	-1.28E-02	8.74E-06	-5.12E-06	2.15E-03	8.62E-07	0.59	0.10
G 25.6	23.05	59.05	1.17E-05	0.0257	1.44E-04	1.93E-02	-1.07E-02	7.73E-06	-4.27E-06	2.29E-03	9.17E-07	0.55	0.12
G 25.5	22.48	58.48	9.50E-06	0.0416	5.80E-05	1.52E-02	-7.07E-03	6.08E-06	-2.83E-06	1.54E-03	6.17E-07	0.47	0.10
G 25.4	22.43	58.43		0.0284									
G 25.3	22.02	58.02	9.42E-06	0.0109	4.53E-05	1.24E-02	-5.28E-03	4.97E-06	-2.11E-06	1.09E-03	4.35E-07	0.43	0.09
G 25.2	21.65	57.65		0.0374									
G 25.1	21.41	57.41	1.45E-05	0.039	4.77E-05	1.85E-02	-7.23E-03	7.39E-06	-2.89E-06	1.70E-03	6.80E-07	0.39	0.09
G 25	20.95	56.95	1.44E-05	0.0284	2.99E-05	1.89E-02	-8.75E-03	7.56E-06	-3.50E-06	1.73E-03	6.92E-07	0.46	0.09
G 24.6	20.87	56.87		0.0234									
G 24.5	20.33	56.33	1.14E-05	0.0187	4.00E-05	1.53E-02	-6.66E-03	6.10E-06	-2.66E-06	1.53E-03	6.14E-07	0.44	0.10
G 24.4	20.05	56.05		0.0323									
G 24.3	19.70	55.70	1.06E-05	0.0207	9.06E-05	1.46E-02	-5.90E-03	5.82E-06	-2.36E-06	1.38E-03	5.53E-07	0.41	0.09
G 24.2	19.35	55.35		0.0318									
G 24.1	19.15	55.15		0.0276									
G 24	18.85	54.85	1.31E-05	0.0416	1.59E-04	1.84E-02	-7.93E-03	7.36E-06	-3.17E-06	2.08E-03	8.30E-07	0.43	0.11
G 23.2	18.60	54.60		0.0322									
G 23.1	18.40	54.40		0.0336									
G 23	18.20	54.20	1.59E-05	0.0251	1.07E-04	1.98E-02	-7.90E-03	7.92E-06	-3.16E-06	2.11E-03	8.43E-07	0.40	0.11
G 22.8	18.12	54.12		0.0382									
G 22.7	17.77	53.77		0.0438									
G 22.6	17.59	53.59		0.0599									

G 22.5	17.38	53.38	1.83E-05	0.0288	1.64E-04	2.21E-02	-1.15E-02	8.83E-06	-4.60E-06	3.03E-03	1.21E-06	0.52	0.14
G 22.4	16.85	52.85		0.0267									
G 22.3	16.65	52.65		0.0292									
G 22.2	16.44	52.44	2.16E-05	0.0443	1.54E-04	2.04E-02	-9.96E-03	8.16E-06	-3.98E-06	2.03E-03	8.11E-07	0.49	0.10
G 22.1	15.90	51.90		0.0582									
G 22	15.46	51.46	3.65E-05	0.0861	3.04E-04	3.35E-02	-1.72E-02	1.34E-05	-6.89E-06	3.67E-03	1.47E-06	0.51	0.11
G 21.2	15.36	51.36		0.0777									
G 21.1	15.22	51.22		0.0694									
G 21	15.03	51.03	2.90E-05		1.69E-04	3.16E-02	-1.34E-02	1.26E-05	-5.34E-06	2.96E-03	1.19E-06	0.42	0.09
G 20.1	14.74	50.74		0.0379									
G 20	14.47	50.47	3.24E-05	0.0469	1.06E-04	3.09E-02	-1.26E-02	1.24E-05	-5.05E-06	3.40E-03	1.36E-06	0.41	0.11
G 19	14.30	50.30		0.0679									
G 18	14.01	50.01	1.79E-05	0.0587	9.09E-05	2.01E-02	-7.65E-03	8.05E-06	-3.06E-06	1.90E-03	7.58E-07	0.38	0.09
G 17.1	13.85	49.85		0.0574									
G 17	13.41	49.41	2.64E-05	0.0655	1.35E-04	2.58E-02	-1.18E-02	1.03E-05	-4.73E-06	2.83E-03	1.13E-06	0.46	0.11
G 16.2	13.29	49.29		0.0516									
G 16.1	13.10	49.10		0.0606									
G 16	12.55	48.55	1.72E-05	0.0509	5.56E-05	1.75E-02	-8.87E-03	7.02E-06	-3.55E-06	1.84E-03	7.37E-07	0.51	0.11
G 15.2	12.43	48.43		0.0413									
G 15.1	12.05	48.05		0.0365									
G 15	11.90	47.90	1.30E-05	0.0433	1.68E-04	1.92E-02	-7.91E-03	7.68E-06	-3.16E-06	2.01E-03	8.03E-07	0.41	0.10
G 14.1	11.28	47.28		0.0602									
G 14	11.03	47.03	2.08E-05	0.0488	1.17E-04	2.25E-02	-9.17E-03	9.00E-06	-3.67E-06	2.04E-03	8.15E-07	0.41	0.09
G 13.1	10.65	46.65		0.0366									
G 13	10.35	46.35	1.50E-05	0.0442	1.28E-04	1.99E-02	-7.50E-03	7.97E-06	-3.00E-06	2.10E-03	8.39E-07	0.38	0.11
G 12.2	10.25	46.25		0.0377									
G 12.1	9.90	45.90		0.0413									
G 12	9.55	45.55	2.00E-05	0.0374		4.28E-02	-2.75E-02	1.71E-05	-1.10E-05	3.04E-03	1.21E-06	0.64	0.07
G 11.2	9.03	45.03		0.0396									
G 11.1	8.61	44.61	1.62E-05	0.0379	1.08E-04	2.17E-02	-8.56E-03	8.69E-06	-3.43E-06	1.95E-03	7.79E-07	0.39	0.09
G 11	8.25	44.25		0.0436									
G 10.2	8.12	44.12		0.0329									
G 10.1	7.65	43.65	1.44E-05	0.038	1.15E-04	1.98E-02	-6.96E-03	7.92E-06	-2.78E-06	2.10E-03	8.41E-07	0.35	0.11
G 10	7.25	43.25		0.0296									
G 9.4	7.19	43.19		0.0374									
G 9.3	6.73	42.73	2.10E-05	0.0418	1.84E-04	3.50E-02	-1.46E-02	1.40E-05	-5.84E-06	4.65E-03	1.86E-06	0.42	0.13
G 9.2	6.60	42.60		0.0361									
G 9.1	6.07	42.07		0.026									
G 9	5.90	41.90	1.63E-05	0.0371	1.36E-04	2.34E-02	-7.21E-03	9.37E-06	-2.88E-06	2.89E-03	1.16E-06	0.31	0.12
G 8.2	6.45	42.45											
G 8.1	5.88	41.88											
G 8	5.52	41.52	2.16E-05	0.0454	1.27E-04	3.22E-02	-1.32E-02	1.29E-05	-5.28E-06	4.13E-03	1.65E-06	0.41	0.13
G 7.2	5.46	41.46											
G 7.1	5.31	41.31		0.0152									
G 7	5.15	41.15	1.77E-05		2.06E-04	2.87E-02	-1.26E-02	1.15E-05	-5.04E-06	4.27E-03	1.71E-06	0.44	0.15
G 6.2	5.05	41.05		0.0362									
G 6.1	4.85	40.85		0.0491									
G 6	4.40	40.40	1.74E-05	0.0384	9.59E-05	2.43E-02	-1.07E-02	9.74E-06	-4.27E-06	3.18E-03	1.27E-06	0.44	0.13
G 5.2	4.23	40.23		0.0394									
G 5.1	3.70	39.70	1.45E-05	0.0266	9.23E-05	3.18E-02	-2.12E-02	1.27E-05	-8.48E-06	6.28E-03	2.51E-06	0.67	0.20
G 5	3.20	39.20	9.69E-06	0.0282	9.39E-05	2.37E-02	-1.47E-02	9.47E-06	-5.86E-06	4.60E-03	1.84E-06	0.62	0.19
G 4.7	2.90	38.90		0.0633									
G 4.6	2.68	38.68		0.0461									
G 4.5	2.29	38.29	2.64E-05	0.0462	2.74E-04	3.04E-02	-1.62E-02	1.21E-05	-6.47E-06	4.48E-03	1.79E-06	0.53	0.15
G 4.4	1.78	37.78		0.0465									
G 4.3	1.44	37.44		0.0557									
G 4.2	0.85	36.85		0.0417									
G 4.1	0.58	36.58		0.0364									
G 3	0.43	36.43	3.23E-05	0.0518	1.77E-04	2.61E-02	-1.61E-02	1.04E-05	-6.45E-06	1.11E-02	4.43E-06	0.62	0.42
G 2	0.35	36.35	2.12E-05	0.0425	2.27E-04	4.32E-02	-2.44E-02	1.73E-05	-9.74E-06	7.73E-03	3.09E-06	0.56	0.18
G 1	0.18	36.18	2.36E-05	0.0453	3.13E-04	5.19E-02	-3.32E-02	2.08E-05	-1.33E-05	1.07E-02	4.30E-06	0.64	0.21
MG 56	0.38	0.38	1.56E-05	0.0210	1.09E-04	3.10E-02	-2.09E-02	1.24E-05	-8.36E-06	4.71E-03	1.88E-06	0.68	0.15
MG 57	0.38	0.38	2.33E-05	0.0259	1.60E-04	4.48E-02	-3.21E-02	1.79E-05	-1.28E-05	8.17E-03	3.27E-06	0.72	0.18
MG 58	1.88	1.88	1.45E-05	0.0260	1.18E-04	2.74E-02	-1.88E-02	1.10E-05	-7.54E-06	5.02E-03	2.01E-06	0.69	0.18
MG 59	6.10	6.10	8.06E-06	0.0118	5.20E-04	3.70E-02	-2.97E-02	1.48E-05	-1.19E-05	7.00E-03	2.80E-06	0.80	0.19
MG 60	6.38	6.38	4.61E-06	0.0084	1.36E-04	2.27E-02	-1.69E-02	9.06E-06	-6.77E-06	4.58E-03	1.83E-06	0.75	0.20
MG 61	7.10	7.10	5.94E-06		6.35E-05	1.46E-02	-1.10E-02	5.84E-06	-4.40E-06	2.75E-03	1.10E-06	0.75	0.19
MG 62	7.10	7.10	6.96E-06	0.0133	1.01E-04	1.50E-02	-1.08E-02	6.01E-06	-4.33E-06	2.67E-03	1.07E-06	0.72	0.18
MG 63	7.70	7.70	1.02E-05	0.0188	1.14E-04	2.48E-02	-1.91E-02	9.92E-06	-7.65E-06	4.81E-03	1.92E-06	0.77	0.19
MG 64	8.50	8.50	7.18E-06	0.0124	6.52E-05	1.87E-02	-1.41E-02	7.47E-06	-5.62E-06	3.48E-03	1.39E-06	0.75	0.19
MG 65	8.80	8.80	1.04E-05	0.0241	9.43E-05	2.07E-02	-1.44E-02	8.26E-06	-5.78E-06	3.71E-03	1.48E-06	0.70	0.18
MG 66	9.35	9.35	1.18E-05	0.0100	1.06E-04	2.96E-02	-2.03E-02	1.19E-05	-8.13E-06	6.82E-03	2.73E-06	0.69	0.23
MG 67	9.95	9.95	7.56E-06	0.0077	1.09E-04	1.99E-02	-1.49E-02	7.94E-06	-5.97E-06	3.64E-03	1.46E-06	0.75	0.18
MG 68	10.20	10.20	6.67E-06	0.0096	9.93E-05	3.00E-02	-2.08E-02	1.20E-05	-8.32E-06	5.96E-03	2.38E-06	0.69	0.20
MG 69	10.85	10.85	1.09E-05	0.0212	1.43E-04	4.38E-02	-3.54E-02	1.75E-05	-1.42E-05	1.02E-02	4.09E-06	0.81	0.23
MG 70	11.20	11.20	1.42E-05	0.0138	1.73E-04	4.37E-02	-3.68E-02	1.75E-05	-1.47E-05	1.04E-02	4.18E-06	0.84	0.24
MG 71	12.10	12.10	7.59E-06	0.0148	1.54E-04	3.34E-02	-2.58E-02	1.33E-05	-1.03E-05	6.75E-03	2.70E-06	0.77	0.20
MG 72	12.55	12.55	1.38E-05	0.0109	1.56E-04	4.31E-02	-3.09E-02	1.72E-05	-1.24E-05	8.46E-03	3.38E-06	0.72	0.20
MG 73	13.90	13.90	5.92E-06	0.0157	6.10E-04	3.05E-02	-2.05E-02	1.22E-05	-8.18E-06	7.26E-03	2.90E-06	0.67	0.24
MG 74	14.50	14.50	1.17E-05	0.0076	1.41E-04	3.23E-02	-2.05E-02	1.29E-05	-8.19E-06	5.43E-03	2.17E-06	0.63	0.17
MG 75	15.15	15.15	1.42E-05	0.0192	1.21E-04	3.26E-02	-3.02E-02	1.30E-05	-1.21E-05	6.36E-03	2.55E-06	0.93	0.20
MG 75A	15.70	15.70	1.00E-05		2.12E-04	3.45E-02	-2.62E-02	1.38E-05	-1.05E-05	7.56E-03	3.02E-06	0.76	0.22
MG 76	17.50	17.50	1.20E-05	0.0162	1.80E-04	4.02E-02	-3.22E-02	1.61E-05	-1.29E-05	6.54E-03	2.62E-06	0.80	0.16
MG 77	19.10	19.10	1.45E-05	0.0156	1.35E-04	3.81E-02	-2.82E-02	1.52E-05	-1.13E-05	5.92E-03	2.37E-06	0.74	0.16
MG 78	19.25	19.25	1.34E-05	0.0120	1.26E-04	4.77E-02	-3.87E-02	1.91E-05	-1.55E-05	8.51E-03	3.40E-06	0.81	0.18

MG	**79**	19.95	19.95	1.50E-05	0.0173	1.68E-04	4.70E-02	-3.36E-02	1.88E-05	-1.35E-05	9.16E-03	3.66E-06	0.72	0.20
MG	**80**	21.60	21.60	1.24E-05	0.0137	1.77E-04	4.35E-02	-3.01E-02	1.74E-05	-1.20E-05	7.26E-03	2.90E-06	0.69	0.17
MG	**81**	22.25	22.25	1.26E-05	0.0144	1.46E-04	4.18E-02	-2.81E-02	1.67E-05	-1.12E-05	8.22E-03	3.29E-06	0.67	0.20
MG	**82**	23.55	23.55	1.67E-05	0.0161	2.66E-04	5.16E-02	-3.88E-02	2.06E-05	-1.55E-05	9.20E-03	3.68E-06	0.75	0.18
MG	**83**	24.60	24.60	1.23E-05	0.0209	7.95E-05	2.91E-02	-1.48E-02	1.16E-05	-5.94E-06	4.20E-03	1.68E-06	0.51	0.14
MG	**84**	25.25	25.25	1.03E-05	0.0212	2.37E-04	4.58E-02	-2.94E-02	1.83E-05	-1.18E-05	8.14E-03	3.26E-06	0.64	0.18
MG	**85**	25.95	25.95	1.42E-05	0.0199	1.59E-04	5.05E-02	-3.49E-02	2.02E-05	-1.40E-05	8.75E-03	3.50E-06	0.69	0.17
MG	**86**	26.80	26.80	1.56E-05	0.0195	6.82E-05	4.07E-02	-2.62E-02	1.63E-05	-1.05E-05	6.11E-03	2.44E-06	0.64	0.15
MG	**87**	27.30	27.30	1.72E-05	0.0319	2.46E-04	3.85E-02	-2.71E-02	1.54E-05	-1.08E-05	6.88E-03	2.75E-06	0.70	0.18
MG	**88**	29.60	29.60	1.45E-05	0.0218	1.82E-04	4.67E-02	-2.96E-02	1.87E-05	-1.18E-05	8.62E-03	3.45E-06	0.63	0.18
MG	**89**	30.50	30.50	1.27E-05	0.0150	9.75E-05	3.00E-02	-2.26E-02	1.20E-05	-9.06E-06	4.78E-03	1.91E-06	0.75	0.16
MG	**90**	31.70	31.70	1.50E-05	0.0223	1.28E-04	3.31E-02	-2.06E-02	1.32E-05	-8.24E-06	5.79E-03	2.32E-06	0.62	0.18
MG	**91**	32.80	32.80	1.49E-05	0.0175	2.12E-04	4.99E-02	-3.88E-02	2.00E-05	-1.55E-05	1.07E-02	4.26E-06	0.78	0.21
MG	**92**	33.90	33.90	9.56E-06	0.0176	9.96E-05	2.18E-02	-1.40E-02	8.74E-06	-5.61E-06	3.19E-03	1.28E-06	0.64	0.15
MG	**93**	33.91	33.91	1.93E-05	0.0166	2.96E-04	6.36E-02	-3.15E-02	2.54E-05	-1.26E-05	1.15E-02	4.58E-06	0.50	0.18
MG	**94**	34.30	34.30	1.97E-05	0.0332	1.42E-04	2.85E-02	-1.67E-02	1.14E-05	-6.70E-06	2.61E-03	1.04E-06	0.59	0.09
MG	**95**	34.85	34.85	1.91E-05	0.0256	1.68E-04	4.13E-02	-2.80E-02	1.65E-05	-1.12E-05	7.33E-03	2.93E-06	0.68	0.18
MG	**96**	35.95	35.95	3.45E-05	0.0496	1.42E-04	3.39E-02	-1.89E-02	1.35E-05	-7.54E-06	2.33E-03	9.33E-07	0.56	0.07
MG	**97**	36.30	36.30	4.54E-05	0.0614	5.24E-04	5.70E-02	-3.17E-02	2.28E-05	-1.27E-05	7.43E-03	2.97E-06	0.56	0.13
MG	**97A**	37.60	37.60	4.62E-05		2.43E-04	3.69E-02	-2.44E-02	1.48E-05	-9.76E-06	4.21E-03	1.69E-06	0.66	0.11
MG	**97A1**	38.00	38.00	5.74E-05		3.06E-04	4.80E-02	-3.31E-02	1.92E-05	-1.32E-05	5.77E-03	2.31E-06	0.69	0.12
MG	**97B**	39.10	39.10	4.11E-05		2.77E-04	3.30E-02	-2.01E-02	1.32E-05	-8.04E-06	3.57E-03	1.43E-06	0.61	0.11
MG	**98**	40.60	40.60	1.19E-05	0.0737	8.57E-05	1.01E-02	-6.42E-03	4.03E-06	-2.57E-06	6.86E-04	2.74E-07	0.64	0.07
MG	**99**	40.80	40.80	3.22E-05	0.0668	1.73E-04	2.84E-02	-1.62E-02	1.14E-05	-6.46E-06	2.35E-03	9.39E-07	0.57	0.08
MG	**100**	44.70	44.70		0.4395									
MG	**101**	45.30	45.30	2.65E-05	0.0290	1.84E-04	2.37E-02	-1.23E-02	9.50E-06	-4.92E-06	1.97E-03	7.90E-07	0.52	0.08
MG	**102**	46.20	46.20	2.61E-05	0.0388	2.03E-04	3.74E-02	-2.46E-02	1.49E-05	-9.84E-06	2.37E-03	9.49E-07	0.66	0.06
MG	**103**	46.40	46.40	2.61E-05	0.0524	1.55E-04	2.63E-02	-1.75E-02	1.05E-05	-7.01E-06	2.44E-03	9.77E-07	0.67	0.09
MG	**104A**	48.10	48.10	2.72E-05		8.42E-05	2.54E-02	-1.57E-02	1.02E-05	-6.29E-06	2.66E-03	1.06E-06	0.62	0.10
MG	**104B**	51.40	51.40	4.00E-05	0.0410	1.50E-04	3.57E-02	-2.30E-02	1.43E-05	-9.22E-06	3.07E-03	1.23E-06	0.65	0.09
MG	**104C**	52.10	52.10	3.59E-05		1.62E-04	2.58E-02	-1.60E-02	1.03E-05	-6.39E-06	2.48E-03	9.92E-07	0.62	0.10
MG	**105**	56.10	56.10	2.83E-05	0.0200	4.22E-04	2.53E-02	-1.62E-02	1.01E-05	-6.49E-06	1.99E-03	7.96E-07	0.64	0.08
MG	**106**	56.40	56.40	1.58E-05	0.0289	9.54E-05	1.79E-02	-1.03E-02	7.16E-06	-4.13E-06	1.57E-03	6.27E-07	0.58	0.09
MG	**107**	57.05	57.05	9.98E-06	0.0214	9.95E-05	1.57E-02	-8.76E-03	6.29E-06	-3.50E-06	1.28E-03	5.10E-07	0.56	0.08
MG	**108**	57.05	57.05	1.74E-05	0.0106	3.61E-04	1.77E-02	-9.90E-03	7.06E-06	-3.96E-06	1.49E-03	5.95E-07	0.56	0.08
MG	**109**	58.60	58.60	9.93E-06	0.0166	1.98E-04	1.31E-02	-7.33E-03	5.26E-06	-2.93E-06	1.04E-03	4.14E-07	0.56	0.08
MG	**110**	59.95	59.95	8.74E-06	0.0263	7.24E-05	6.71E-03	-5.24E-03	2.68E-06	-2.10E-06	7.64E-04	3.05E-07	0.78	0.11
MG	**111**	60.30	60.30	1.90E-05	0.0172	2.70E-04	2.33E-02	-1.37E-02	9.30E-06	-5.49E-06	2.06E-03	8.22E-07	0.59	0.09
MG	**112**	60.65	60.65	1.43E-05	0.0189	2.65E-04	2.02E-02	-1.30E-02	8.08E-06	-5.19E-06	1.87E-03	7.46E-07	0.64	0.09
MG	**113**	61.10	61.10	1.95E-05	0.0155	1.75E-04	3.19E-02	-1.95E-02	1.27E-05	-7.79E-06	2.71E-03	1.08E-06	0.61	0.09
MG	**114**	61.70	61.70	1.95E-05	0.0155	1.84E-04	2.86E-02	-1.71E-02	1.14E-05	-6.86E-06	2.77E-03	1.11E-06	0.60	0.10
MG	**115**	63.60	63.60	5.29E-06	0.0124	7.27E-05	9.69E-03	-5.64E-03	3.88E-06	-2.26E-06	7.40E-04	2.96E-07	0.58	0.08
MG	**116**	64.85	64.85	3.68E-06	0.0058	1.06E-04	1.12E-02	-6.07E-03	4.47E-06	-2.43E-06	1.12E-03	4.46E-07	0.54	0.10
MG	**117**	77.80	77.80	-3.14E-06	-0.0046	3.54E-05	3.31E-03	-1.77E-03	1.32E-06	-7.10E-07	1.00E-04	4.00E-08	0.54	0.03
MG	**118**	78.40	78.40	-1.37E-06	-0.0061	7.25E-04	8.88E-03	-6.68E-03	3.55E-06	-2.67E-06	1.74E-04	6.96E-08	0.75	0.02
MG	**119**	78.90	78.90	-2.58E-06	-0.0070	2.89E-05	4.57E-03	-2.72E-03	1.83E-06	-1.09E-06	1.44E-04	5.76E-08	0.59	0.03
MG	**120**	80.00	80.00	7.54E-07	-0.0081	4.70E-05	8.89E-03	-7.61E-03	3.56E-06	-3.04E-06	2.20E-04	8.81E-08	0.86	0.02

Sample	[m]	[m] succession	GRS								
			Dose [nGy/h]	Total [ppm]	K [%]	K [cpm]	U [ppm]	U [cpm]	Th [ppm]	Th [cpm]	CGR [API]
G 49	39.75	75.75	8.3	138.0	0.0	5.7	1.0	20.3	1.0	9.4	4
G 48	39.50	75.50	8.8	107.3	0.0	0.4	1.3	24.5	0.6	6.2	2
G 47	39.00	75.00	5.5	120.6	0.0	12.3	0.9	15.5	0.3	3.1	1
G 45	38.55	74.55	9.7	143.1	0.0	15.4	1.7	29.7	0.2	3.1	1
G 43	38.05	74.05	11.4	159.8	0.0	7.7	1.7	31.8	0.1	7.6	0
G 42	37.80	73.80	9.6	151.7	0.0	9.5	1.4	25.5	0.8	8.0	3
G 40	37.35	73.35	7.8	154.9	0.0	15.1	1.4	24.2	0.1	2.1	0
G 39	37.10	73.10	8.0	146.4	0.0	4.6	1.4	25.2	0.1	1.7	0
G 38	36.90	72.90	10.2	138.9	0.0	12.6	1.6	28.7	0.6	6.6	2
G 37	36.70	72.70	8.2	142.5	0.0	15.1	1.2	22.4	0.6	6.2	2
G 36	36.40	72.40	9.3	165.5	0.0	17.1	1.5	27.3	0.4	4.5	2
G 35	36.20	72.20	9.7	183.4	0.0	17.5	1.6	28.7	0.4	4.5	2
G 33	35.85	71.85	10.4	152.7	0.0	13.0	1.7	30.8	0.4	4.5	2
G 32	35.65	71.65	11.1		0.0		1.4		1.3		5
G 31	35.40	71.40	10.9	206.7	0.0	5.3	1.5	28.3	1.1	10.4	4
G 30.3	35.30	71.30	11.9	203.9	0.0	3.2	1.6	30.8	1.0	11.5	4
G 30.1	34.85	70.85	10.3	210.1	0.0	16.1	1.2	24.5	1.3	12.5	5
G 29.4	34.20	70.20	12.4	234.0	0.0	26.5	1.8	33.5	0.9	9.4	4
G 29.3	34.00	70.00	2.8	175.6	0.1	18.9	0.3	5.7	0.0	0.0	2
G 29.2	33.60	69.60	3.9	190.8	0.1	22.7	0.5	8.8	0.0	0.0	2
G 29.1	33.20	69.20	14.1	204.0	0.0	24.4	2.1	39.5	0.9	9.4	4
G 28.13	32.60	68.60	16.8	135.7	0.0	1.5	0.0	6.4	6.3	53.9	25
G 28.12	32.40	68.40	6.8	120.0	0.0	10.5	1.1	20.3	0.2	2.8	1
G 28.11	32.10	68.10	8.7	104.6	0.0	7.4	1.4	25.5	0.4	4.1	2
G 28.10	31.70	67.70	7.1		0.0		1.3		0.1		
G 28.9	31.22	67.22	6.2	107.7	0.0	8.1	1.0	17.5	0.4	3.8	2
G 28.7	30.60	66.60	6.6	98.2	0.0	2.5	1.0	18.9	0.4	3.8	2
G 28.5	29.89	65.89	5.4	76.0	0.0	0.0	0.8	15.1	0.4	3.8	2
G 28.4	29.33	65.33	2.4	75.9	0.0	0.0	0.3	5.4	0.4	3.4	2
G 28.3	28.95	64.95	5.4	70.2	0.0	0.0	0.8	14.8	0.4	4.1	2
G 28.2	28.45	64.45	4.5	53.2	0.0	0.0	0.6	11.6	0.5	4.5	2
G 28.1	27.75	63.75	4.0	52.9	0.0	0.0	0.7	12.0	0.1	1.7	0
G 27	27.05	63.05	2.4	60.5	0.0	0.0	0.3	6.4	0.2	2.1	1
G 26.10	26.40	62.40	3.1	70.5	0.0	0.0	0.5	8.8	0.2	2.1	1
G 26.9	26.02	62.02	3.0	59.2	0.0	0.0	0.3	6.4	0.5	4.8	2
G 26.7	25.47	61.47	3.8	56.0	0.0	0.0	0.4	8.8	0.5	4.8	2
G 26.6	25.15	61.15	4.1	77.6	0.0	0.0	0.5	9.5	0.6	5.2	2
G 26.3	24.65	60.65	3.2	61.3	0.0	0.0	0.3	6.4	0.6	5.5	2
G 26.1	24.20	60.20	5.4	89.5	0.0	6.0	0.8	14.4	0.5	4.5	2
G 26	23.80	59.80	5.4	93.3	0.0	0.0	0.6	12.7	0.7	6.9	3
G 25.8	23.53	59.53	3.6	92.9	0.0	0.8	0.4	7.8	0.6	5.5	2
G 25.6	23.05	59.05	4.1	84.2	0.0	0.8	0.3	7.8	0.9	7.6	4
G 25.5	22.48	58.48	5.7	105.5	0.0	14.0	0.8	14.4	0.5	4.8	2
G 25.3	22.02	58.02	6.3	88.2	0.0	11.6	0.9	16.8	0.5	5.2	2
G 25.1	21.41	57.41	6.8	163.5	0.0	14.7	0.8	16.2	0.8	7.6	3
G 25	20.95	56.95	8.1	99.0	0.0	13.0	1.1	21.4	0.8	7.3	3
G 24.6	20.87	56.87	6.0	81.3	0.0	8.8	1.0	17.5	0.2	2.8	1
G 24.4	20.05	56.05	6.5	79.7	0.0	14.4	1.1	19.6	0.2	2.4	1
G 24.2	19.35	55.35	3.0	58.8	0.0	14.0	0.3	6.1	0.2	2.1	1
G 24	18.85	54.85	4.4	51.6	0.0	1.1	0.5	9.9	0.7	6.2	3
G 23.2	18.60	54.60	5.4	70.4	0.0	10.2	0.8	14.4	0.5	4.5	2
G 23	18.20	54.20	3.0	56.9	0.0	10.5	0.2	4.3	0.6	5.5	2
G 22.7	17.77	53.77	6.8	134.3	0.1	23.4	0.5	11.6	1.2	10.4	6
G 22.5	17.38	53.38	5.4	71.6	0.0	11.9	0.4	10.2	1.0	9.4	4
G 22.4	16.85	52.85	4.0	79.1	0.0	1.8	0.4	8.8	0.6	5.9	2
G 22.2	16.44	52.44	3.4	61.6	0.0	0.0	0.4	8.5	0.4	3.4	2
G 22	15.46	51.46	6.8	108.1	0.0	13.7	0.9	17.5	0.6	6.2	2
G 21.2	15.36	51.36	5.7	105.1	0.1	28.3	0.5	10.6	0.5	4.8	4
G 20.1	14.74	50.74	5.8	70.4	0.0	1.8	0.8	15.1	0.6	5.5	2
G 19	14.30	50.30	5.2	72.5	0.0	6.7	0.6	12.3	0.7	6.2	3
G 18	14.01	50.01	4.3	50.8	0.0	6.4	0.4	8.8	0.8	7.3	3
G 17	13.41	49.41	3.6	66.9	0.0	1.1	0.2	6.1	0.9	7.6	4
G 16.1	13.10	49.10	4.9	71.3	0.0	2.9	0.5	10.9	0.8	6.9	3
G 15.2	12.43	48.43	4.0	70.8	0.0	6.0	0.5	9.9	0.5	4.5	2
G 15	11.90	47.90	2.8	60.4	0.0	0.4	0.3	5.7	0.5	4.8	2
G 14.1	11.28	47.28	8.6	88.8	0.0	0.0	1.2	23.1	0.7	6.9	3
G 14	11.03	47.03	3.0	47.1	0.0	2.2	0.2	5.4	0.7	5.9	3
G 13.1	10.65	46.65	4.0	53.4	0.0	0.8	0.5	9.2	0.6	5.2	2
G 12.2	10.25	46.25	3.4	86.6	0.0	8.8	0.4	7.8	0.4	3.8	2
G 12	9.55	45.55	4.2	51.2	0.0	8.4	0.6	10.9	0.4	3.8	2
G 11.2	9.03	45.03	3.6	52.9	0.0		0.5		2.8		11
G 11	8.25	44.25	5.4	86.4	0.0	7.4	0.4	10.2	1.1	10.1	4
G 10.2	8.12	44.12	3.2	76.1	0.0	0.0	0.3	7.1	0.5	4.8	2
G 10	7.25	43.25	2.4	57.7	0.0	4.3	0.2	4.3	0.5	4.5	2
G 9.4	7.19	43.19	5.5	102.4	0.0	9.8	0.4	10.2	1.2	10.4	5
G 9.2	6.60	42.60	3.7	66.1	0.0	2.2	0.4	7.5	0.6	6.2	2
G 9	5.90	41.90	5.9	86.0	0.0	18.5	0.6	11.6	0.8	7.6	3
G 7.1	5.31	41.31	3.7	66.1	0.0	2.2	0.3	7.5	0.7	6.2	3
G 6.1	4.85	40.85	3.9	69.1	0.0	0.0	0.4	8.1	0.7	6.2	3
G 5.2	4.23	40.23	3.8	68.4	0.0	1.5	0.4	8.1	0.6	5.9	2
G 5.1	3.70	39.70	5.1	86.9	0.0	9.1	0.7	13.3	0.5	5.2	2
G 5	3.20	39.20	5.7	98.7	0.0	13.3	0.7	13.4	0.7	6.6	3
G 4.7	2.90	38.90	13.4	148.2	0.0	29.3	1.9	34.9	1.2	11.5	5
G 4.5	2.29	38.29	9.8	165.3	0.0	24.1	1.2	23.5	1.1	10.1	4
G 4.3	1.44	37.44	20.6	254.2	0.2	73.5	2.6	48.5	1.5	14.6	9
G 4.1	0.58	36.58	17.1	210.5	0.0	42.2	2.6	46.8	1.0	10.1	4
G 3	0.43	36.43	21.3	249.8	0.1	66.6	2.9	53.7	1.3	13.5	7
G 1	0.18	36.18	8.7	134.5	0.1	25.5	0.9	17.9	1.2	11.1	6
MG 120	80.00	80.00	4.9	72.20	0.00	0.00	0.70	13.70	0.3	3.4	1
MG 119	78.90	78.90	4.5	67.70	0.00	0.00	0.70	12.70	0.3	2.8	1

Th (ACME)			
Sample	[m]	[m] succession	PPM
G 30.3	35.30	71.30	0.3
G 30.1	34.85	70.85	0.2
G 30	34.50	70.50	0.1
G 29.2	33.60	69.60	0.1
G 29	32.95	68.95	0.2
G 28.11	32.10	68.10	0.2
G 28.9	31.22	67.22	0.1
G 28.7	30.60	66.60	0.2
G 28.5	29.89	65.89	0.2
G 28.4	29.33	65.33	0.1
G 28.2	28.45	64.45	0.1
G 28.1	27.75	63.75	0.2
G 28	27.28	63.28	0.2
G 27	27.05	63.05	0.4
G 26.8	25.80	61.80	0.5
G 26.6	25.15	61.15	0.2
G 26.2	24.45	60.45	0.2
G 26.1	24.20	60.20	0.3
G 26	23.80	59.80	0.1
G 25.6	23.05	59.05	0.1
G 25.3	22.02	58.02	0.2
G 25	20.95	56.95	0.1
G 24.5	20.33	56.33	0.2
G 24.3	19.70	55.70	0.1
G 24	18.85	54.85	0.2
G 23	18.20	54.20	0.3
G 22.5	17.38	53.38	0.2
G 22.2	16.44	52.44	0.2
G 22	15.46	51.46	0.2
G 21	15.03	51.03	0.2
G 20	14.47	50.47	0.2
G 18	14.01	50.01	0.2
G 17	13.41	49.41	0.3
G 16	12.55	48.55	0.2
G 15	11.90	47.90	0.3
G 14	11.03	47.03	0.2
G 13	10.35	46.35	0.3
G 12	9.55	45.55	0.2
G 11.1	8.61	44.61	0.3
G 10.1	7.65	43.65	0.2
G 9.3	6.73	42.73	0.4
G 9	5.90	41.90	0.4
G 7	5.15	41.15	0.3
G 6	4.40	40.40	0.4
G 5.1	3.70	39.70	0.3
G 5	3.20	39.20	0.4
G 4.5	2.29	38.29	0.5
G 3	0.43	36.43	0.7
G 1	0.18	36.18	0.6
MG 56	0.38	0.38	0.3
MG 58	1.88	1.88	0.3
MG 60	6.38	6.38	0.5
MG 63	7.70	7.70	0.2
MG 66	9.35	9.35	0.3
MG 68	10.20	10.20	0.2
MG 70	11.20	11.20	0.7
MG 72	12.55	12.55	0.4
MG 75	15.15	15.15	0.4
MG 77	19.10	19.10	0.6
MG 80	21.60	21.60	0.5
MG 82	23.55	23.55	1.0
MG 84	25.25	25.25	0.9
MG 87	27.30	27.30	0.7
MG 89	30.50	30.50	1.2
MG 92	33.90	33.90	0.7
MG 95	34.85	34.85	0.5
MG 97	36.30	36.30	0.5
MG 97A	37.60	37.60	0.5
MG 97B	39.10	39.10	0.3
MG 99	40.60	40.60	0.3
MG 100	44.70	44.70	0.3
MG 104A	48.10	48.10	0.3
MG 104B	51.40	51.40	0.3
MG 107	57.05	57.05	0.2
MG 109	58.60	58.60	0.2
MG 113	61.10	61.10	0.1
MG 116	64.85	64.85	0.2
MG 119	78.90	78.90	0.1
MG 120	80.00	80.00	0.1

MG 118	78.40	78.40	3.2	67.80	0.00	0.00	0.40	8.10	0.4	3.4	2
MG 117	77.80	77.80	4.3	108.00	0.00	0.00	0.50	9.90	0.6	5.9	2
MG 117B	76.10	76.10	3.9	104.40	0.00	0.00	0.30	7.80	0.8	6.9	3
MG 117A	75.10	75.10	4.1	98.30	0.00	0.00	0.50	10.20	0.5	4.5	2
MG 116	64.85	64.85	7.8	128.80	0.00	1.10	1.00	18.90	1	9	4
MG 115	63.60	63.60	5.7	130.10	0.00	5.70	0.90	15.80	0.4	3.8	2
MG 114	61.70	61.70	7.5	117.10	0.00	2.50	1.20	21.40	0.4	4.5	2
MG 113	61.10	61.10	10	141.20	0.00	8.40	1.70	29.70	0.3	4.1	1
MG 112	60.65	60.65	6.2	125.80	0.00	0.00	0.90	16.80	0.5	4.8	2
MG 111	60.30	60.30	5.2	121.60	0.00	0.00	0.70	13.40	0.5	5.2	2
MG 110	59.95	59.95	6.6	135.50	0.00	0.00	0.80	15.50	0.9	8.3	4
MG 109	58.60	58.60	4.8	78.00	0.00	0.00	0.60	11.30	0.7	6.2	3
MG 108	57.05	57.05	4	86.70	0.00	0.00	0.40	9.20	0.6	5.5	2
MG 107	57.05	57.05	3.5	116.50	0.00	0.00	0.20	6.10	0.8	7.3	3
MG 106	56.10	56.10	4.3	86.90	0.00	0.00	0.40	8.50	0.8	7.6	3
MG 105	56.10	56.10	5.4	133.40	0.00	0.00	0.60	12.30	0.8	7.3	3
MG 104C	52.10	52.10	10.7	202.90	0.10	28.60	0.50	15.50	2.5	22.2	11
MG 104B	51.40	51.40	6.5	164.20	0.00	11.20	0.30	9.50	1.7	15.3	7
MG 104A	48.10	48.10	4.5	170.10	0.00	8.40	0.40	9.50	0.8	6.9	3
MG 104	47.20	47.20	4.7	110.40	0.00	0.00	0.30	8.10	1.1	9.7	4
MG 103	46.00	46.00	4.9	110.40	0.00	0.00	0.20	7.10	1.4	12.1	6
MG 102	46.00	46.00	5.3	133.80	0.00	0.40	0.50	11.30	0.9	8.3	4
MG 101	45.30	45.30	3.1	131.00	0.00	4.60	0.30	6.10	0.6	5.5	2
MG 100	44.70	44.70	3.9	119.80	0.00	1.50	0.20	6.40	1	8.7	4
MG 99A	41.30	41.30	8.1	221.30	0.00	17.80	0.70	15.10	1.6	13.9	6
MG 98	40.60	40.60	7.8	209.10	0.00	17.50	0.70	15.50	1.3	12.1	5
MG 99	40.60	40.60	8.7	223.40	0.00	16.80	0.80	17.50	1.6	14.2	6
MG 97B	39.10	39.10	7.1	173.10	0.00	11.60	1.00	18.60	0.6	6.2	2
MG 97A	37.60	37.60	8.5	171.50	0.00	13.70	1.10	21.70	0.9	8.3	4
MG 97	36.30	36.30	17.1	283.00	0.00	41.90	2.20	42.60	1.6	15.3	6
MG 96	35.95	35.95	9.9	190.70	0.00	11.20	0.90	20.70	1.8	16	7
MG 95A	35.25	35.25	5.3	154.70	0.00	6.70	0.50	10.60	1	9.4	4
MG 95	34.85	34.85	5	112.50	0.00	3.60	0.40	9.90	1	9	4
MG 94	34.30	34.30	6.6	156.20	0.00	5.00	0.60	13.70	1.2	10.8	5
MG 93	33.90	33.90	3.8	137.30	0.00	6.00	0.00	2.90	1.4	11.8	6
MG 92	33.90	33.90	5.6	147.50	0.00	12.30	0.30	8.80	1.3	11.8	5
MG 91	32.80	32.80	6.1	241.00	0.10	24.40	0.10	6.10	1.6	13.5	8
MG 90	31.70	31.70	5.1	195.90	0.00	2.50	0.30	8.80	1.2	10.8	5
MG 89	30.50	30.50	6.2	186.50	0.10	17.50	0.10	6.10	1.9	16.3	9
MG 88	29.60	29.60	8.7	168.50	0.20	39.80	0.30	9.20	2	17	11
MG 87	27.30	27.30	9.2	188.10	0.20	51.20	0.40	9.90	1.7	14.6	10
MG 86	26.80	26.80	1.4	138.60	0.00	0.00	0.00	1.20	0.5	4.5	2
MG 85	25.95	25.95	6.2	155.80	0.10	29.30	0.10	5.70	1.5	12.8	8
MG 84	25.25	25.25	5.8	139.20	0.10	32.10	0.20	6.10	1.1	9.7	6
MG 83	24.60	24.60	2.5	77.10	0.00	2.20	0.10	4.00	0.7	5.9	3
MG 82	23.55	23.55	5.5	164.80	0.10	22.00	0.10	5.00	1.4	12.5	7
MG 81	22.25	22.25	8.3	175.70	0.10	36.30	0.30	9.50	1.8	15.6	9
MG 80	21.60	21.60	4.1	130.20	0.00	4.30	0.00	2.90	1.5	13.2	6
MG 79	19.95	19.95	5.5	152.40	0.00	8.40	0.30	8.10	1.5	13.2	6
MG 78	19.25	19.25	5.6	133.00	0.00	13.70	0.10	5.70	1.7	14.9	7
MG 77	19.10	19.10	7.2	174.90	0.10	24.80	0.30	9.50	1.6	14.2	8
MG 76	17.50	17.50	6.1	178.40	0.10	20.60	0.10	5.40	1.8	15.6	9
MG 75	15.15	15.15	6.4	142.90	0.10	31.80	0.30	7.80	1.2	10.4	6
MG 74	14.50	14.50	2.5	98.80	0.00	0.00	0.10	2.90	0.8	7.3	3
MG 73	13.90	13.90	3	85.50	0.00	0.00	0.10	4.30	0.9	7.6	4
MG 72	12.55	12.55	3.6	99.60	0.10	12.30	0.00	0.80	1.1	9.4	6
MG 71	12.10	12.10	3.3	87.40	0.00	3.20	0.10	4.30	1	9	4
MG 70	11.20	11.20	4.1	86.80	0.00	4.30	0.10	5.40	1.2	10.8	5
MG 69	10.85	10.85	3.5	82.60	0.00	1.10	0.00	0.00	1.3	11.1	5
MG 68	10.20	10.20	2.3	80.60	0.00	0.00	0.00	0.10	0.8	7.3	3
MG 67	9.95	9.95	1.6	81.80	0.00	0.00	0.00	0.80	0.6	5.2	2
MG 66	9.35	9.35	2.7	98.20	0.00	1.10	0.00	1.20	1	8.7	4
MG 65	8.80	8.80	1.9	53.20	0.00	0.00	0.00	1.90	0.7	5.9	3
MG 64	8.50	8.50	2.7	75.50	0.00	0.00	0.30	6.40	0.4	3.4	2
MG 63	7.70	7.70	3.4	113.50	0.00	4.60	0.10	4.70	1	8.7	4
MG 62	7.10	7.10	2.9	112.30	0.00	0.00	0.20	4.70	0.7	6.6	3
MG 61	7.10	7.10	3.2	115.30	0.00	0.00	0.30	6.80	0.6	5.2	2
MG 60	6.38	6.38	2.4	99.90	0.00	0.00	0.00	1.20	0.9	7.6	4
MG 59	6.10	6.10	3.6	119.90	0.00	2.50	0.30	7.50	0.7	5.9	3
MG 58	1.88	1.88	3.3	84.80	0.00	0.00	0.40	7.50	0.5	4.8	2
MG 57	0.38	0.38	1.8	80.30	0.00	0.00	0.10	2.90	0.5	4.1	2
MG 56	0.38	0.38	2.2	71.80	0.00	5.70	0.10	2.60	0.6	5.5	2

Sample	[m]		$\delta^{13}C$ [‰ VPDB]	$\delta^{18}O$ [‰ VPDB]
G 49	39.75	75.75	2.40	-4.88
G 48	39.50	75.50	2.45	-5.47
G 47	39.00	75.00	2.18	-5.22
G 45	38.55	74.55	2.12	-5.81
G 43	38.05	74.05	2.28	-5.41
G 41	37.60	73.60	2.15	-5.52
G 39	37.10	73.10	2.29	-5.30
G 37	36.70	72.70	2.17	-5.54
G 35	36.20	72.20	0.53	-6.55
G 33	35.85	71.85	2.16	-5.52
G 32	35.65	71.65	1.81	-6.43
G 31	35.40	71.40	2.16	-6.29
G 30.3	35.30	71.30	2.09	-5.83
G 30.2	35.15	71.15	2.04	-5.69
G 30.1	34.85	70.85	1.95	-5.60
G 30	34.50	70.50	2.17	-6.50
G 29.4	34.20	70.20	0.99	-4.91
G 29.3	34.00	70.00	2.18	-3.61
G 29.2	33.60	69.60	2.02	-3.87
G 29.1	33.20	69.20	1.78	-4.42
G 29	32.95	68.95	2.03	-2.63
G 28.13	32.60	68.60	1.78	-4.10
G 28.12	32.40	68.40	1.70	-3.83
G 28.11	32.10	68.10	1.73	-3.91
G 28.10	31.70	67.70	1.77	-4.64
G 28.9	31.22	67.22	1.88	-4.29
G 28.8	30.98	66.98	1.76	-4.17
G 28.7	30.60	66.60	2.01	-3.98
G 28.6	30.30	66.30	1.88	-4.48
G 28.5	29.89	65.89	1.69	-3.68
G 28.4	29.33	65.33	1.89	-4.42
G 28.3	28.95	64.95	1.90	-7.80
G 28.2	28.45	64.45	1.97	-4.41
G 28.1	27.75	63.75	2.07	-5.07
G 28	27.28	63.28	1.83	-7.66
G 27	27.05	63.05	1.91	-4.61
G 26.11	26.60	62.60	2.00	-3.91
G 26.10	26.40	62.40	1.60	-3.98
G 26.9	26.02	62.02	1.80	-3.59
G 26.8	25.80	61.80	1.61	-3.81
G 26.7	25.47	61.47	2.04	-3.85
G 26.6	25.15	61.15	1.85	-3.72
G 26.5	24.95	60.95	1.97	-3.55
G 26.4	24.85	60.85	2.01	-4.10
G 26.3	24.65	60.65	1.98	-3.63
G 26.2	24.45	60.45	2.03	-3.90
G 26.1	24.20	60.20	1.91	-3.70
G 26	23.80	59.80	2.08	-3.26
G 25.8	23.53	59.53	1.79	-3.80
G 25.7	23.40	59.40	1.88	-3.86
G 25.6	23.05	59.05	1.76	-4.06
G 25.5	22.48	58.48	1.42	-3.21
G 25.4	22.43	58.43	1.84	-3.42
G 25.3	22.02	58.02	1.72	-4.36
G 25.2	21.65	57.65	1.80	-4.29
G 25.1	21.41	57.41	1.92	-3.80
G 25	20.95	56.95	2.00	-3.94
G 24.6	20.87	56.87	1.90	-3.08
G 24.5	20.33	56.33	1.83	-4.12
G 24.4	20.05	56.05	1.98	-4.14
G 24.3	19.70	55.70	1.84	-3.83
G 24.2	19.35	55.35	1.85	-3.87
G 24.1	19.15	55.15	1.98	-3.82
G 24	18.85	54.85	1.88	-3.70
G 23.2	18.60	54.60	1.62	-3.60
G 23.1	18.40	54.40	1.74	-3.37

Sample	[m]		$\delta^{13}C$ [‰ VPDB]	$\delta^{18}O$ [‰ VPDB]
MG 120	80.00	80.00	2.35	-4.77
MG 119	78.90	78.90	1.99	-5.25
MG 116	64.85	64.85	1.79	-2.73
MG 113	61.10	61.10	1.88	-3.43
MG 110	59.95	59.95	1.52	-3.03
MG 109	58.60	58.60	1.70	-3.40
MG 107	57.05	57.05	0.97	-3.44
MG 105	56.10	56.10	1.81	-2.88
MG 104B	51.40	51.40	1.73	-2.97
MG 104A	48.10	48.10	1.39	-3.41
MG 102	46.20	46.20	1.59	-2.45
MG 100	44.70	44.70	1.72	-3.63
MG 99	40.80	40.80	1.61	-4.80
MG 98	40.60	40.60	-0.37	-4.86
MG 97B	39.10	39.10	1.71	-2.97
MG 97A	37.60	37.60	1.68	-3.09
MG 97	36.30	36.30	1.83	-2.69
MG 95	34.85	34.85	1.81	-2.12
MG 93	33.90	33.90	1.84	-1.82
MG 92	33.90	33.90	1.77	-2.20
MG 90	31.70	31.70	2.04	-1.80
MG 89	30.50	30.50	1.97	-2.10
MG 87	27.30	27.30	2.36	-1.80
MG 85	25.95	25.95	2.26	-1.47
MG 84	25.25	25.25	2.09	-1.90
MG 82	23.55	23.55	2.35	-1.51
MG 80	21.60	21.60	2.47	-1.63
MG 79	19.95	19.95	2.51	-1.73
MG 77	19.10	19.10	2.42	-1.21
MG 75	15.15	15.15	2.45	-1.39
MG 72	12.55	12.55	2.48	-2.56
MG 70	11.20	11.20	2.47	-2.25
MG 68	10.20	10.20	2.57	-2.01
MG 66	9.35	9.35	2.56	-2.83
MG 63	7.70	7.70	2.58	-2.98
MG 62	7.10	7.10	2.55	-3.43
MG 60	6.38	6.38	2.57	-3.56
MG 58	1.88	1.88	2.55	-3.63
MG 57	0.38	0.38	2.59	-2.28
MG 56	0.38	0.38	2.60	-3.90

XXX samples excluded from analysis

G 23	18.20	54.20	1.93	-3.70
G 22.8	18.12	54.12	1.93	-3.26
G 22.7	17.77	53.77	2.07	-3.55
G 22.5	17.38	53.38	1.90	-4.40
G 22.4	16.85	52.85	1.95	-4.67
G 22.3	16.65	52.65	1.79	-3.65
G 22.2	16.44	52.44	1.93	-4.15
G 22.1	15.90	51.90	1.77	-4.32
G 22	15.46	51.46	1.79	-4.39
G 21.2	15.36	51.36	1.92	-4.70
G 21.1	15.22	51.22	1.91	-4.29
G 21	15.03	51.03	1.72	-5.16
G 20.1	14.74	50.74	1.89	-4.60
G 20	14.47	50.47	1.84	-4.51
G 19	14.30	50.30	1.81	-3.47
G 18	14.01	50.01	1.94	-4.54
G 17.1	13.85	49.85	1.84	-3.45
G 17	13.41	49.41	1.68	-5.76
G 16.2	13.29	49.29	1.85	-3.72
G 16.1	13.10	49.10	1.79	-4.08
G 16	12.55	48.55	2.01	-3.44
G 15.2	12.43	48.43	1.78	-3.39
G 15.1	12.05	48.05	1.95	-3.50
G 15	11.90	47.90	1.90	-3.71
G 14.1	11.28	47.28	1.95	-2.59
G 14	11.03	47.03	1.85	-3.49
G 13.1	10.65	46.65	1.96	-3.69
G 13	10.35	46.35	1.88	-3.50
G 12.2	10.25	46.25	2.03	-3.24
G 12.1	9.90	45.90	1.92	-3.34
G 12	9.55	45.55	1.90	-3.69
G 11.2	9.03	45.03	1.81	-3.23
G 11.1	8.61	44.61	1.95	-3.63
G 11	8.25	44.25	2.03	-3.48
G 10.2	8.12	44.12	1.93	-3.55
G 10.1	7.65	43.65	1.88	-3.71
G 10	7.25	43.25	2.01	-4.65
G 9.4	7.19	43.19	1.87	-3.17
G 9.3	6.73	42.73	1.74	-3.01
G 9.2	6.60	42.60	2.25	-3.83
G 9.1	6.07	42.07	1.84	-3.78
G 9	5.90	41.90	1.86	-3.18
G 8	5.52	41.52	1.99	-2.88
G 7.2	5.46	41.46	1.94	-3.15
G 7.1	5.31	41.31	1.90	-2.47
G 7	5.15	41.15	1.93	-3.57
G 6.2	5.05	41.05	1.86	-3.87
G 6.1	4.85	40.85	1.91	-3.31
G 6	4.40	40.40	2.02	-2.90
G 5.2	4.23	40.23	1.89	-3.08
G 5.1	3.70	39.70	1.83	-5.41
G 5	3.20	39.20	1.91	-4.15
G 4.7	2.90	38.90	1.80	-2.67
G 4.6	2.68	38.68	1.72	-2.69
G 4.5	2.29	38.29	1.73	-3.06
G 4.4	1.78	37.78	1.89	-2.61
G 4.3	1.44	37.44	1.68	-2.55
G 4.2	0.85	36.85	1.75	-2.60
G 4.1	0.58	36.58	1.54	-2.81
G 3	0.43	36.43	1.73	-2.25
G 2	0.35	36.35	1.92	-2.22
G 1	0.18	36.18	1.62	-3.22

Giewont section			Calcareous dinoflagellates										
Sample	[m]	[m] succession	*Cadosina semiradiata fusca*	*Colomisphaera carpathica*	*Stomiosphaera moluccana*	*Cadosina semiradiata semiradiata*	*Colomisphaera sublapidosa*	*Parastomiosphaera malmica*	*Colomisphaera tenuis*	*Colomisphaera lapidosa*	*Colomisphaera pulla*	*Schizosphaerella minutissima*	*Cadosina parvula*
G 49	39.75	75.75											
G 48	39.50	75.50											
G 47	39.00	75.00											
G 46	38.80	74.80											
G 45	38.55	74.55											
G 44	38.30	74.30											
G 40	37.35	73.35											
G 37	36.70	72.70											
G 36	36.40	72.40											
G 34	36.05	72.05											
G 33	35.85	71.85											
G 31	35.40	71.40											
G 30.3	35.30	71.30											
G 30.2	35.15	71.15											
G 29.4	34.20	70.20		X									
G 29.2	33.60	69.60			aff.		cf.						
G 29.1	33.20	69.20											
G 29	32.95	68.95		X									
G 28.13													
G 28.11													
G 28.9	31.22	67.22		cf.									
G 28.7													
G 28.5													
G 28.4	29.33	65.33		cf.									
G 28.3	28.95	64.95											
G 28.2	28.45	64.45								cf.			
G 28.1	27.75	63.75											
G 28	27.28	63.28					c.f						
G 27	27.05	63.05		X	cf.					X			
G 26.8													
G 26.6	25.15	61.15											
G 26.2	24.45	60.45											
G 26.1	24.20	60.20			cf.								
G 26													
G 25.7													
G 25.5													
G 25.3	22.02	58.02											cf.
G 25.1	21.41	57.41					cf.						
G 25	20.95	56.95											
G 24.5	20.33	56.33											
G 24.3	19.70	55.70											
G 24	18.85	54.85											
G 23	18.20	54.20			aff.								
G 22.5	17.38	53.38										cf.	cf.
G 22.2	16.44	52.44		cf.						X			
G 22	15.46	51.46		cf.	X				cf.	X		X	
G 21	15.03	51.03			X								
G 20	14.47	50.47			X				cf.		cf.		
G 18	14.01	50.01							cf.	cf.			
G 14	11.03	47.03			cf.				cf.				
G 13	10.35	46.35							cf.				
G 12	9.55	45.55			X		cf.						
G 11.1	8.25	44.25			X								
G 10.1	7.25	43.25											
G 9.3	6.73	42.73			cf.		cf.	X					
G 9	5.90	41.90											
G 8													
G 7	5.15	41.15			cf.								
G 6	4.40	40.40		cf.			cf.						
G 5.1	3.70	39.70		X		X	X			X			
G 5	3.20	39.20											
G 4.5	2.29	38.29		cf.	aff.					X			
G 3	0.43	36.43			aff.					X			
G 2	0.35	36.35		cf.	aff.								
G 1	0.18	36.18	X	cf.	aff.								

Sample	Foraminifers																						
	Lenticulina sp.	*Spirillina* sp.	*Conoglobigerina* sp.	*Ammodiscus* sp.	*Pseudomarsonella bipartita*	*Redmondoides* sp.	*Lenticulina muensteri*	*Lenticulina* ex gr. *uhligi-muensteri*	*Conoglobigerina gulekhensis*	*Lenticulina angulosa*	*Praehedbergella infracretacea*	*Preahedbergella sigali*	*Paleogaudryina* sp.	*Textularia* sp.	*Haghimashella arcuata*	*Praedorothia praehauteriviana*	*Protomarsonella kummi*	*Protomarsonella hechti*	*Bigenerina* sp.	*Praehedbergella rudis*	*Uvigerinammina uvigeriniformis*	*Protomarsonella* sp.	*Pseudonerinea vaceki* (snail)
G 49																							cf.
G 48																						X	
G 47	X														cf.								
G 46															cf.	X	cf.						
G 45																X	cf.			cf.	X		
G 44																	cf.		cf.				
G 40	X																						
G 37	X																						
G 36																		cf.					
G 34																cf.	cf.						
G 33															cf.								
G 31		cf.																					
G 30.3	X					X							X										
G 30.2						cf.							X	X									
G 29.4		X	X							cf.	cf.	cf.											
G 29.2								X	cf.														
G 29.1	X							X															
G 29	X																						
G 28.13																							
G 28.11																							
G 28.9																							
G 28.7																							
G 28.5																							
G 28.4																							
G 28.3				X																			
G 28.2																							
G 28.1	X																						
G 28																							
G 27																							
G 26.8																							
G 26.6	X																						
G 26.2	X																						
G 26.1																							
G 26																							
G 25.7																							
G 25.5																							
G 25.3																							
G 25.1																							
G 25	X																						
G 24.5																							
G 24.3							cf.																
G 24							cf.																
G 23																							
G 22.5																							
G 22.2																							
G 22	X																						
G 21																							
G 20	X																						
G 18																							
G 14																							
G 13																							
G 12						X																	
G 11.1					cf.																		
G 10.1																							
G 9.3			X																				
G 9																							
G 8																							
G 7	X																						
G 6																							
G 5.1																							
G 5																							
G 4.5	X	X	X	X																			
G 3	X			X																			
G 2		X																					
G 1	X	X	X																				

Sample	Saccomidae elements							INTERPRETATION	Sample
	Sac1	Sac2	Sac3	Sac4	Sac5	Sac6	Sac7		
G 49									**G 49**
G 48									**G 48**
G 47									**G 47**
G 46									**G 46**
G 45									**G 45**
G 44									**G 44**
G 40									**G 40**
G 37									**G 37**
G 36									**G 36**
G 34									**G 34**
G 33									**G 33**
G 31									**G 31**
G 30.3									**G 30.3**
G 30.2									**G 30.2**
G 29.4									**G 29.4**
G 29.2									**G 29.2**
G 29.1									**G 29.1**
G 29									**G 29**
G 28.13	X	X	**X**	**X**	**X**	**X**	**X**		**G 28.13**
G 28.11		X	X	**X**	**X**	**X**	X		**G 28.11**
G 28.9		X	X	**X**	**X**	**X**	X		**G 28.9**
G 28.7			X	X	X	X	X		**G 28.7**
G 28.5			**X**	**X**	**X**	**X**	X		**G 28.5**
G 28.4			**X**	**X**	**X**	**X**	X		**G 28.4**
G 28.3			**X**	**X**	**X**	**X**	X		**G 28.3**
G 28.2	X	**X**	**X**	**X**	**X**	**X**			**G 28.2**
G 28.1	X	X	X	**X**	**X**	**X**	X		**G 28.1**
G 28			**X**	**X**	**X**	**X**	X		**G 28**
G 27			X	**X**	**X**	**X**	X	**Sac6**	**G 27**
G 26.8			X	**X**	**X**	**X**	X		**G 26.8**
G 26.6		X	X	X	X	X			**G 26.6**
G 26.2			X	**X**	**X**	**X**	X		**G 26.2**
G 26.1		X	X	X	X	**X**	X		**G 26.1**
G 26			X	X	X	X	X		**G 26**
G 25.7	X	X	**X**	**X**	X	X			**G 25.7**
G 25.5		X	**X**	**X**	**X**	**X**			**G 25.5**
G 25.3				**X**	**X**	**X**	X		**G 25.3**
G 25.1			X	X	**X**	**X**	X		**G 25.1**
G 25	X	X	**X**	**X**	**X**	**X**	X		**G 25**
G 24.5	X	X	**X**	**X**	**X**	X	X		**G 24.5**
G 24.3			**X**	**X**	**X**	**X**	X		**G 24.3**
G 24			X	**X**	**X**	**X**	X		**G 24**
G 23				X	X	X			**G 23**
G 22.5									**G 22.5**
G 22.2	X	X	X	**X**	**X**	**X**	**X**		**G 22.2**
G 22	X	X	X	**X**	**X**	X		**Sac5**	**G 22**
G 21				X	X	X	X		**G 21**
G 20		X	**X**	**X**	**X**	X	X		**G 20**
G 18				X	X	X			**G 18**
G 14	X	X	**X**	**X**	**X**	X	X		**G 14**
G 13			X	X	**X**	**X**	**X**		**G 13**
G 12		X	X	**X**	**X**	**X**	X		**G 12**
G 11.1	X	**X**	**X**	**X**					**G 11.1**
G 10.1		X	**X**	**X**	X	X	X		**G 10.1**
G 9.3	X	X	**X**	**X**	X				**G 9.3**
G 9	X	X	**X**	**X**	**X**	X			**G 9**
G 8		**X**	**X**	**X**	**X**	X	X		**G 8**
G 7			**X**	**X**	**X**	X	X		**G 7**
G 6			X	X	X			**Sac4**	**G 6**
G 5.1		X	**X**	**X**	**X**	X	X		**G 5.1**
G 5			**X**	**X**	X	X			**G 5**
G 4.5			**X**	**X**	X				**G 4.5**
G 3			**X**	**X**	X	X	X		**G 3**
G 2	X	X	**X**	**X**	X	X	X		**G 2**
G 1			**X**	**X**	**X**	X			**G 1**

X ocurrence
cf. *conformis* ocurrence
aff. *affinis* ocurrence